

University of New Mexico

UNM Digital Repository

Nanoscience and Microsystems ETDs

Engineering ETDs

Spring 5-15-2022

Application of Bismuth Oxychloride as a Colorimetric UV Sensor Material

Kyle James Troche
University of New Mexico

Follow this and additional works at: https://digitalrepository.unm.edu/nsms_etds



Part of the [Nanoscience and Nanotechnology Commons](#)

Recommended Citation

Troche, Kyle James. "Application of Bismuth Oxychloride as a Colorimetric UV Sensor Material." (2022). https://digitalrepository.unm.edu/nsms_etds/60

This Thesis is brought to you for free and open access by the Engineering ETDs at UNM Digital Repository. It has been accepted for inclusion in Nanoscience and Microsystems ETDs by an authorized administrator of UNM Digital Repository. For more information, please contact disc@unm.edu.

Kyle Troche

Department of Nanoscience and Microsystems Engineering

This thesis is approved, and it is accepted in quality
and form for publication:

Approved by the Thesis Committee:

Fernando Garzon, Chairperson

Kannan Ramaiyan

Lok-kun Tsui

**APPLICATION OF BISMUTH OXYCHLORIDE AS A
COLORIMETRIC UV SENSOR MATERIAL**

BY

KYLE TROCHE

B.S., Chemical Engineering, University of New Mexico, 2021

THESIS

Submitted in Partial Fulfillment of the
Requirements for the Degree of

Master of Science

Nanoscience and Microsystems Engineering

The University of New Mexico
Albuquerque, New Mexico

May 2022

ACKNOWLEDGMENTS

I heartily acknowledge Fernando Garzon, my advisor and thesis chair, for continuing to encourage me throughout my academic journey and during the past couple of months writing these chapters. I want to thank Kannan Ramaiyan, my research advisor for the vast amounts of feedback to ensure that it is the best it could be. I am truly thankful for all of your help and advice. from the bottom of my heart. Your guidance and professional style will remain with me as I continue my career.

APPLICATION OF BISMUTH OXYCHLORIDE AS A COLORIMETRIC UV SENSOR MATERIAL

BY

KYLE TROCHE

B.S., Chemical Engineering, University of New Mexico, 2021

M.S., Nanoscience and Microsystems Engineering, University of New Mexico, 2022

ABSTRACT

Sunlight contains about 9% UV radiation with roughly one-third of it penetrating the atmosphere and reaching the Earth's surface. UV radiation from the sun is classified into three different types: UVA (315- 499 nm), UVB (280- 314nm), and UVC (100- 279 nm). Prolonged exposure to artificial UV radiation or direct sunlight can still induce many adverse effects such as sunburn, weakening of the immune system, and skin cancer. A wide variety of photoresistor, photodiode and colorimetric UV sensors are currently being researched to help monitor UV radiation. Our research is focused on developing a colorimetric UV sensor that is inherently safe and environmentally friendly and is composed of bismuth (III) chloride (BiCl_3) and 6-carboxyfluorescein (6-CF). Two different UV sensors were prepared, a solution state with ethanol and a solid-state with a Grade 597 Whatman filter paper substrate. Our proposed mechanism involves the spontaneous hydrolysis of BiCl_3 in ethanol to produce bismuth oxychloride (BiOCl). Upon UV exposure, BiOCl is excited and changes color from white to black. This extent of black color formation provides a direct measure of UV exposure. Other

dye molecules including 5-Carboxyfluorescein (5-CF), prussian blue (PB), and rhodamine-b (RhB) were also tested. The 6-CF/BiCl₃ solid-state sensor is very cheap and easy to scaleup production due to the filter paper substrate and readily available chemicals. The work presented here paves the way for a commercially viable sensor that is cheap to produce and more importantly easy to analyze the results leading to wide variety of applications across multiple industries.

TABLE OF CONTENTS

LIST OF FIGURES	viii
LIST OF TABLES	xiii
CHAPTER 1: INTRODUCTION.....	1
UV Sensors Overview.....	3
Photoresistors and Photodiode UV Sensors.....	3
Zinc Oxide UV Sensor	4
Titanium Dioxide UV Sensor	5
Bismuth Oxychloride Photocatalyst	6
Colorimetric UV Sensors	7
Polydiacetylene UV Sensor	7
Phenylsulfonium UV Sensor.....	9
Chlorine Radical Fluorescent Quenching	10
Our Research.....	11
Materials and Instrumentation	12
CHAPTER 2: 6-CARBOXYFLUORESCEIN – BiCl₃ BASED	
UV SENSOR.....	14
6-CF Solution Sensor	15
Solid-State 6-CF UV Sensor.....	25
CHAPTER 3: 5-CARBOXYFLUORESCEIN – BiCl₃ BASED	
UV SENSOR.....	27
5-CF Solution Sensor	29
Solid-State 5-CF UV Sensor.....	33

CHAPTER 4: UV SENSOR MECHANISM	35
6-CF and KCl Sensor	37
SEM, EDS, and Powder XRD Analysis	40
Mechanism	44
CHAPTER 5: OTHER DYES IN BiCl₃ SENSORS.....	47
PB Solution Sensor	48
Solid-State PB UV Sensor	50
RhB Solution Sensor.....	51
XRD Analysis	57
Solid-State RhB UV Sensor.....	58
CHAPTER 6: PRACTICAL APPLICATIONS FOR THE UV SOLID-STATE SENSORS.....	60
Sunscreen Efficiency Measurements	60
302 nm SPF 30 Testing.....	61
Sunlight SFP 30 Testing	63
Optical Density Measurements on Solid-State Sensors.....	67
CHAPTER 7: CONCLUSION.....	72
APPENDIX A: REFERENCE UV-VIS ABSORPTION SPECTRUMS.....	76
APPENDIX B: 6-CF FLUORESCENCE AND FRONTIER MOLECULAR ORBITALS	79
APPENDIX C: TAUC PLOT FOR 100 mM BiCl₃.....	80
REFERENCES.....	81

LIST OF FIGURES

Figure 1.1. a) Schematic representation of UV exposure from sunlight through The atmosphere and Ozone as well as b) layers of the skin. c) Positive and negative effects of UV radiation on the human skin.....	2
Figure 1.2. Diagram of a photodiode	4
Figure 1.3. a) Schematic design of an integrated ZnO nanowire UV sensor and b) Photoresponse of the integrated ZnO nanowire UV sensor under UV irradiance of 4.5 mW cm^{-2} and bias voltage of 1 V	5
Figure 1.4. Chemical structure of PCDA used in PDA colorimetric UV sensors	8
Figure 1.5. PDA UV sensor color change of different polymer assemblies after various irradiation times	9
Figure 1.6. a) Chemical structure of 4-phenoxyphenyl)diphenylsulfonium triflate (PPDPS-TF) used in a phenylsulfonium colorimetric UV sensors, b) color change of PPDPS-TF UVA sensor using crystal violet lactone and a UVB filter, and c) color change of PPDPS-TF UVB sensor using Congo red and a UVA filter	10
Figure 1.7. Mechanism for DPI-BP quenching upon exposure to γ radiation.....	11
Figure 2.1. Chemical structure of 6-carboxyfluorescein (6-CF).....	14
Figure 2.2. a) UV absorption spectrum of 1mM 6-CF prior to UV exposure, b) solution picture of 1 mM 6-CF under 302 nm UV light (right) and under visible light (left), c) UV absorption spectrum of 100 mM BiCl_3 prior to UV exposure, d) solution picture of 100 mM BiCl_3 under 302 nm UV light (right) and under visible light (left).....	16
Figure 2.3. UV absorption of 1 mM 6-CF and 1 mM BiCl_3 in ethanol when exposed to 302 nm UV light	18

Figure 2.4. UV absorption of 1 mM 6-CF and 1 mM BiCl ₃ in ethanol when exposed to sunlight	19
Figure 2.5. UV absorption of 1 mM 6-CF and 5 mM BiCl ₃ in ethanol when exposed to sunlight	20
Figure 2.6. UV absorption of 5 mM 6-CF and 5 mM BiCl ₃ in ethanol when exposed to sunlight	21
Figure 2.7. UV absorption of 5 mM 6-CF and 10 mM BiCl ₃ in ethanol when exposed to sunlight	22
Figure 2.8 Various volume percentages of 1 mM 6-CF and 100 mM BiCl ₃ solution state UV Sensors a) as prepared, b) continuous 3 hour direct sunlight exposure, and c) 72 hour settling	24
Figure 2.9. Soaked and dried filter paper squares in 50% 1 mM 6-CF and 100 mM BiCl ₃ in ethanol exposed to a) 365 nm UV, b) 302 nm UV, c) 254 nm UV and d) sunlight for various durations	26
Figure 3.1. Comparison of the chemical structure, 1 mM ethanol solutions, and UV absorption spectra of a) 5-carboxyfluorescein (5-CF) and b) 6-carboxyfluorescein (6-CF).....	28
Figure 3.2. UV absorption spectrum of 1 mM 5-CF in ethanol when exposed to 302 nm UV light	29
Figure 3.3. UV absorption of 1 mM 5-CF and 10 mM BiCl ₃ in ethanol when exposed to 302 nm UV light	31
Figure 3.4. Various volume percentages of 1 mM 5-CF and 100 mM BiCl ₃ solution state UV Sensors a) as prepared, b) continuous 3 hour 302 nm UV exposure, and c) 72 hour settling	32
Figure 3.5. Soaked and dried filter paper squares in 50% 1 mM 5-CF and 100 mM BiCl ₃ in ethanol exposed to 302 nm UV light at various times	34

Figure 4.1. Proposed reaction mechanism for generation of reactive oxygen species and free chlorine on irradiation of AgCl	36
Figure 4.2. UV absorption of 1 mM 6-CF and 100 mM KCl in ethanol when exposed to sunlight	38
Figure 4.3. UV absorption of a) 100 mM KCl and b) 100 mM BiCl ₃ in ethanol when exposed to a) sunlight and b) 302 nm UV light	39
Figure 4.4. SEM images of 400 mM BiCl ₃ in ethanol.....	41
Figure 4.5. EDS spectrum of 400 mM BiCl ₃ in ethanol	42
Figure 4.6. XRD analysis comparing reference BiOCl and room temperature dried 400 mM BiCl ₃ in ethanol	43
Figure 4.7 Schematic of the electronic band structure of BiOCl.....	45
Figure 4.8. 100 mM BiCl ₃ filter paper sample a) exposed to 1 hour of sunlight, b) 3 weeks after initial exposure, c) additional 1 hour exposure of sunlight on unexposed side and initially exposed side	46
Figure 5.1. Chemical structure of a) Prussian Blue (PB) and b) Rhodamine-B (RhB) as well as photos of c) 0.1 mM PB in ethanol and d) 0.1 mM RhB in ethanol.....	48
Figure 5.2. UV absorption of as prepared solutions of a) 0.01 mM PB, b) 0.1 mM PB, and c) 1 mM PB	49
Figure 5.3. UV absorption of 0.01 mM PB and 10 mM BiCl ₃ in ethanol when exposed to 302 nm UV light	50
Figure 5.4. Soaked and dried filter paper squares in 50% 1 mM PB and 100 mM BiCl ₃ in ethanol exposed to 302 nm UV light at various times	51
Figure 5.5. UV absorption spectrum of 0.1 mM RhB in ethanol when exposed to 302 nm UV light	52

Figure 5.6. UV absorption of a) 50% 0.1 mM RhB and 100 mM BiCl ₃ and b) 50% 1 mM RhB and 100 mM BiCl ₃ in ethanol when exposed to 302 nm UV light	53
Figure 5.7. UV absorption of 0.1 mM RhB and 100 mM BiCl ₃ in ethanol when exposed to 302 nm UV light	54
Figure 5.8. Picture of 0.1 mM RhB and 100 mM BiCl ₃ solution sensor	56
Figure 5.9. XRD Whole Pattern Fitting of black precipitate formed from 5 continuous hours of 302 nm UV light exposure of 50% 0.1 mM RhB and 100 BiCl ₃ solution sensor	58
Figure 5.10. Soaked and dried filter paper squares in 50% 1 mM RhB and 100 mM BiCl ₃ in ethanol exposed to 302 nm UV light at various times	59
Figure 6.1. a) schematic and b) picture of experimental setup of 302 nm UV light SPF 30 sunscreen test.....	61
Figure 6.2. 50% 1 mM 6-CF and 100 mM BiCl ₃ UV sensor SPF 30 sunscreen test with 302 nm UV light	63
Figure 6.3. Schematic of sunlight SPF 30 sunscreen test	64
Figure 6.4. 50% 1 mM 6-CF and 100 mM BiCl ₃ UV sensor SPF 30 sunscreen test with sunlight.....	66
Figure 6.5. Kodak No. 3 Calibrated Step Tablet scanned with an Epson Expression 1680 Professional Scanner	67
Figure 6.6. 8-bit gray scale conversion of 302 nm solid-state sensor image	68
Figure 6.7. Plot of optical density values of 50% 1 mM 6-CF and 100 mM BiCl ₃ solid-state sensor when exposed to 365 nm light, 302 nm light, 254 nm light, and sunlight as a function of a) time and b) dosage	69

Figure 6.8. a) Filter paper squares soaked in 500 mM BiCl ₃ and ethanol exposed to 302 nm UV light for various durations. b) Plot of optical density values with respect to 302 nm exposure time	71
Figure 7.1. Illustration of an application that relates the optical density of a solid-state sensor the duration of UV exposure	75
Figure A1. UV absorption spectrum of blank quartz cuvette	76
Figure A2. UV absorption spectrum of ethanol.....	76
Figure A3. UV absorption spectrum of as prepared 5 mM 6-CF in ethanol	77
Figure A4. UV absorption spectrum of as prepared 1 mM BiCl ₃ in ethanol.....	77
Figure A5. UV absorption spectrum of as prepared 5 mM BiCl ₃ in ethanol.....	78
Figure A6. UV absorption spectrum of as prepared 10 mM BiCl ₃ in ethanol.....	78
Figure B1. Absorption and emission spectra of 6-CF.....	79
Figure B2. HOMO and LUMO frontier molecular orbitals of fluorescein.....	79
Figure C1. UV absorption spectrum of as prepared 10 mM BiCl ₃ in ethanol	80

LIST OF TABLES

Table 2.1. Maximum exposure time for various 6-CF/BiCl ₃ solution sensors.....	17
Table 4.1. Average atomic percentages of bismuth and chlorine from EDS.....	42
Table 6.1. Optical density values of 50% 1 mM 6-CF and 100 mM BiCl ₃ solid-state UV sensor exposed to 365 nm, 302 nm, 254 nm, and sunlight.....	70
Table 7.1. Comparison of three different commercial UV dosimeters, PCE-UV34 Light Meter, Grainger UV Light Meter, and UVC Dosimeters UVC 254 TRI Card.....	73

Chapter 1:

Introduction

A large range of wavelengths are observed from solar radiation. Sunlight contains about 9% UV radiation with roughly one-third of it penetrating the atmosphere and reaching the Earth's surface.¹ UV radiation from the sun is classified into three different types; UVA (315- 499 nm), UVB (280- 314nm), and UVC (100- 279 nm).² Among the three types of UV radiation, the high energy UVC and to a greater extent UVB can be very lethal to human life as it causes a wide variety of skin diseases. Thankfully, UVC is filtered completely by the ozone layer, eliminating the risk of UVC exposure from sunlight. UVB is partially absorbed by the ozone while all UVA passes through to reach Earth's surface. The UV radiation in ambient sunlight is predominantly 90%-95% UVA and 5%-10% UVB.² UV radiation has been successfully utilized in many applications from the medical industry to food sterilization. Nevertheless, prolonged exposure to artificial UV radiation or sunlight can still induce many adverse effects such as sunburn, weakening of the immune system, and skin cancer.^{1,2} While controlled exposure of UV radiation such as sterilization can be useful, unintended long term exposure should be prevented. Figure 1.1.a. depicts solar UV radiation as it passes through the atmosphere and Ozone while Figure 1.1.b. depicts where the solar radiation is absorbed in the skin. Figure 1.1.c. illustrates the positive and negative effects of UV exposure on human skin. UV radiation helps produce vitamin D and to regulate immune system, it also creates various health problems related to skin.

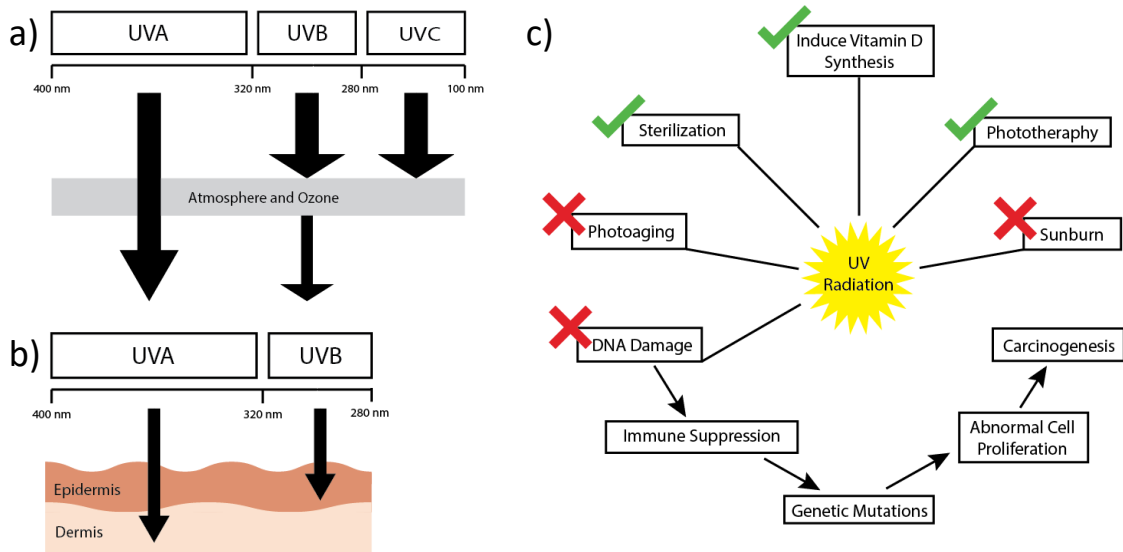


Figure 1.1. a) Schematic representation of UV exposure from sunlight through the atmosphere and Ozone as well as b) layers of the skin. c) Positive and negative effects of UV radiation on the human skin.

Since UV radiation can be both beneficial and harmful, monitoring the exposure is essential. Necessary protective measures such as sunscreen and UV protective clothing are available.³ Similarly, monitoring the UV radiation exposure is also possible through a wide variety of UV sensors that will further help mitigate UV exposure and limit skin damage. While UV sensors do not provide direct protection to UV radiation, their potential to monitor UV exposure is a valuable tool in a variety of industries such as sunscreen testing, food processing, and phototherapy. In this respect, significant research is being done on developing efficient and cheap UV sensors for wide range of applications. A wide variety of materials have been tested for UV sensor applications such as metal oxide nanostructures^{4,5}, organic dyes^{6,7}, and functional materials.^{8,9}

UV Sensors Overview

A sensor is a device that measures a physical property and either responds to it in a quantifiable manner or is recorded a signal. In the case of a UV sensor, the dosage of UV radiation is the physical property that the sensor responds to. In the following sections, I will introduce three different types of UV sensors that are commonly studied, photoresistors, photodiode UV sensors and colorimetric UV sensors.

Photoresistors and Photodiode UV Sensors

Photoresistors are a type of sensor that decreases its resistance when the active area of sensor is exposed to light.¹⁰ Photodiode sensors are a type of sensor that requires a photon of sufficient energy to interact with the active area of the sensor that contains an electron-hole pair to create a measurable change in current.¹¹ Figure 1.2 depicts the function of a photodiode. The incident photons interact with the photodiode to provide enough energy for the electrons (black circles) to move toward the cathode side and the holes (white circles) toward the anode which generates a current. Zinc oxide (ZnO) based sensors are photoresistors while titanium dioxide (TiO₂) based sensors are photodiode sensors. Both ZnO and TiO₂ UV sensors will be discussed in their relative subheadings in this chapter. It should be noted that other semiconductor materials have been researched for UV sensor applications but is outside of the scope of this thesis.

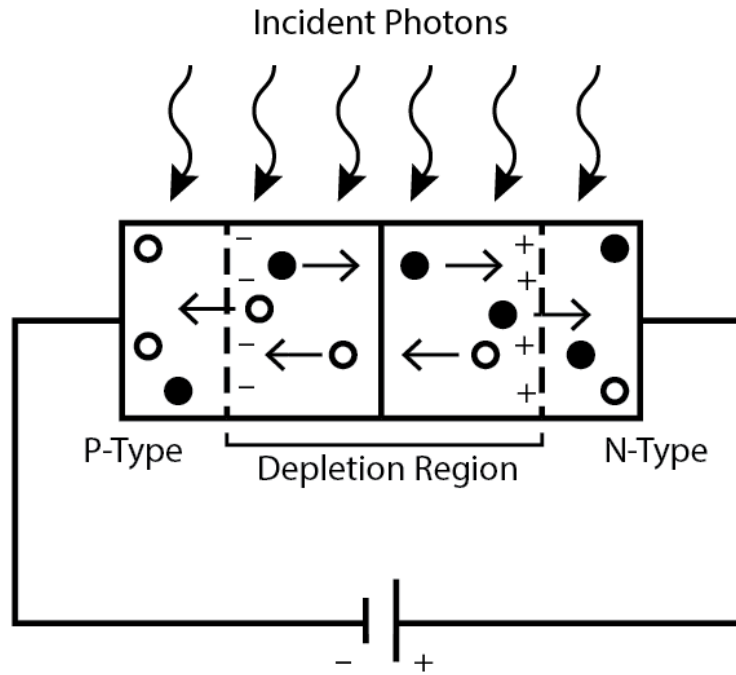


Figure 1.2. Diagram of a photodiode.

Zinc Oxide UV Sensor

Zinc oxide (ZnO) is one of the most promising metal oxides for UV sensors due to its high on/off current ratio, fast response and recovery, and large photoresponse current.^{4,5} ZnO UV sensors stand out amongst other photoresistors for UV sensor applications because of its large energy gap of 3.37 eV as well as an excitation binding energy of 60 meV.¹² ZnO UV sensors function based on the depletion of electrons in ZnO caused by the surface adsorbed oxygen.¹³ When illuminated by UV light, the high electron mobility contributes to the increasing photocurrent of sensor.¹⁴ ZnO nanostructures have a large surface-to-volume ratio and can produce a low electron density in ZnO without UV illumination¹⁴ allowing for a more accurate sensor. Precise dosage measurements can be achieved using ZnO nanostructure sensors along with high-precision voltage and current measuring systems. Furthermore, fabrication for ZnO nanowires⁴, ZnO nanoneedle networks⁵, and ZnO nanotetrapod⁵ networks are more expensive

compared to photodiode sensors such as TiO_2 , GaN, and SnO_2 . ZnO UV sensors produce a precise UV dosage measurement but rely on external monitoring tools such as a source measure unit. This limits the application of these sensors as well as reduces the range of target customers. Figure 1.3 illustrates the high performance ZnO nanowire UV sensor researched in Bai et al.⁴ Figure 1.3.a. is a schematic diagram of the UV sensor. Figure 1.3.b. is the photoresponse of ZnO nanowire UV sensor under UV irradiance of 4.5 mW cm^{-2} and a bias voltage of 1 V. When exposed to UV radiation a 1.0 mA current is measured followed by an immediate decrease in current after the UV radiation is turned off.

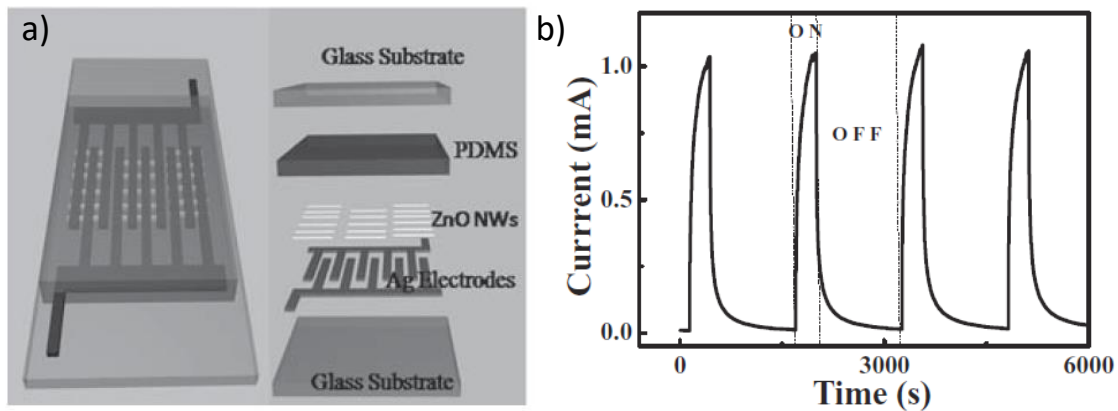


Figure 1.3. a) Schematic design of an integrated ZnO nanowire UV sensor and b) Photoresponse of the integrated ZnO nanowire UV sensor under UV irradiance of 4.5 mW cm^{-2} and bias voltage of 1 V. This Figure was reused from the Bai et al. article regarding high performance ZnO nanowire UV sensors.⁴

Titanium Dioxide UV Sensor

Titanium dioxide (TiO_2) UV sensors are another promising photodiode sensor because of its large band gap of 3.26 eV.^{15,16} When TiO_2 nanorod arrays are exposed to UV light, the irradiation provides enough energy to excite the electrons from the valence band to the conducting band thus leaving a hole in the valence band that leads to a low resistance state.¹⁵ After the UV exposure the sensor returns to its initial state. A fast response wearable p-

CuZnS/n-TiO₂ nanotube array UV photodetector was developed. Titanium microwire was used as an inner electrode surrounded by a fiber shaped p-CuZnS/n-TiO₂ nanotube array and wrapped with a carbon nanotube fiber as the outer electrode.¹⁶ This fiber-shaped design allows for more flexibility as well as faster response speeds in the UVA and UVB regions compared to the p-CuZnS/n-TiO₂ nanotube array planar design.¹⁶ While TiO₂ UV sensors have great potential, the largest challenges associated with these sensors are their high production cost and small sensing area.

Bismuth Oxychloride Photocatalyst

A photocatalyst is a type of material that upon exposure to light absorbs its energy to create an excited electron/hole pair that raises the material's energy enough to induce a chemical reaction. Notable photocatalysts include metal oxides semiconductors¹⁷ such as TiO₂ and ZnO as well as layered materials¹⁸ such as graphene, perovskites, and bismuth oxychloride (BiOCl). While both ZnO and TiO₂ have been studied for UV sensor applications, BiOCl has not been examined for this application. Interestingly, BiOCl has a wide band gap of 3.46 eV¹⁹ and an indirect trap level of 2.45 eV.²⁰ BiOCl only responds to UV light resulting in a low light utilization efficiency in conventional photocatalyst applications²¹⁻²³ but could be ideally suited for UV sensor application. Research efforts have been focused on doping BiOCl with iron, cobalt, zinc, or sulfur in order to broaden BiOCl's light absorption range from UV to visible light.¹⁸ BiOCl's inherent sensitivity to UV light should make for better a UV sensor rather than a photocatalyst however, no such research has been conducted with regard to BiOCl as a UV sensing material.

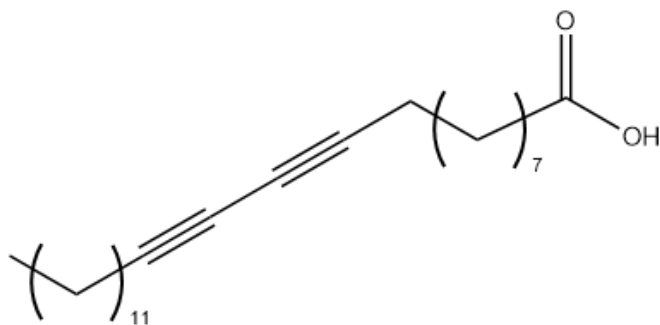
Colorimetric UV Sensors

Colorimetric sensors are another type of chemical sensor that produces a visible color change on the sensor upon exposure to UV radiation.⁶⁻⁹ Polydiacetylene UV sensors change color due to the transition between two order states.²⁴ On the other hand, phenylsulfonium UV sensors use a UV sensitive dye that undergoes a chemical reaction when exposed to UV radiation.⁹ Colorimetric UV sensors allow for the monitoring of UV dosage without the need for external monitoring devices required for photodiode sensors. A visual color change is produced and can be analyzed to determine a correlation between UV dosage and color change. Colorimetric UV sensors have a low production cost and can be used in a wide variety of applications. The Beer-Lambert Law could also be used for solution state sensors to determine the relationship between absorbance of light and concentration. Polydiacetylene and phenylsulfonium UV sensors will be discussed in detail under their relative subheadings in this chapter.

Polydiacetylene UV Sensor

Colorimetric UV sensors using polydiacetylenes (PDAs) function based on the color changing of the PDA chemical. PDAs have been studied widely due to their ability to change color from blue to red with prolonged exposure to UV radiation.⁶ This could help produce a better contrast for colorimetric UV sensors. One proposed mechanism for the color transition of PDA is the change in molecular orientation to a more ordered state of the alkyl chains. This orientation is constricted by hydrogen bonding and imposes strain on the polymer backbone which leads to a drastic decrease in the π -electron-conjugation length.²⁵ The color change in PDA also depends on the functional groups present in it and hence its sensitivity could be tuned by modifying the functional groups. Figure 1.4 shows the chemical structure of 10,12-pentacosadiynoic acid (PCDA) used as a diacetylene monomer in the PDA colorimetric

sensors. For example, Ngampeungpis et al. tested mono- and diamide head groups with variable lengths of methylene spacers in comparison with their diacetylene fatty acid analogues and found that varying the chain length allowed for UV sensitivity tuning.⁶



10,12-pentacosadiynoic acid (PCDA)

Figure 1.4. Chemical structure of PCDA used in PDA colorimetric UV sensors.

Pankaew et al. added polyvinylpyrrolidone, poly(N-vinyl formamide) and poly(N,N-dimethyl acrylamide) to PDA's in ethanol to tune the sensors sensitivity to UV radiation.⁷ The addition of these polymers to the PDA based sensors caused the blue to red color shift to occur at longer exposure times and in some cases changed the shade of red ranging from a light tan to a deep purple.⁷ Figure 1.5 shows a study from *Colloids and Surfaces A: Physicochemical and Engineering Aspects* where various PDA UV sensors change color from blue to red based on the polymer added.⁷ The different polymers effected the irradiation needed to induce the color change. For example, the pure PCDA's first red square was seen at 8400 seconds while PCDA/PDMA12's first red square was seen at 6000 seconds. While this distinct color change greatly improves this colorimetric UV sensor, it was also found that these PDA sensors also change color based on heat, mechanical stress, and pH.⁶ Hence, due to PDA's unstable color,

UV monitoring in hot environments as well as in direct sunlight will cause challenges and may even be impossible to get an accurate reading.

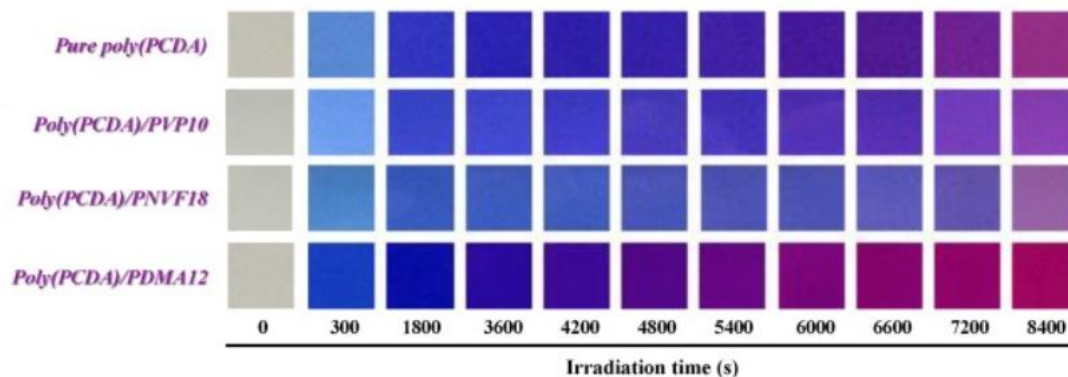


Figure 1.5. PDA UV sensor color change of different polymer assemblies after various irradiation times. This Figure was reused from the Pankaew et al. article regarding the tunability of PDA UV sensors with the addition of various polymers.

Phenylsulfonium UV Sensor

Another type of colorimetric UV sensor uses a phenylsulfonium indicator. Phenylsulfonium sensors utilize a photosensitive phenylsulfonium molecule that interact with a dye resulting in a color change. Figure 1.6.a. shows the chemical structure of (4-phenoxyphenyl)diphenylsulfonium triflate (PPDPS-TF), one of the photosensitive indicators used in a phenylsulfonium UV sensors with another being triphenylsulfonium. Figure 1.6.b. depicts the color change associated with the PPDPS-TF and crystal violet lactone UVA sensor with UVB filter. Figure 1.6.c. depicts the color change associated with the PPDPS-TF and Congo red UVB sensor with UVA filter. An epidermal patch was designed utilizing PPDPS-TF with crystal violet lactone and Congo red to maximize UVA and UVB sensing.⁸

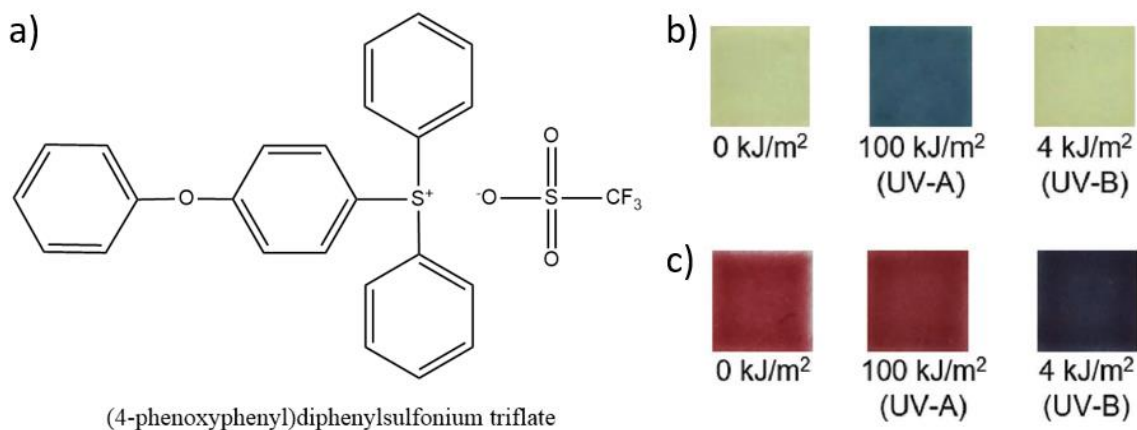


Figure 1.6. a) Chemical structure of (4-phenoxyphenyl)diphenylsulfonium triflate (PPDPS-TF) used in a phenylsulfonium colorimetric UV sensors, b) color change of PPDPS-TF UVA sensor using crystal violet lactone and a UVB filter, and c) color change of PPDPS-TF UVB sensor using Congo red and a UVA filter. Figures 1.6.b-c. were reused from Araki et al article regarding an epidermal UV colorimetric dosimeter.⁸

Upon UV exposure, the PPDPS-TF decomposes releasing a positively charged benzene compound that protonates the dye. The dye protonation acidifies the solution and induces the color change seen in these sensors.⁸ A similar paper on colorimetric UV sensors was published by Kurz et. al. where triphenylsulfonium emits a hydride upon UV exposure, which interacts with the leucobase dye to induce a color change.⁹ Their proposed sensor could be used in a wrist band, textile patch or epidermal patch however, the largest drawback for these phenylsulfonium UV sensors as well as the PDA UV sensors are the chemical hazards associated with dyes and indicators. Both PDA, triphenylsulfonium, and their products are toxic and category 2 skin and eye irritants listed on their respective safety data sheets from Sigma Aldrich.

Chlorine Radical Fluorescent Quenching

The previous two examples of colorimetric sensors demonstrate the changes in color due to structural changes associated with acidity, heat, and UV radiation as well as chemical

reactions. Similar to these UV sensors, there can be a quantifiable color change due to a molecule forming an adduct as a result of an exposure to high energy radiation. This could lead to a significant reduction in a chemicals UV adsorption properties. This kind of low dose high energy sensors for x-ray or γ radiation research could help lay the groundwork for UV sensors. Recently, Han et al. utilized halogenated solvents, such as chloroform (CHCl_3) or dichloromethane (CH_2Cl_2), in combination with 4,4'-di(1H-phenanthro[9,10-d]imidazol-2-yl)biphenyl (DPI-BP), a fluorescent indicator to detect γ radiation.²⁶ Upon exposure to γ radiation, the solvents decompose to produce chlorine radicals that in turn reacted with hydrogen radicals to form HCl. Then, DPI-BP interacts with the HCl to form a DPI-BP/HCl adduct causing a fluorescence quenching via π - π stacking.²⁶ This fluorescence quenching was then measured to detect low dose radiation. Figure 1.7 shows the mechanism for DPI-BP fluorescent quenching.

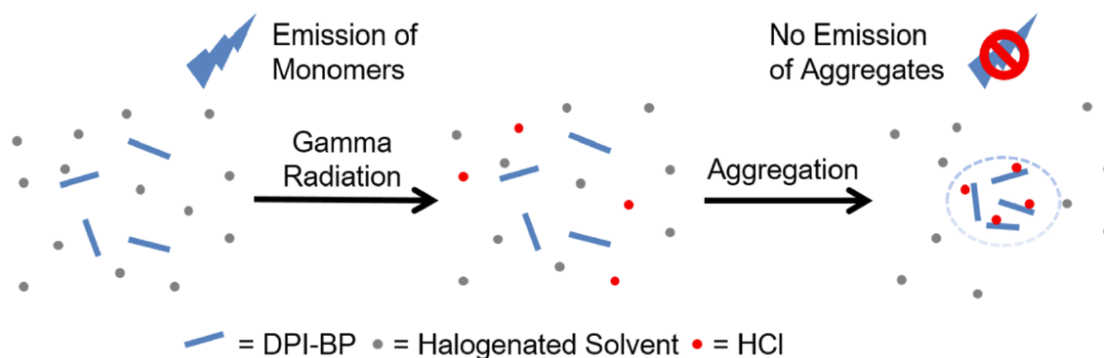


Figure 1.7. Mechanism for DPI-BP quenching upon exposure to γ radiation. This Figure was reused from the Han et al. article regarding low dose γ radiation by fluorescent quenching.²⁶

Our Research

Our initial idea for the UV sensor discussed in this thesis was a fluorescent quenching method similar to the Han et al article discussed in the previous subsection.²⁶ The idea that free chlorine

radicals help form an adduct to quench the fluorescence led us in to search for molecules that produce chlorine radicals readily. Metal chlorides have weak metal-Cl bonds that enable the rapid production of Cl radicals upon exposure to radiation.²⁷ A stronger focus was set on the chemical hazards associated with the compounds that helped us identify bismuth (III) chloride for this application. BiCl₃ and many Bi based molecules are non-hazardous in nature and are being used in many medical applications^{28,29} including those in tissue engineering, therapeutics, and diagnostic imaging. Therefore, BiCl₃ was chosen to replace the halogenated solvent. For the fluorescent dye, we chose 6-carboxyfluorescein (6-CF) which is a non-hazardous organic dye³⁰, used in the sequencing of nucleic acids, labeling of nucleotides, and tracking the division of cells.³¹ In Chapter 2, an analysis of a 6-CF/BiCl₃ sensor will be conducted in solution as well as solid-state on a Grade 597 Whatman filter paper substrate. Chapter 3 will discuss the results of a 5-carboxyfluorescein (5-CF)/BiCl₃ sensor in solution state and solid-state for a comparison to the 6-CF/BiCl₃ sensor. In Chapter 4, a mechanism is proposed based on the previous sensor results, SEM images, EDS analysis, and powder XRD. In Chapter 5, two different sensors using prussian blue (PB) and rhodamine-b (RhB) were prepared and tested with BiCl₃. Finally, Chapter 6 analyze the practical applications of the 6-CF/BiCl₃ sensor which includes a sunscreen test as well as optical density measurements.

Materials and Instrumentation

The following chemicals were purchased from Sigma-Aldrich, 6-carboxyfluorescein (6-CF), 5-carboxyfluorescein (5-CF), prussian blue (PB), and rhodamine-b (RhB), BiCl₃, and BiOCl. Anhydrous ethanol was used to make the dye and BiCl₃ solutions used to make our sensors. Grade 597 Whatman filter paper was used as the substrate to make our solid-state sensors. UV radiation at 254 nm, 302 nm, and 365 nm wavelengths were produced using a UVLMS-38 EL

Series 3UV Lamp. The intensity of the UV lamp was measured using a Thorlabs 9.5 mm aperture UV extended Si Photodiode. All UV-Vis absorption spectra were collected using a Varian Cary 50 Bio UV Vis Spectrophotometer with a quartz cuvette. SEM images were taken using a Hitachi S-5200 Nano SEM and EDS spectra were taken using an Oxford Aztec X-MAX 80 EDS. Powder XRD data was obtained using a Panalytical X'Pert PRO. Photos of the solution state and solid-state sensors were taken using an iPhone 11. ImageJ was used to determine the optical density measurements of our solid-state UV sensors.³²

Chapter 2:

6-Carboxyfluorescein – BiCl₃ based UV Sensor

This section will discuss the measurements and results of our UV sensors prepared using 6-Carboxyfluorescein (6-CF) and bismuth (III) chloride (BiCl₃). 6-CF was chosen as our UV sensor dye because of its chemical safety³⁰ as well as its aromatic rings that could result in π - π interactions. 6-CF's fluorescent properties have also been used to determine the pH in biological applications.³³ The chemical structure of 6-CF is shown in Figure 2.1. The numbering indicates the location of the carboxylic acid group on the fluorescein molecule. BiCl₃ was also chosen for its ability to produce chlorine radicals²⁷ as well as Bi based molecules' non-hazardous properties and current medical applications^{28,29} as stated in the introduction.

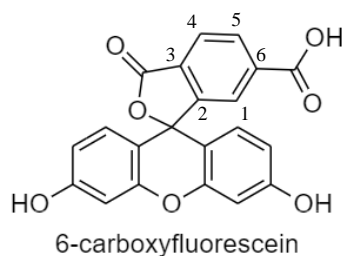


Figure 2.1. Chemical structure of 6-carboxyfluorescein (6-CF).

Both 6-CF and BiCl₃ were separately dissolved in anhydrous ethanol to make their respective solutions. While 6-CF formed a homogeneous solution, BiCl₃ formed a turbid solution that was sonicated or shaken vigorously before mixing with the 6-CF solution. A wide range of 6-CF and BiCl₃ concentrations and volume percentages (Table 2.1) were prepared and tested under a UV lamp at a UV wavelength of 302 nm representing UVB as well as under direct

sunlight. The intensity of the UVLMS-38 EL Series 3UV Lamp at 302 nm was determined to be 1.16 mW/cm². The UV intensity of sunlight is approximately 4.61 mW/cm² with 4.54 mW/cm² associated with UVA and 0.07 mW/cm² associated with UVB. The intensity of UV from sunlight was calculated using the ASTM G-173-03 international standard AM1.5 Global Standard Solar Spectra.³⁴ For direct sunlight exposure, clear sunlit days were chosen and almost all of the data was taken during the months of June, July, and August. The UV sensitivity of these mixtures in the solution state was monitored by measuring the UV absorption spectrum of these solutions using a Varian Cary 50 Bio UV Vis Spectrophotometer before and after UV irradiation. The reference UV-Vis absorption spectra for the blank quartz cuvette, ethanol, 5 mM 6-CF, 1 mM BiCl₃, 5 mM BiCl₃, and 10 mM BiCl₃ are located in Appendix A. A similar comparison of before and after UV irradiation was used for a solid-state UV sensor. This solid-state UV sensor was also fabricated using these the same unexposed solutions with a Whatman filter paper as the substrate. Filter paper squares of approximately 1.15 cm by 1.15 cm sizes were soaked in the UV sensor solution and dried at room temperature then exposed to 365 nm, 302 nm, and 254 nm UV radiation as well as direct sunlight. Although the parent compound fluorescein was not used in our sensors, the frontier molecular orbitals for fluorescein³⁵ are located in appendix B.

6-CF Solution Sensor

Before the addition of BiCl₃, the UV-Vis absorption spectrum of the 6-CF dye was collected. Figure 2.2 shows the UV absorption spectrum of 1 mM 6-CF in ethanol. The 1 mM 6-CF solution has one large absorption peak at 450 nm and a small shoulder at 490 nm. This unexposed UV absorption spectrum of 6-CF allows for an easy comparison to mixtures of 6-CF and BiCl₃ solutions as well as after their exposure to 302 nm UV light and sunlight.

Similarly, upon exposure to 302 nm UV light the 1 mM 6-CF solution had a bright green fluorescence as expected (Figure 2.2.b.). At neutral pH, 6-CF fluoresces at 518 nm.³⁶ The absorption and emission spectra of 6-CF is located in Appendix B. The UV absorption spectrum of 100 mM BiCl₃ is given in Figure 2.2.c. shows no characteristic peaks in the UV range from 400 – 800 nm although its absorption values goes beyond the instrument range in the 250-350 nm UV range with significant noise. The BiCl₃ solutions shows no fluorescence under the 302 nm UV light shown in Figure 2.2.d.

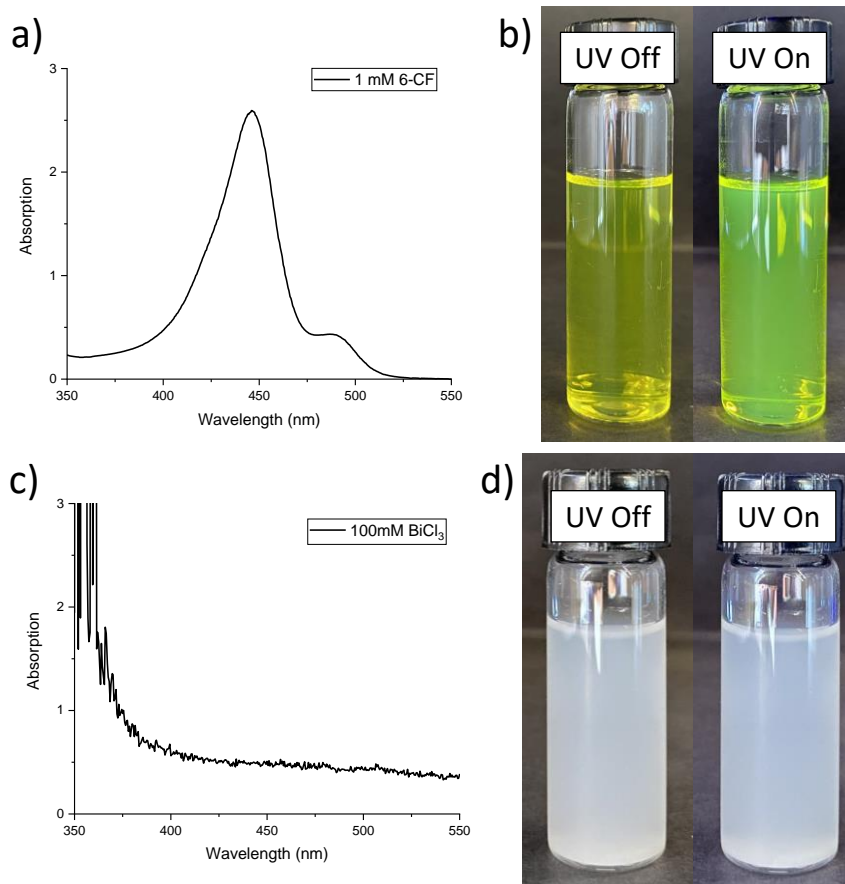


Figure 2.2. a) UV absorption spectrum of 1mM 6-CF prior to UV exposure, b) solution picture of 1 mM 6-CF under 302 nm UV light (right) and under visible light (left), c) UV absorption spectrum of 100 mM BiCl₃ prior to UV exposure, d) solution picture of 100 mM BiCl₃ under 302 nm UV light (right) and under visible light (left).

The numerous concentrations of the 6-CF/BiCl₃ solutions and their maximum exposure times to UV radiation are shown in Table 2.1. These compositions were made by mixing the individual solutions of 6-CF in ethanol and BiCl₃ in ethanol at the specified concentrations. Only the 50%, 34%, and 17% 6-CF solutions were measured for the 5 mM 6-CF and 5 mM as well as the 5 mM 6-CF and 10 mM BiCl₃ solutions because the UV absorption spectra of these solutions showed the largest change after UV exposure.

Table 2.1. Maximum exposure time for various 6-CF/BiCl₃ solution sensors

	302 nm UV Light	Sunlight			
Volumetric Percentage of 6-CF	1 mM 6-CF 1 mM BiCl ₃ (1:1)	1 mM 6-CF 1 mM BiCl ₃ (1:1)	1 mM 6-CF 5 mM BiCl ₃ (1:5)	5 mM 6-CF 5 mM BiCl ₃ (5:5)	5 mM 6-CF 10 mM BiCl ₃ (5:10)
83%	5 hours	5 hours	5 hours	-	-
66%	5 hours	5 hours	5 hours	-	-
50%	5 hours	5 hours	5 hours	2 hours	2 hours
34%	5 hours	5 hours	5 hours	2 hours	2 hours
17%	5 hours	5 hours	5 hours	2 hours	2 hours

For example, 1 mM BiCl₃ was mixed with 1 mM 6-CF in varying ratios. Figure 2.3 shows the UV absorption of 83%, 50% and 17% 6-CF by volume when exposed to a 302 nm UV lamp for 1 to 5 hours. The vials containing the solution state sensors were placed horizontally in a glass baking dish under the UV lamp. From the UV absorption spectra, the first noticeable trend is the decreased peak intensity in the 450 nm peak as the volume percentage of 6-CF decreases. This is anticipated as 6-CF has a characteristic absorption at this wavelength while BiCl₃ does not. 83% 1:1 6-CF (Figure 2.3.a.) and 50% 1:1 6-CF (Figure 2.3.b.) both have a slight increase in the 450 nm 6-CF peak upon exposure to UV light while 17% 1:1 6-CF shows a slight decrease in the 450 nm 6-CF peak. The increase in intensity for 83% and 50% 1:1 6-CF solutions could be attributed to the settling of BiCl₃ in solution allowing more 6-CF

molecules to absorb the light during the UV absorption measurement. Nevertheless, in the case of 17% 1:1 6-CF there is a linear reduction in the peak intensity for the peak at 450 nm. Finally in the 17% 1:1 6-CF UV absorption, a peak at 295 nm is formed from the BiCl_3 and increases in intensity as exposure time increases although not in significant quantity.

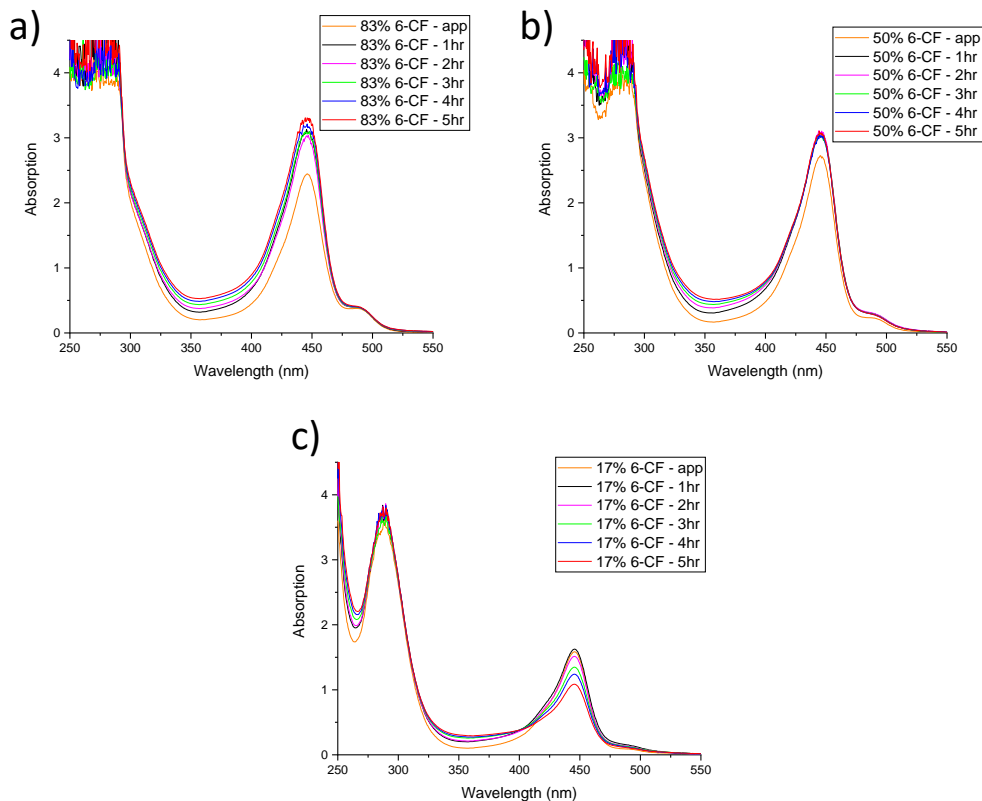


Figure 2.3. UV absorption of 1 mM 6-CF and 1 mM BiCl_3 in ethanol when exposed to 302 nm UV light for 1, 2, 3, 4, and 5 hours at a) 83% volume 6-CF, b) 50% volume 6-CF, and c) 17% volume 6-CF.

We next exposed fresh solutions made from 1 mM 6-CF and 1 mM BiCl_3 to sunlight and evaluated their UV-Vis spectra. Figure 2.4.a-c. compares UV absorption spectrums obtained from 83%, 50%, and 17% 1:1 6-CF solutions respectively after direct sunlight exposure. A decrease in the 450 nm 6-CF peak is seen as the percentage of 6-CF decrease, similar to the trends in the 302 nm exposure. The 295 nm BiCl_3 peak is present again in the 17% 1:1 6-CF

(Figure 2.4.c.) and remains unchanged with increasing exposure to sunlight. The most noticeable change was the large decreases in the 450 nm 6-CF peak for all samples unlike the exposure to 302 nm UV light, where only the 17% 1:1 6-CF showed a linear decrease in intensity with increasing exposure. This change could be due to the generation of Cl radicals from BiCl_3 that may have helped to stack the 6-CF molecules. This reduction in peak intensity behavior led us to believe that our sensing mechanism is similar to the fluorescent quenching mechanism discovered by Han et al.,²⁶ with the chlorine radical generation occurring from BiCl_3 and the 6-CF dye undergoing π - π stacking. Nevertheless, we also noticed some black precipitate after exposure to sunlight in these mixtures that could have played a role in the peak intensity reduction as well.

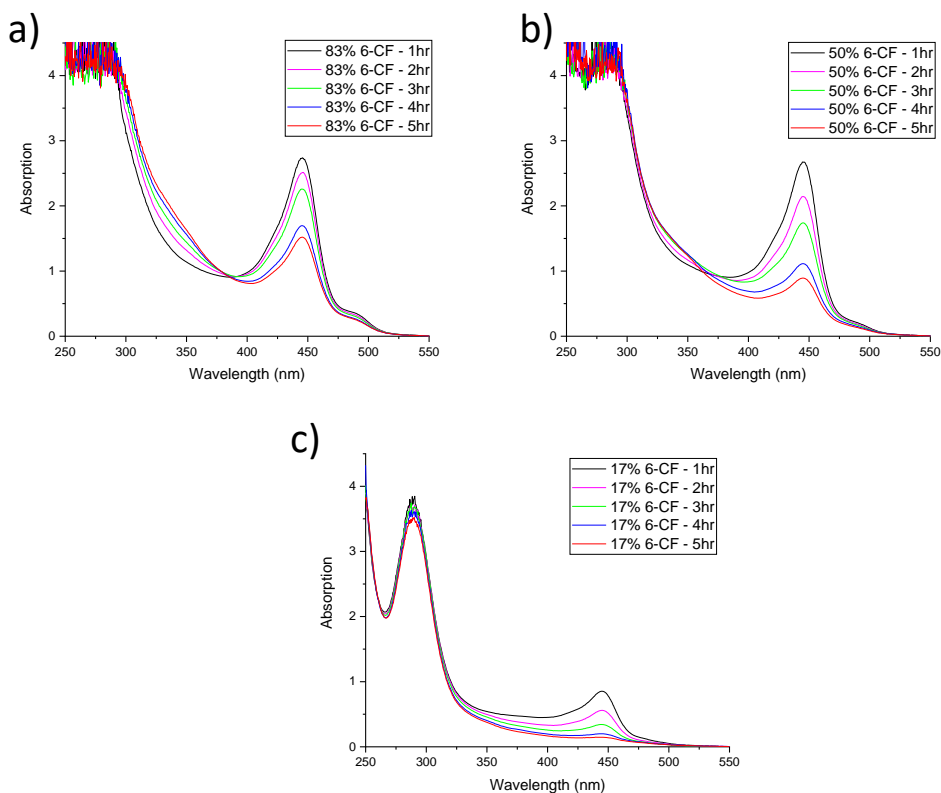


Figure 2.4. UV absorption of 1 mM 6-CF and 1 mM BiCl_3 in ethanol when exposed to sunlight for 1, 2, 3, 4, and 5 hours at a) 83% volume 6-CF, b) 50% volume 6-CF, and c) 17% volume 6-CF.

Next, the concentration of BiCl_3 was increased from 1 mM to 5 mM while leaving the 6-CF concentration unchanged and similar compositions were prepared. Figure 2.5 shows the UV absorption spectrum for 1 mM 6-CF and 5 mM BiCl_3 at 83%, 50%, and 17% 1:5 6-CF when exposed to sunlight for 5 hours on one hour intervals. Surprisingly, the 450 nm 6-CF peak does not decrease with the decrease in volume percentage of 6-CF. However, the increase in BiCl_3 concentration caused about a 25 nm widening of the 450 nm 6-CF peak in the 83% 1:5 6-CF and 50% 1:5 6-CF as prepared samples and a 5 nm widening in the 17% 1:5 6-CF. An increase in exposure time led to a decrease in the 450 nm 6-CF peak as well as width shrinking.

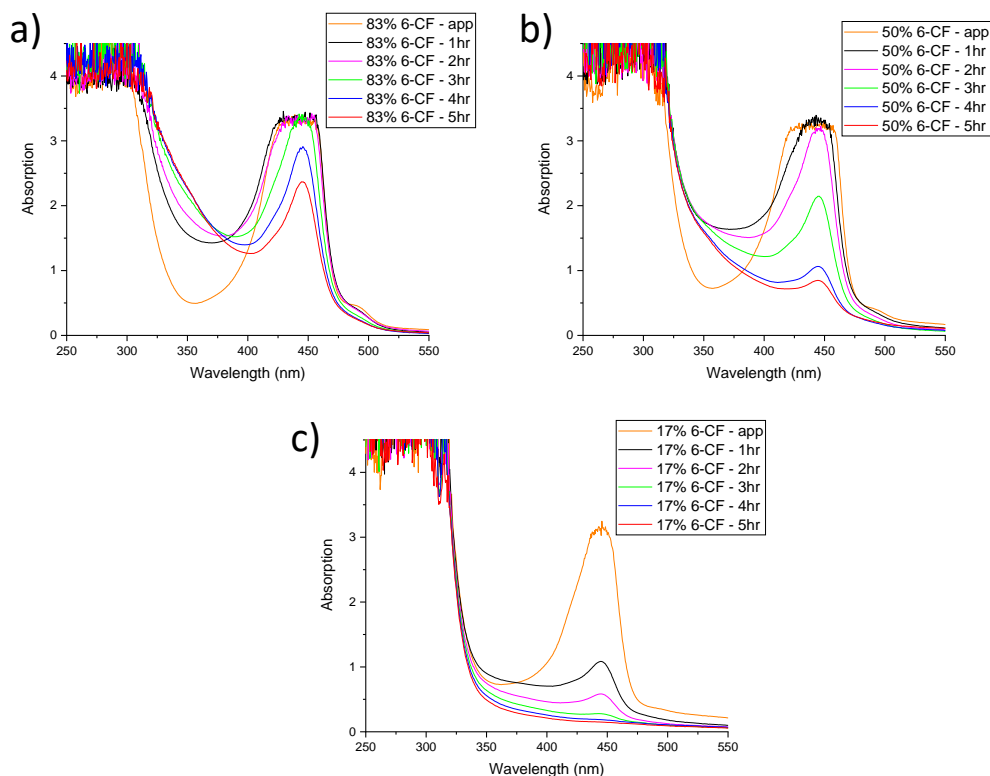


Figure 2.5. UV absorption of 1 mM 6-CF and 5 mM BiCl_3 in ethanol when exposed to sunlight for 1, 2, 3, 4, and 5 hours at a) 83% volume 6-CF, b) 50% volume 6-CF, and c) 17% volume 6-CF.

Following above observations, we increased the concentration of 6-CF to 5 mM as well and repeated these measurements. Figure 2.6 compares 50% 5:5 6-CF and 17% 5:5 6-CF solutions prepared from 5 mM 6-CF and 5 mM BiCl₃ solutions after exposure to 1 and 2 hours of sunlight. The 450 nm 6-CF peak widened by 100 nm for 50% 5:5 6-CF and by 75 nm for 17% 5:5 6-CF. Again, no change in the 450 nm peak intensity was seen as 6-CF volume percentage was decreased however a slight increase of the 450 nm peak was noticed in both samples when the exposure time was increased. The 17% 5:5 6-CF sample saw its width shrink almost by half after 2 hour sunlight exposure.

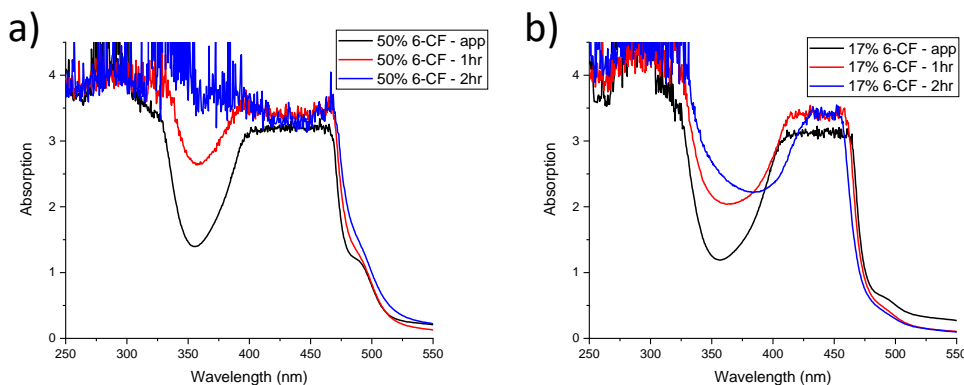


Figure 2.6. UV absorption of 5 mM 6-CF and 5 mM BiCl₃ in ethanol when exposed to sunlight for 1 and 2 hours at a) 50% volume 6-CF and b) 17% volume 6-CF.

Comparing with the previous spectra, the 83% 1:5 6-CF and 50% 1:5 6-CF solutions, the 450 nm peak widened by about 25 nm which may be due to the increase in BiCl₃ concentration. The 450 nm peak was also widened by the increase in 6-CF concentration. After exposure to UV, a flat peak was formed from 250 nm to 490 nm for the 50% 5:5 6-CF solution while in the 83% 1:5 6-CF and 50% 1:5 6-CF solutions the 450 nm peak was reduced. This drastic change in the 6-CF/BiCl₃ UV spectra could be due to the decreased permeability of light during

the UV-Vis absorption in the 1:5 solutions. The smaller concentration of 6-CF was being blocked by the higher concentration of BiCl_3 .

Another 6-CF and BiCl_3 solution sensor studied was with a BiCl_3 concentration of 10 mM. Figure 2.7 compares the 50% 5:10 6-CF and 17% 5:10 6-CF solutions prepared with 5 mM 6-CF and 10 mM BiCl_3 and exposed to 1 and 2 hours of sunlight. Similar to the 1 mM 6-CF 5 mM BiCl_3 solution, the width of the 450 nm peak was broadened by 100 nm for 50% 5:10 6-CF and 75 nm for 17% 5:10 6-CF. Again, the characteristic 6-CF peak was slightly increased as exposure time increased for both samples. The 17% 5:10 6-CF sample saw its 450 nm peak width shrink by roughly half after 2 hours of sunlight exposure. A wide 490 nm peak broadening ranging from 250 nm to 490 is seen in the 50% 5:10 6-CF sample after 2 hours of sunlight exposure. The UV absorption spectra for the 17% 5:10 6-CF solution was easier to discern the changes in 6-CF peak intensity while the 50% 5:10 6-CF solution was not.

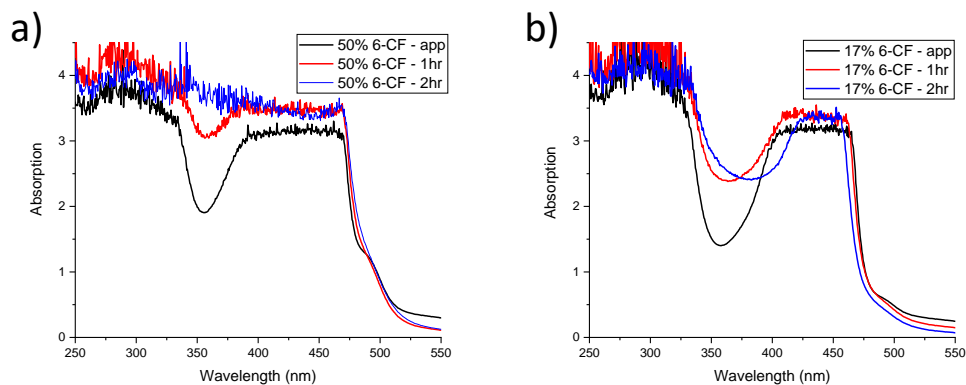


Figure 2.7. UV absorption of 5 mM 6-CF and 10 mM BiCl_3 in ethanol when exposed to sunlight for 1 and 2 hours at a) 50% volume 6-CF and b) 17% volume 6-CF.

One final solution state UV sensor was prepared with 1 mM 6-CF and 100 mM BiCl₃. From the previous UV absorption spectra, it appeared that a lower concentration of 6-CF and a higher concentration of BiCl₃ produced the best solution state sensor. Figure 2.8 compares the a) unexposed solutions to b) 3 hours of continuous sunlight exposure followed by c) 72 hours of settling with no additional sunlight exposure. The solutions are listed from left to right, 100% 6-CF, 83% 1:100 6-CF, 50% 1:100 6-CF, 17% 1:100 6-CF, and 100% BiCl₃. Figure 2.8.b. shows that the 100% 6-CF solution remained unchanged after 3 continuous hours in sunlight while the remaining BiCl₃ solutions turned completely black. The black particles were observed in the other concentrations discussed above as well. This points to the conclusion that the BiCl₃ could be the major contributor in our UV sensor although the role of 6-CF is not clear. Figure 2.8.c. shows a black precipitate formed in the BiCl₃ solutions after 72 hours of settling. The stability of 6-CF should be noted with the 100% 6-CF solution remaining its original color. The 83%, 50%, and 17% 1:100 6-CF solutions did not return to the original 6-CF color due to the suspension of fine black particles in solution. The 100% BiCl₃ solution also had a small amount of white BiCl₃ precipitate out of solution along with the black precipitate. The Beer-Lambert Law was not applied further than the collection of our UV absorption spectra of our solution state sensors.

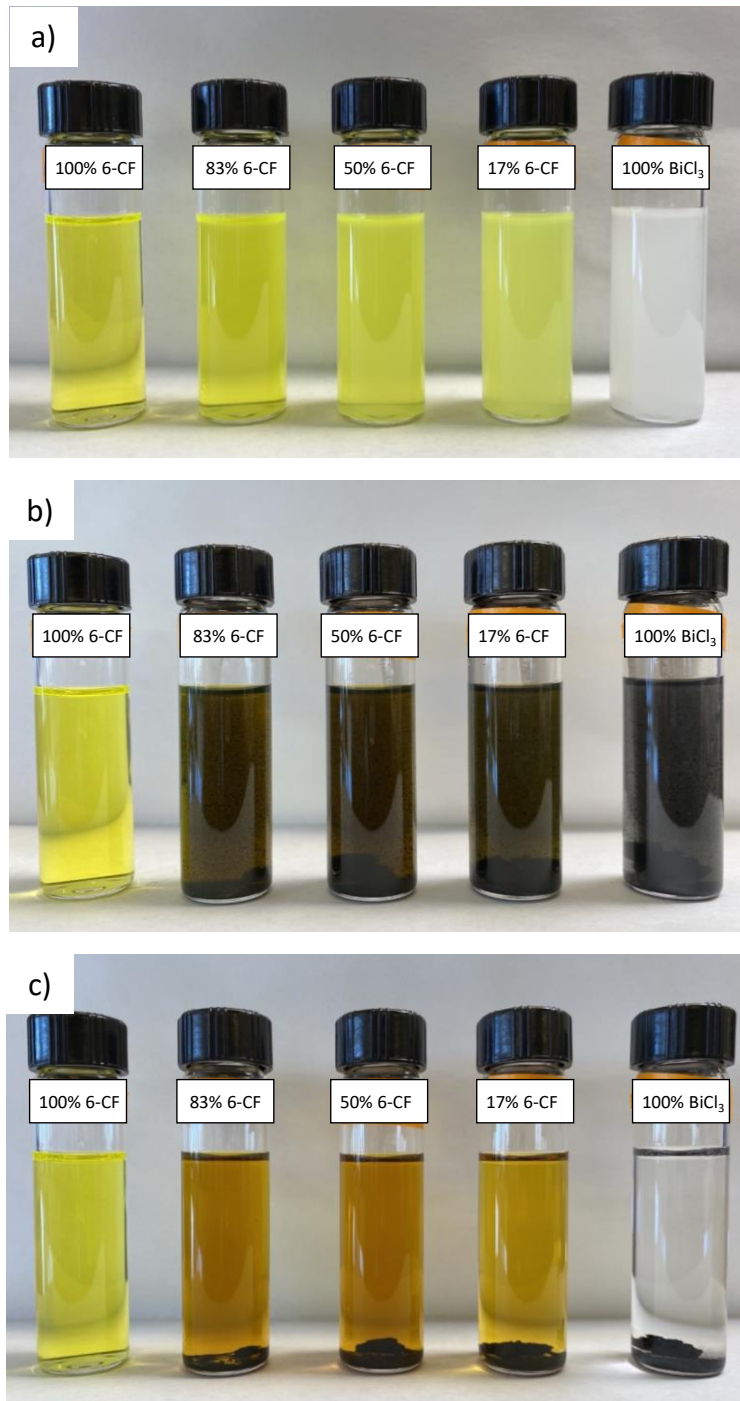


Figure 2.8. Various volume percentages of 1 mM 6-CF and 100 mM BiCl₃ solution state UV Sensors a) as prepared, b) continuous 3 hour direct sunlight exposure, and c) 72 hour settling.

Solid-State 6-CF UV Sensor

We wanted to extend the UV sensor measurements from solution state to solid-state due to ease of fabrication for solid-state devices along with challenges associated in dealing with solutions such as solvent evaporation, leakage, and spillage. Besides, if the fine black suspension formed in the solution state sensors could be regulated in a solid state device, it may help monitor the UV exposure systematically. From the solution state measurements and analysis of the UV exposure measurement data, it was determined that the ideal combination between 6-CF and BiCl_3 would be a lower concentration of 6-CF and a higher concentration of BiCl_3 . Whatman filter paper was used as the substrate. A 50% mixture of 1 mM 6-CF and 100 mM BiCl_3 was used to prepare the solid-state UV sensor. Filter paper squares with a dimension of 1.15 cm, used as the substrate, were soaked in the 50% 1:100 6-CF solution for 10 minutes followed by drying at room temperature away from direct sunlight exposure. The BiCl_3 loading on the filter paper square was approximately 0.09 mg. The prepared sensors were exposed under the UV lamp to 365 nm, 302 nm, and 254 nm as well as in direct sunlight for different durations of time. Figure 2.9 compares the sensor's response to a) 365 nm UV, b) 302 nm UV, c) 254 nm UV, and d) direct sunlight at specified time intervals. For every time interval, the left side of the sensor was blocked using a piece of metal while the right side of the sensor was exposed to UV radiation. This allows for an easy comparison between different exposure times as well as different UV wavelengths. For every type of UV exposure, a color change from yellow to brown can be seen with the shade of brown darkening as the duration of UV exposure increases. The 365 nm UVA test showed considerably less color change compared to 302 nm UVB and 254 nm UVC. While the 302 nm UV, 254 nm UV, and direct sunlight showed similar color change over the 2 hour interval. Based on the solid-state sensor

results, the 50% 1 mM 6-CF and 100 mM BiCl₃ sensor can be tuned to either 365nm UV or 302 nm UV with a greater selectivity toward 302 nm UV. The solid-state UV sensors showed a clear advantage over the solution-state UV sensors as the color change is proportionate to the duration of the UV radiation exposure. The solid-state devices did not show any color change for prolonged periods and only showed color change when exposed to sunlight or UV radiation. In the next chapter, solution state and solid-state UV sensors were prepared and analyzed using 5-carboxyfluorescein and BiCl₃ to better determine the role 6-CF had in our previous UV sensors.

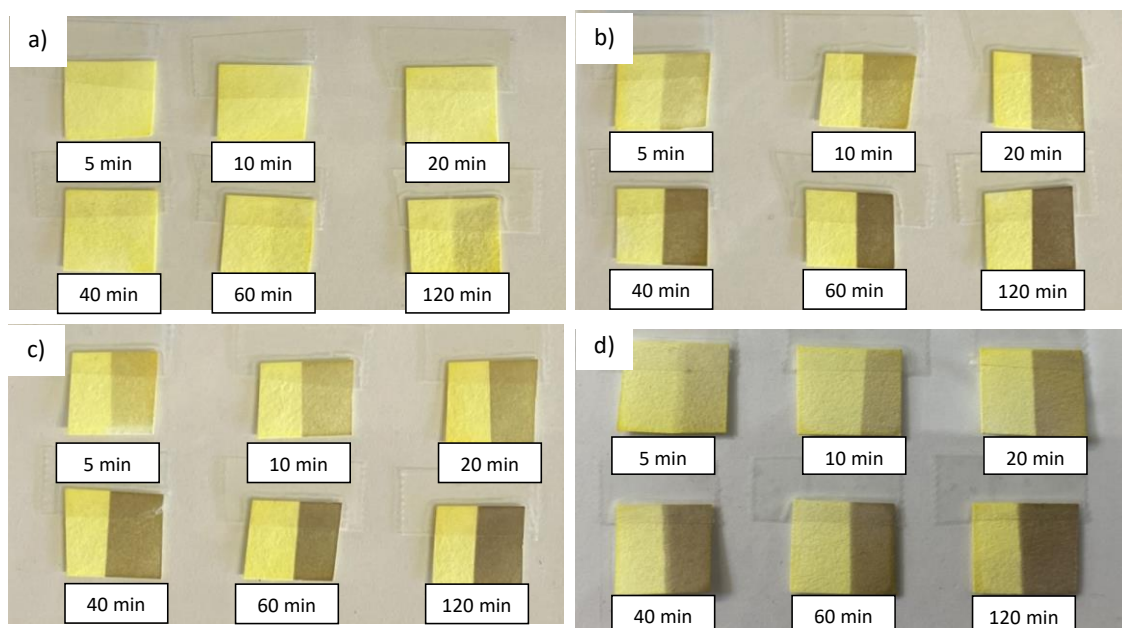


Figure 2.9. Soaked and dried filter paper squares in 50% 1 mM 6-CF and 100 mM BiCl₃ in ethanol exposed to a) 365 nm UV, b) 302 nm UV, c) 254 nm UV and d) sunlight for various durations.

Chapter 3:

5-Carboxyfluorescein – BiCl₃ based UV Sensor

The constitutional isomers in organic chemistry can have vastly different properties and as a result may interact differently in solutions and mixtures. Constitutional isomers are isomers that have identical chemical composition but have a different chemical structure. A common example is butane and isobutane. The same is true for Bis(thiophen-2-yl)-diketopyrrolopyrrole (DDP) dyes with each isomer having vastly different morphologies, as well as optical and electronic properties.³⁷ Hence, after evaluating the role of 6-CF in forming an adduct with H and Cl radicals from BiCl₃, we decided to carry out the UV sensor fabrication with one of its readily available constitutional isomer, 5-carboxyfluorescein (5-CF). The molecular structure of 5-CF is given in Figure 3.1. The carboxylic acid group is connected to the fifth position on the numbered benzene ring while the carboxylic acid group is connected to the sixth position for 6-CF. A comparison of 1 mM 5-CF and 1 mM 6-CF in ethanol shows that the 5-CF solution is a transparent yellow while the 6-CF solution is a saturated yellow. The most noticeable difference is the UV absorption spectra of these solutions. For the 1 mM 5-CF UV absorption spectrum, three absorption peaks at 430 nm, 460 nm, and 490 nm are present. For the 1 mM 6-CF UV absorption spectrum, a single peak at 450 nm is seen with twice the intensity of the 460 nm peak associated with 5-CF. The 490 nm peak is present in both spectra and appears at the same intensity for both solutions. These slight changes in the UV absorption could help us determine the function of 6-CF/5-CF in these BiCl₃ sensors.

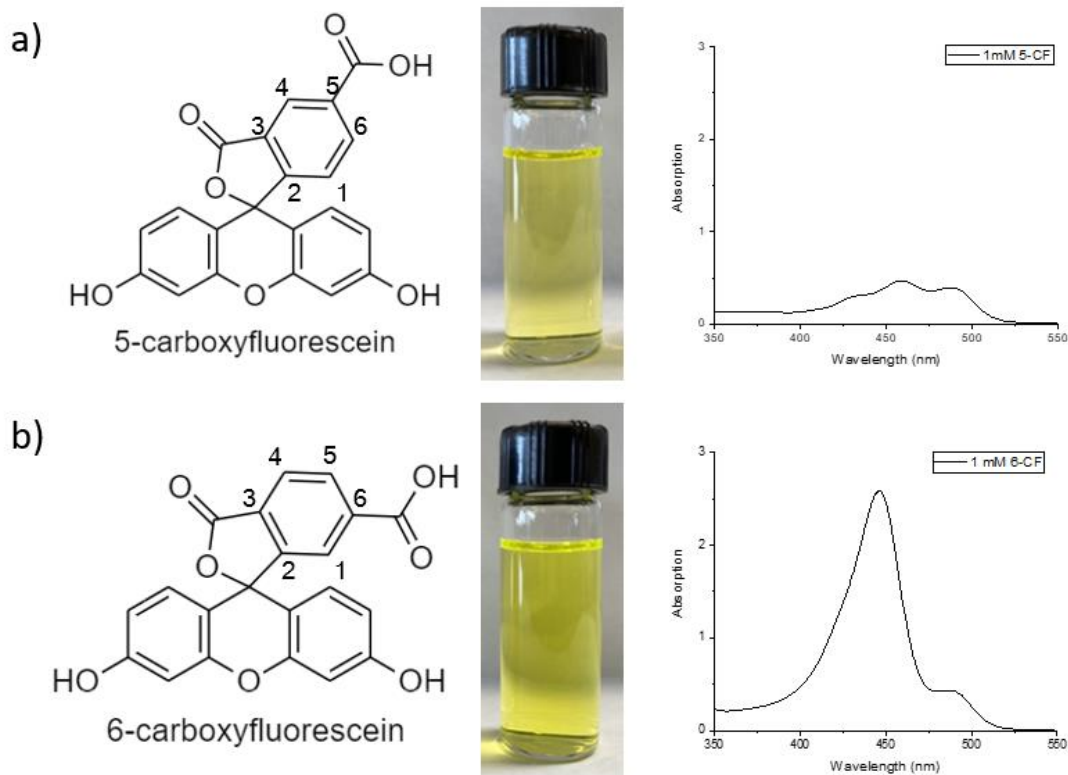


Figure 3.1. Comparison of the chemical structure, 1 mM ethanol solutions, and UV absorption spectra of a) 5-carboxyfluorescein (5-CF) and b) 6-carboxyfluorescein (6-CF).

We prepared a 1 mM 5-CF ethanol solution and mixed it with 10 mM BiCl_3 in ethanol. Similar to our experiments with 6-CF, the solution state and solid state sensors were analyzed. Hence, in this section will discuss the results of our 5-Carboxyfluorescein (5-CF) and bismuth (III) chloride (BiCl_3) UV sensors. Both 5-CF and BiCl_3 were dissolved in ethanol to make their respective solutions. 6-CF was swapped with 5-CF to determine the effect 6-CF had on the sensor by changing the location of the carboxylic acid group from a sixth site to fifth site as seen in Figure 3.1. Before assembling the sensor, the UV stability of 5-CF was analyzed under 302 nm UV light. Next, a 1 mM 5-CF and 10 mM BiCl_3 sensor was tested under a 302 nm UV lamp. We chose this concentration as we observed this to be best suited to analyze the UV sensing properties in the case of 6-CF. Similar to the 6-CF solution sensors, the UV absorption

spectrum for the UV solution sensor was obtained using a Varian Cary 50 Bio UV Vis Spectrophotometer. A solid-state UV sensor was also tested using Whatman filter paper as the substrate. Filter paper squares were soaked in a 50% 1 mM 5-CF and 100 mM BiCl₃ UV sensor solution and dried at room temperature then exposed to 302 nm UV light.

5-CF Solution Sensor

A 1 mM 5-CF in ethanol solution was used to test the UV stability of 5-CF under 302 nm UV light. Figure 3.2 shows the UV absorption spectrum of the 1 mM 5-CF solution before and after 302 nm UV exposure. After exposure to 302 nm UV light for 5 hours at 1 hour intervals, all three 5-CF peaks do not show any significant change in peak intensities and the slight change in intensity could be due to handling of the sample. It appears that both the 5-CF dye and 6-CF dye have similar stability properties and do not change upon exposure UV radiation. Overall, the 5-CF dye is stable under 302 nm UV light conditions similar to 6-CF allowing for its use as a dye in our UV sensor measurements.

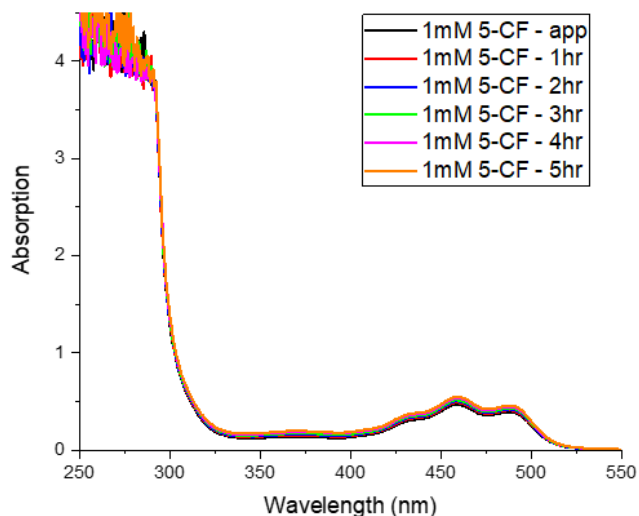


Figure 3.2. UV absorption spectrum of 1 mM 5-CF in ethanol when exposed to 302 nm UV light for 1, 2, 3, 4, and 5 hours.

After testing the UV stability of 5-CF, 1 mM 5-CF and 10 mM BiCl₃ were combined at three different volume percentages 83% 5-CF, 50% 5-CF, and 17% 5-CF. The solutions were exposed to 302 nm UV light with the UV spectra of each sensor shown in Figure 3.3. For all three sensors, the 430 nm and 460 nm 5-CF peaks combine into a peak around 450 nm with a much larger intensity compared to the 5-CF dye alone while the 490 nm peak became a shoulder with the same intensity as the 1 mM 5-CF solution. The peaks intensities seem to be amplified in the presence of BiCl₃ which would explain the large intensity increase although we do not know the exact reason for this increase. Figure 3.3.a. shows the UV absorption spectrum for the 83% 5-CF solution. The addition of 10 mM BiCl₃ caused a small 20 nm widening of the 450 nm 5-CF peak. After an hour of exposure, the 450 nm peak widened another 10 nm with a slight increase in the peak intensity. This absorption spectrum did not show any further widening of the peak or increase in peak intensity upon further exposure to the UV radiation for further 4 hours. Between 300 nm and 400 nm as well as the 490 nm shoulder saw an increase in UV absorption. Figure 3.3.b. shows the UV absorption spectrum for the 50% 5-CF solution. After 5 hours of 302 nm UV light exposure, the peak intensity at 450 nm remained the same with an increase in UV absorption in the 300-400 nm range as well as in in the 490 nm shoulder. Figure 3.3.c. shows the UV absorption spectrum for 17% 5-CF solution. The 450 nm 5-CF peak widening seen in the 83% and 50% 5-CF solutions was not present in the 17% 5-CF solution. After 5 hours of 302 nm UV light exposure, the peak intensity saw a steady decrease similar to 17% 1 mM 6-CF and 1 mM BiCl₃ exposed to 302 nm UV light. This reduction in UV absorption could be a result of the change in solution transmission of light at the higher volume percentage of BiCl₃ as higher concentrations of

BiCl_3 produced finely dispersed black nanoparticles. A detailed discussion on these nanoparticles is included in our discussion on the UV sensing mechanism in Chapter 4.

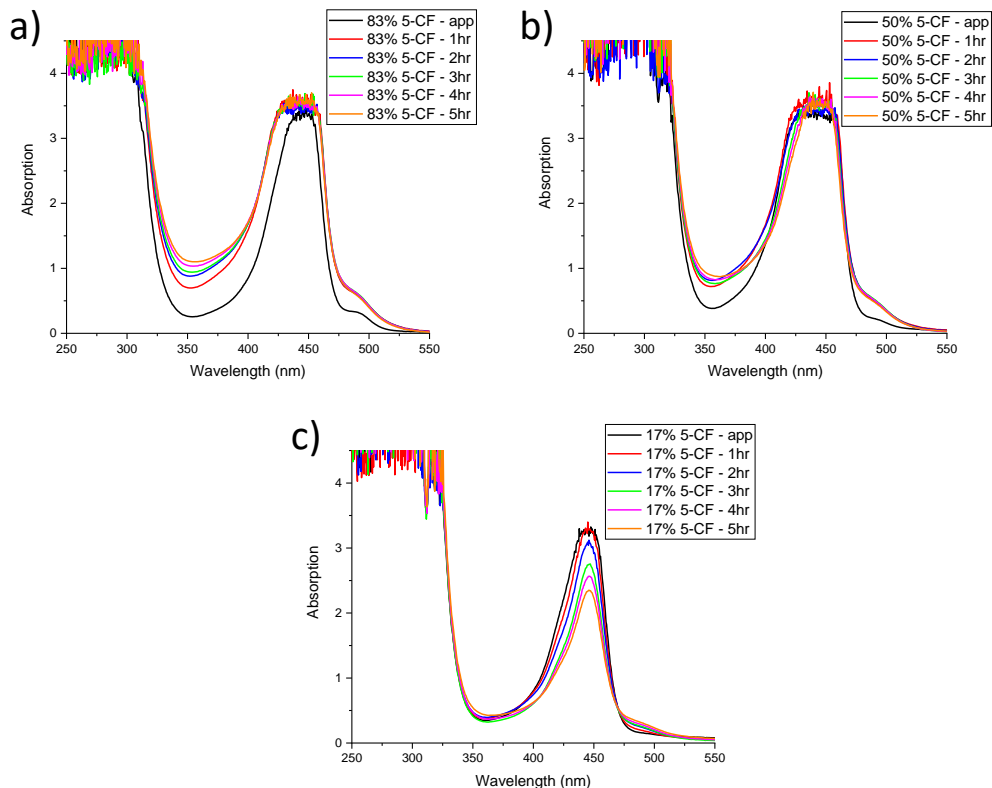


Figure 3.3. UV absorption of 1 mM 5-CF and 10 mM BiCl_3 in ethanol when exposed to 302 nm UV light for 1, 2, 3, 4, and 5 hours of 302 nm UV light and a) 83% volume 5-CF, b) 50% volume 5-CF, and c) 17% volume 5-CF.

The last 5-CF solution state sensor prepared was a 1 mM 5-CF and 100 mM BiCl_3 . Figure 3.4. compares the a) unexposed solutions to b) 3 hours of continuous 302 nm UV exposure followed by c) 72 hours of settling with no additional UV exposure. The solutions are listed from left to right, 100% 5-CF, 83% 1:100 5-CF, 50% 1:100 5-CF, 17% 1:100 5-CF, and 100% BiCl_3 . A complete blackening of all the BiCl_3 solutions after continuous exposure to 302 nm UV light can be seen in Figure 3.4.b. It should be noted that the 100% 5-CF solution did not show any color change under similar UV irradiation. Figure 3.4.c. shows a black precipitate forming

after 72 hours of settling. The 100% 5-CF still maintained its original color however, the 83%, 50%, and 17% 1:100 5-CF solutions were slightly darker due to possible suspension of the fine black particles in the solution. These results are extremely similar to the 1 mM 6-CF and 100 mM BiCl_3 solutions discussed in Chapter 2 leading to the conclusion that 5-CF and 6-CF dyes have similar solution properties under the conditions studied here and may not provide any clear advantage over the other.

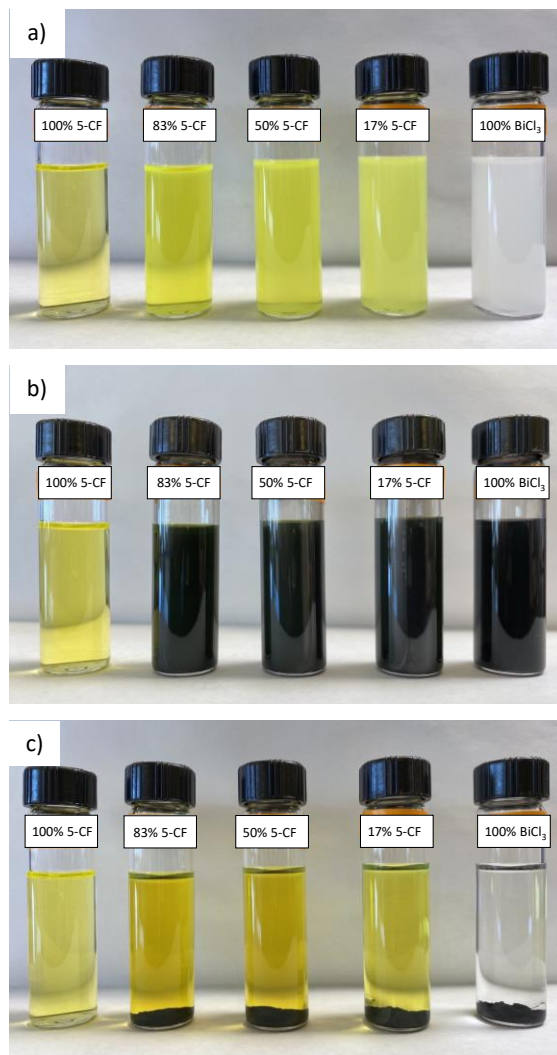


Figure 3.4. Various volume percentages of 1 mM 5-CF and 100 mM BiCl_3 solution state UV Sensors a) as prepared, b) continuous 3 hour 302 nm UV exposure, and c) 72 hour settling.

Solid-State 5-CF UV Sensor

Filter paper squares were soaked in 50% 1 mM 5-CF and 100 mM BiCl₃ in ethanol and dried at room temperature. Figure 3.5 depicts their exposure to 302 nm UV light for various durations. A UV blocker was placed over the left side of the sensor while the right side was exposed to UV radiation. The 5 minute exposure time shows a slight color change while the 2 hour exposure time produced the darkest image and maximum color change. The 40 minute and 1 hour exposure times produced a similar amount of darkening. Comparing the 6-CF solid-state sensor, the same shades of darkening are seen for the 5, 10, 20, and 40 minutes exposures, however, there appears to be no difference in color between the 40 minute and 1 hour exposures for the 5-CF solid-state sensor. The 6-CF solid-state sensor showed a slight color change between the 40 minute and 1 hour exposures. Ultimately, both the 5-CF solution sensor as well the 5-CF solid-state sensor produced similar sensor results when compared to the 6-CF based UV sensors. Both 6-CF and 5-CF dyes do not show any significant difference when mixed with BiCl₃ in producing the UV sensor response and that the sensor response may only be dependent on BiCl₃. In the next chapter, we will further discuss and analyze our UV sensor mechanism.

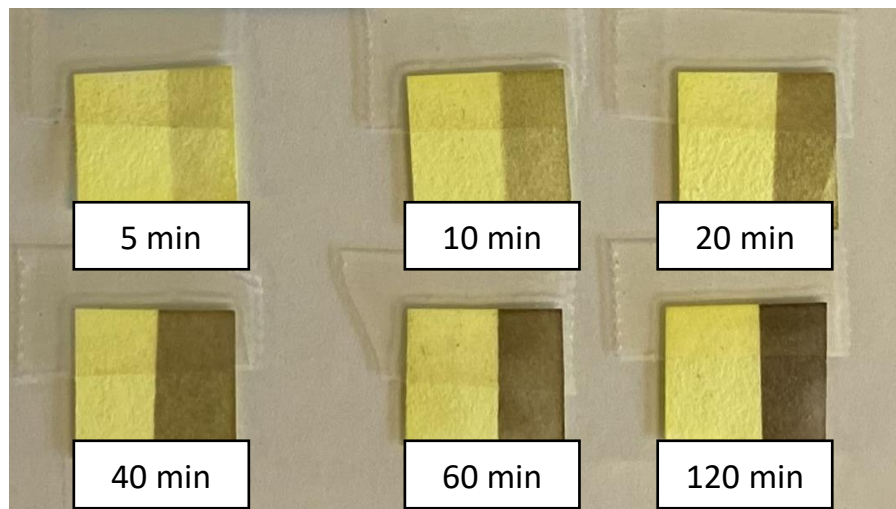


Figure 3.5. Soaked and dried filter paper squares in 50% 1 mM 5-CF and 100 mM BiCl₃ in ethanol exposed to 302 nm UV light at various times.

Chapter 4:

UV Sensor Mechanism

Understanding the mechanism responsible for the color change is necessary to develop successful colorimetric UV sensors. BiCl_3 is known to readily form Cl radical agents.²⁷ Our belief is that the produced Cl radical will interact with an organic dye, such as 6-CF, limiting the UV adsorption properties of the organic dye similar to the mechanism of DBI-BP fluorescence quenching.²⁶ In their work, exposing CHCl_3 to γ radiation resulted in the formation of H and Cl radicals, which in turn formed an adduct with DPI-BP. This DPI-BP/HCl adduct has a planar structure that helped form π - π stacking interaction and thus molecular aggregation. The aggregated product did not possess the high fluorescence properties of DPI-BP thus resulting in quenching (see Figure 1.7). The 6-CF dye does fluoresce under UV light as seen in Figure 2.2.b., however the quenching does not occur in the presence of BiCl_3 . Interestingly, we observed a black precipitate in our 6-CF/ BiCl_3 and 5-CF/ BiCl_3 mixtures upon prolonged exposure to sunlight and 302 nm UV radiation. Further, the solid-state sensors soaked in the sensor solution also turned dark upon exposure to UV radiation. This sparked the discussion on the possibility of Bi metal nanoparticle formation that could lead to the formation of black particles and black color change in the solid UV sensors. A similar type of mechanism was reported in the case of AgCl, where AgCl was photochemically reduced using UV light to produce Ag nanoparticles.³⁸ Figure 4.1 shows the proposed mechanism for the generation of reactive oxygen species and free chlorine on irradiation of AgCl. AgCl absorbs photons from the UV light resulting in the excitation of electrons into the conduction band which then react with Ag^+ to form Ag nanoparticles.³⁸

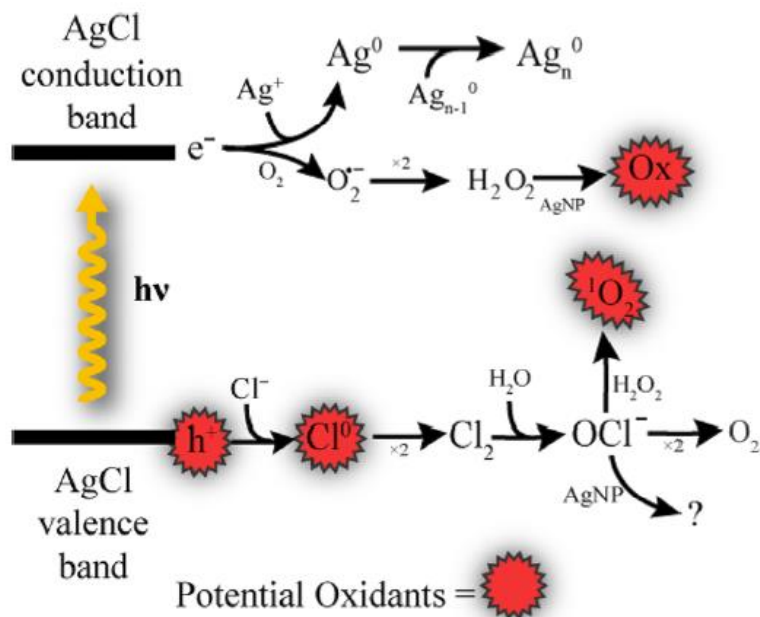


Figure 4.1. Proposed reaction mechanism for generation of reactive oxygen species and free chlorine on irradiation of AgCl. This Figure was reused from the Garg et al. article regarding the mechanism for producing free chlorine and reactive oxygen species from the irradiation of silver chloride particles.³⁸

It was still unclear what the underlying mechanism is for the color change in our sensors. We decided to systematically analyze the products and evaluate the UV sensing mechanism of our sensor. In this section, we will discuss our results and propose a mechanism for our sensor activity. First, we varied the Cl source by substituting BiCl₃ with KCl and evaluated the sensor response. Then Scanning Electron Microscopy (SEM), Electron Dispersive Spectroscopy (EDS), and powder X-Ray Diffraction (XRD) were performed on various BiCl₃ samples dissolved in ethanol and dried. Finally, our UV sensing mechanism is proposed.

6-CF and KCl Sensor

To test the chloride radical quenching mechanism seen with DPI-BP²⁶, the chlorine radical generator in the previous 6-CF and 5-CF based UV sensors, BiCl₃, was substituted with KCl. Figure 4.2 shows the UV spectrum for 83% 6-CF, 50% 6-CF, and 17% 6-CF formulations between 1 mM 6-CF and 100 mM KCl before and after exposure to sunlight for 5 hours on 1 hour intervals. In the case of 83% 6-CF and 50% 6-CF solutions in KCl, the peak at 450 nm remained unchanged although a new shoulder at 490 nm was observed. However, there is no significant change in the peak intensity for both 450 nm and 490 nm peaks upon exposure to sunlight although the background absorption values seen an increase between 300 nm and 400 nm, similar to the 1 mM 6-CF 1 mM BiCl₃ sunlight exposure but at a lower intensity. In the case of 17% 6-CF in KCl, the inset shows the 450 nm 6-CF peak is barely present with a max intensity of 0.1 while the peak at 290 nm seen in the 50% 6-CF solution was also present. Once again, the 17% 6-CF in KCl, did not show any significant change in its UV spectra upon exposure to sunlight for various intervals. The inset in Figure 4.2.c. illustrates the very small peak intensity associated with 6-CF within the 400 nm to 550 nm wavelength region. From the results, the KCl as a chlorine radical source does not appear to have any effect on the UV absorption/quenching of the 6-CF dye.

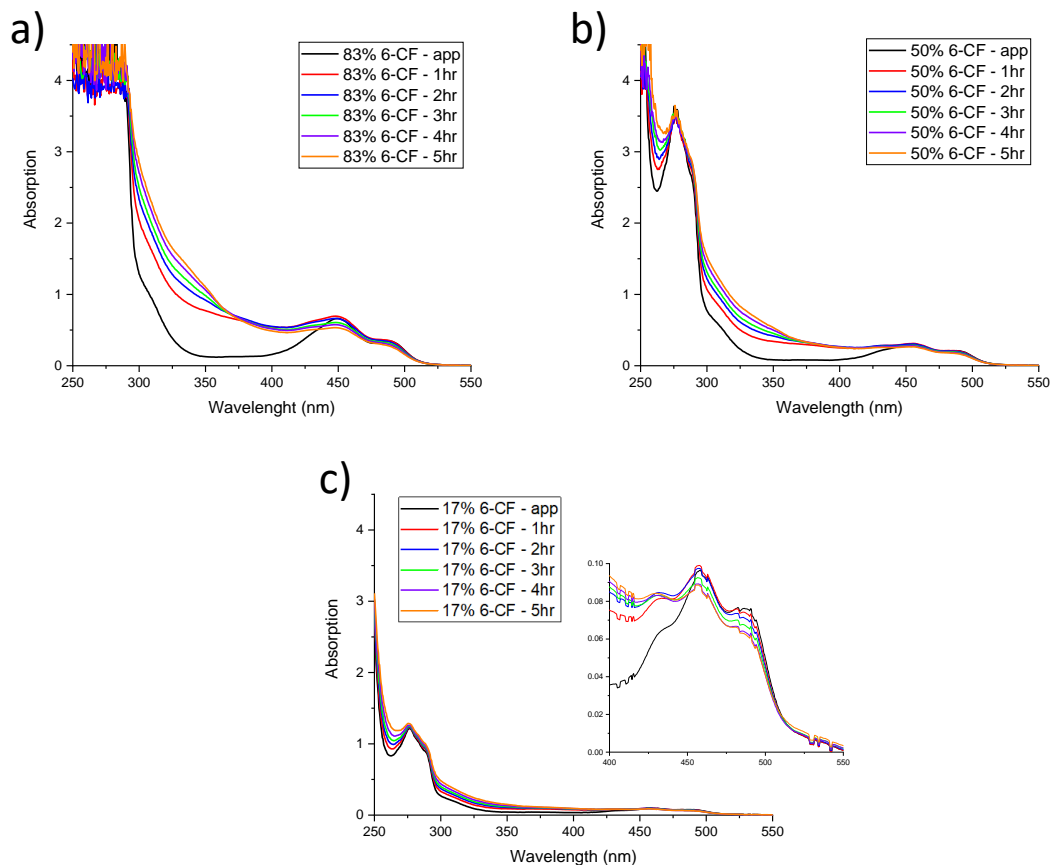


Figure 4.2. UV absorption of 1 mM 6-CF and 100 mM KCl in ethanol when exposed to sunlight for 1, 2, 3, 4, and 5 hours at a) 83% volume 6-CF, b) 50% volume 6-CF, and c) 17% volume 6-CF.

Figure 4.3 compares the UV spectra of individual solutions of 100 mM KCl and 100 mM BiCl₃ in ethanol when exposed to UV radiation from sunlight for KCl and 302 nm UV light for BiCl₃. For all of the KCl samples, no change in the UV spectrum occurred as expected since KCl is not known to have any characteristic UV adsorption behavior. As for the BiCl₃ samples, while no significant change is observed, a small increase in the absorption baseline from 400 nm to 600 nm is observed for all samples. The 3 hour exposure spectrum matched that of the as prepared because the solution was left overnight before continuing the exposure the next day. The color of the KCl solution remained the same clear solution while the BiCl₃ solution turned

from a cloudy white solution to a cloudy light grey solution. After continuously exposing the 100 mM BiCl_3 in ethanol solution to 302 nm UV light as well as sunlight the solution turned black and produced a black precipitate. This observation clearly suggests that a BiCl_3 derivative must be responsible for the black color observed in both the solution state measurements as well as the solid-state UV sensor measurements. While BiCl_3 is known to readily hydrolyze to form bismuth oxychloride (BiOCl) in aqueous solvents,^{39–42} BiOCl does not readily form metallic bismuth unless under strong reducing conditions. For example, Bi nanoparticles are formed from BiOCl nanosheets when using strong reducing agents such as NaBH_4 for reduction⁴³ or under electrochemical reduction in KHCO_3 .⁴⁴ Hence, we carried out detailed analysis on the blackened precipitate as well as evaporated and irradiated BiCl_3 /ethanol solutions under different conditions followed by analyzing the resultant powders using SEM, EDS, and powder XRD analysis.

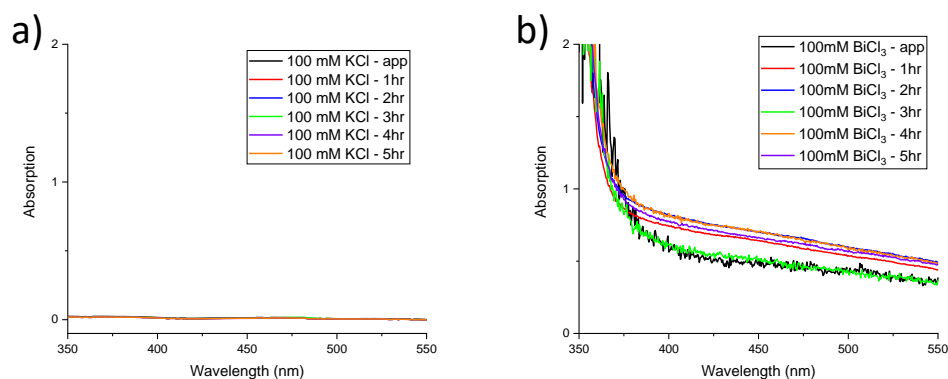


Figure 4.3. UV absorption of a) 100 mM KCl and b) 100 mM BiCl_3 in ethanol when exposed to a) sunlight and b) 302 nm UV light for 1, 2, 3, 4, and 5 hours.

SEM, EDS, and Powder XRD Analysis

To understand the possible role of hydrolysis of BiCl_3 to BiOCl and the effect of drying conditions, we processed BiCl_3 into dry powder in different methods. First, approximately 2 mL of 400 mM BiCl_3 dispersed in ethanol was drop casted on a glass slide and set to dry at room temperature with no UV/sunlight exposure (Sample A). Similarly, a second sample was prepared by casting the 400 mM BiCl_3 solution in a glass slide but was dried under a hot air gun to see the impact of heat (Sample B). A third sample was prepared similar to the first one but after drying under room temperature, the dried sample was exposed to sunlight for two hours (Sample C). Finally, a fourth sample was prepared where the 400 mM BiCl_3 solution was drop casted on the glass plate in direct sunlight and left to dry (Sample D). All the four samples were scraped with a razor and analyzed through Scanning Electron Microscopy (SEM) and Electron Dispersive Spectroscopy (EDS). The resulting SEM images are shown in Figure 4.4.a-d. The SEM image of sample A shown in Figure 4.4.a. indicates that the formed particles are cubes with an average size of $0.44\ \mu\text{m}$ by $0.34\ \mu\text{m}$. Sample B shown in Figure 4.4.b., show a similar morphology to sample A. The structure of the particles are almost identical to the room temperature drying except for the larger particle size, $0.85\ \mu\text{m}$ by $0.66\ \mu\text{m}$ on average. No color change was observed in the powder appearance for both sample A and sample B confirming that heat does not induce a color change. Sample C that was room temperature dried but post exposed to sunlight, produced particles roughly the same size as the heated sample, $0.87\ \mu\text{m}$ by $0.61\ \mu\text{m}$, however, the corners of the cube have been worn down. The physical appearance of the powder was also changed as a light grey color was observed in comparison to the pure white color for samples A and B. In Sample D, where the solution was cast and dried in direct sunlight, interestingly nanoneedles are seen instead of the cubes and

plates of the previous samples. The nanoneedles have an average size of $0.76\ \mu\text{m}$ and $0.06\ \mu\text{m}$. This powder sample's appearance was dark grey and showed the largest physical and color change of the four samples. The results observed here indicate that the BiCl_3 did not undergo any color change under room temperature or hot air conditions but turned into greyish powders upon exposure to sunlight suggesting that the color change observed in our UV sensors could completely be due to BiCl_3 and the organic dye may not play any crucial role at all.

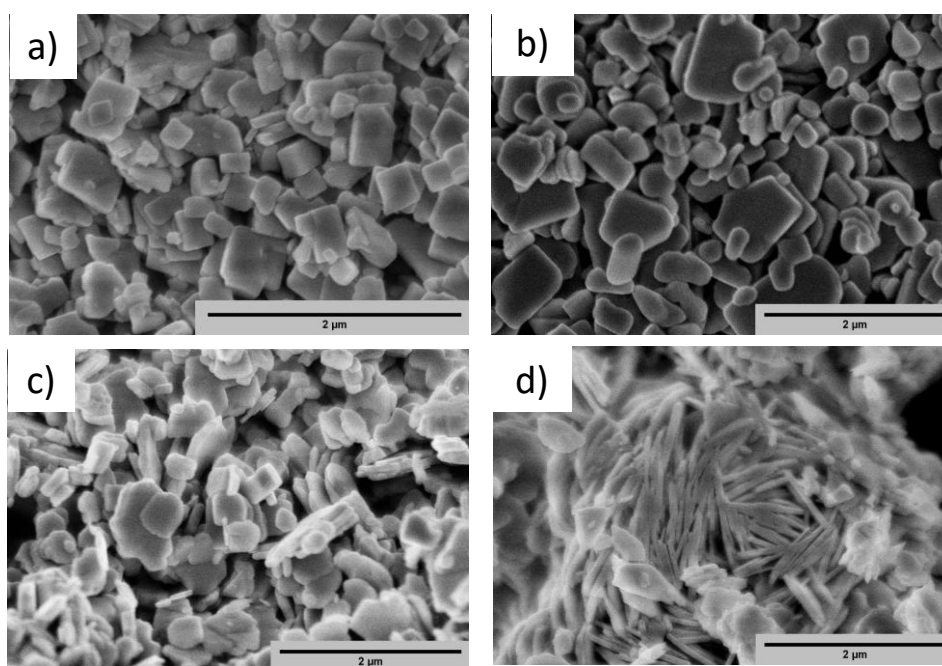


Figure 4.4. SEM images of 400 mM BiCl_3 in ethanol a) room temperature drying with no UV exposure, b) heat gun drying with no UV exposure, c) room temperature drying with 2 hours of sunlight exposure, and d) drying in sunlight for 2 hours.

Figure 4.5 shows the EDS spectrum for all the four SEM samples discussed above, Sample A room temperature drying with no exposure, Sample B heat gun drying with no exposure, Sample C room temperature drying with sunlight exposure, and Sample D sunlight drying. The EDS peaks for oxygen, bismuth, and chlorine were isolated for comparing their relative ratios. For the room temperature no exposure sample, bismuth and chlorine have a one-to-one atomic

ratio when the expected ratio was one-to-three. The same one-to-one bismuth to chlorine ratio can be seen in all four samples as presented in Table 4.1 leading to the conclusion that BiCl_3 was readily hydrolyzed to BiOCl . Further, it also indicated that even though there was a color change in samples exposed to sunlight (Sample C and Sample D), there was no change in chemical composition as it retained the one-to-one ratio between bismuth and chlorine seen in Table 4.1.

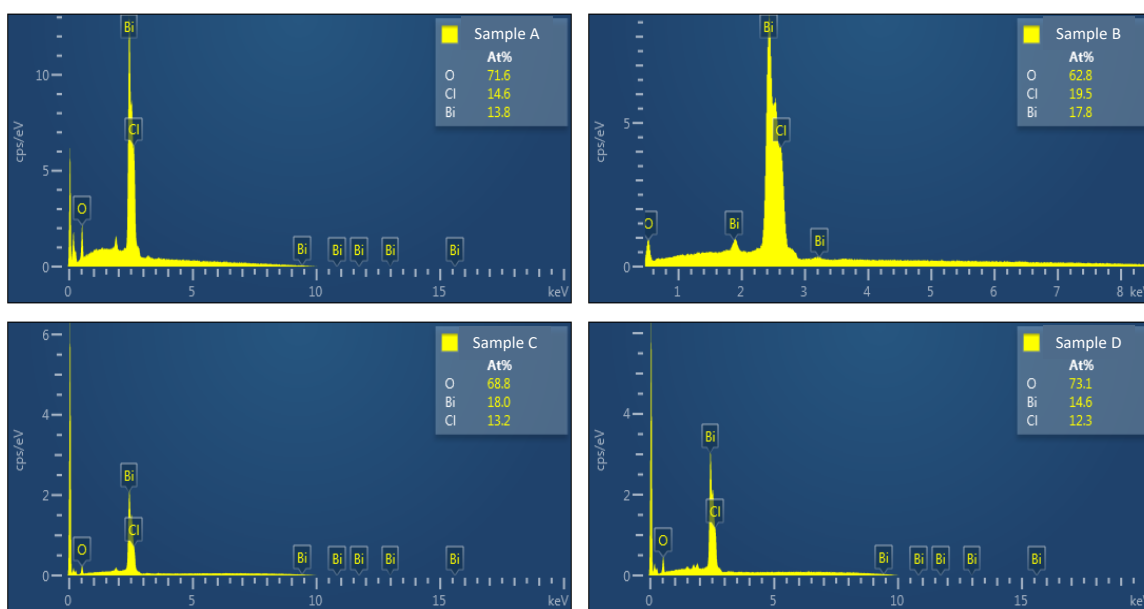


Figure 4.5. EDS spectrum of 400 mM BiCl_3 in ethanol. Sample A, room temperature drying with no exposure. Sample B, heat gun drying with no exposure. Sample C, room temperature drying with sunlight exposure. Sample D, sunlight drying.

Table 4.1. Average atomic percentages of bismuth and chlorine from EDS

Element	No Exposure Drying (Sample A)	Heat Gun Drying (Sample B)	Dry Exposure (Sample C)	Sunlight Drying (Sample D)
Bismuth	16.3%	16.3%	17.4%	15.8%
Chlorine	15.9%	18.6%	15.1%	14.1%

Further confirmation of the BiOCl formation in the aqueous BiCl₃ solutions was obtained through a powder XRD analysis performed on a 400 mM BiCl₃ in ethanol solution dried at room temperature. The BiCl₃ powder XRD was collected and compared to the powder XRD of BiOCl purchased from Sigma Aldrich which confirms BiCl₃ was completely hydrolyzed to form BiOCl and only BiOCl was present in the powder. Figure 4.6 compares the two XRD pattern for BiOCl (top) and dried BiCl₃ from ethanol solution (bottom). The XRD pattern of dried BiCl₃ in ethanol matches the BiOCl pattern almost perfectly with similar peak ratios for every peak excluding the (001) and (101) peaks meaning the dried BiCl₃ sample has more BiOCl orientated along those planes. Two very small peaks corresponding to (103) and (213) were identified on the dried BiCl₃ sample also correspond to BiOCl.

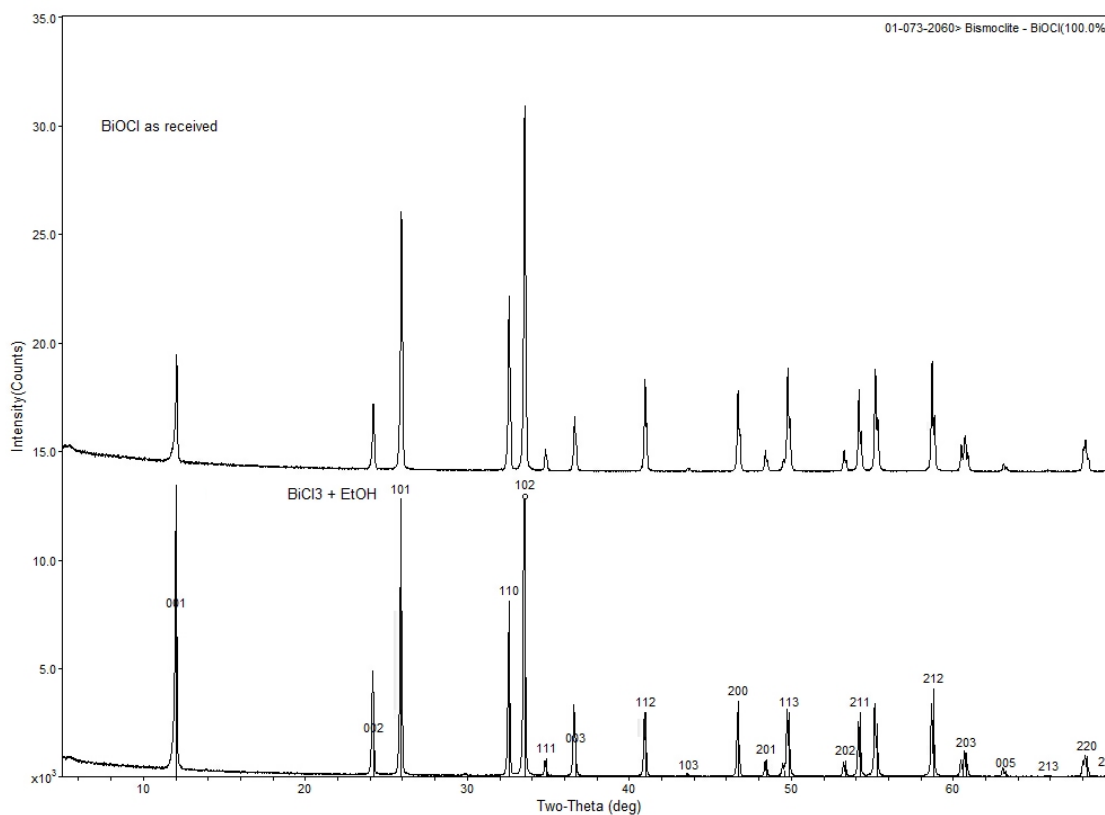
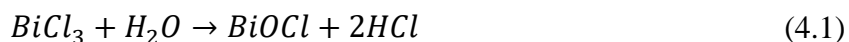


Figure 4.6. XRD analysis comparing reference BiOCl (top) and room temperature dried 400 mM BiCl₃ in ethanol (bottom).

Mechanism

After carefully analyzing the SEM, EDS, and XRD data, we can confirm that the active species in the UV sensor is BiOCl formed upon the addition of BiCl₃ to ethanol, where BiCl₃ undergoes hydrolysis to form BiOCl shown as in equation 4.1.



BiOCl is a well-known photocatalyst with a band gap of 3.46 eV¹⁹ and is being studied for applications in clean energy utilization as it has good chemical stability and is non-toxic. Its band gap is ideally suited for absorbing UV radiation while research has been on focus to reduce this band gap and make it respond to visible light.^{18,19,21-23} A direct band gap of 4.43 eV was calculated from the UV absorption spectrum of 100 mM BiCl₃, which also confirms the BiCl₃ hydrolysis to BiOCl. The Tauc plot is located in Appendix C. Interestingly, this unique UV adsorption property has the potential to be used for UV sensor applications that has not been explored. BiOCl upon exposure to UV light undergoes an excitation process from its ground state to an excited state. While most chemicals once excited can radiate energy to return to the ground state, BiOCl transfers its energy to a trap level⁴⁵⁻⁴⁷ where this transition back to the ground state is a forbidden transition. In the trap level, BiOCl remains at this level for several weeks to months slowly dissipating heat to return to its ground state. Figure 4.7 is a schematic of the electronic band structure of BiOCl. The circle insets are pictures of Whatman filter paper squares soaked in 100 mM BiCl₃ in ethanol prior to UV exposure (valence band), immediately after UV exposure (conduction band and trap level). During this excitation, BiOCl also changes its color from crystal white into a black color. We are uncertain if BiOCl's excited state causes the color change or if the transfer of energy from the excited state to the trap level

is the cause. Bulk powders of BiOCl produce a less noticeable color transition after UV exposure. By dispersing BiOCl on a filter paper, we amplified this color transformation and are able to track the UV radiation that is involved in exciting the BiOCl molecule.

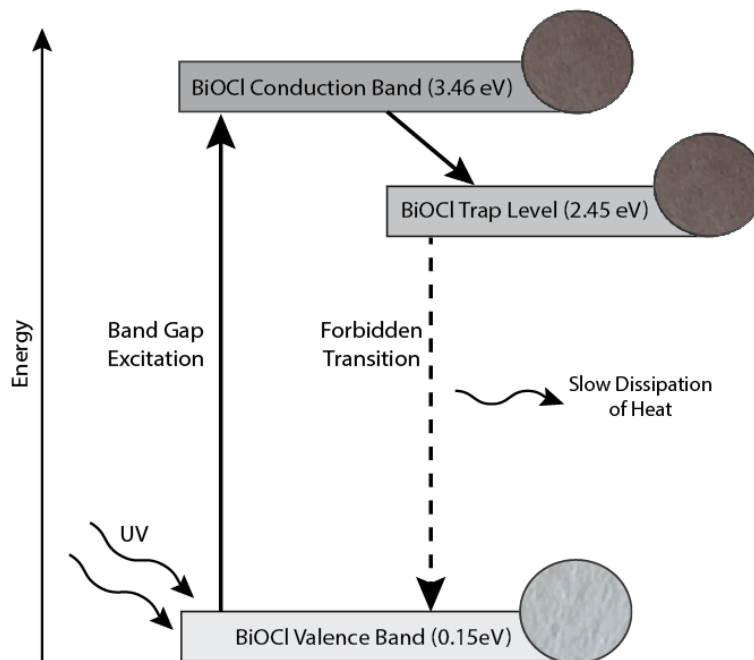


Figure 4.7. Schematic of the electronic band structure of BiOCl.

We prepared solid samples by soaking filter paper in BiCl₃ solution in ethanol to confirm that the UV sensing is produced completely from BiOCl while the organic dyes is used to provides a better contrast. Figure 4.8 shows the digital image of these samples before and after sunlight exposure. Figure 4.8.a. shows 1 hour exposure of sunlight on the right half of the sample. A UV blocking material was placed on the left side of sample and a dark color change was seen on the area exposed to UV radiation. We left that sample inside a cupboard without any additional exposure to sunlight or UV radiation for three weeks and took a digital image that is shown in Figure 4.8.b. Clearly, the exposed side changed from a dark brown to a pale grey, illustrating the dissipation of heat by BiOCl from its trap level. We exposed both sides of the

sample again to sunlight for an hour and Figure 4.8.c. shows that both sides of the filter paper have turned to dark black. The black color transition of BiOCl is likely due an increase in oxygen vacancies or an increase in surface disorder upon UV exposure and resulted in more absorption in the visible light region.^{47,48} This further clarifies that BiOCl is stable for prolonged periods and did not degrade into Bi metal or bismuth oxide (BiO) upon exposure to sunlight. The relaxation of excited BiOCl leads to disappearance of dark black color that reappears when exposed to sunlight. This result shows that the 6-CF dye or other dyes could be used to help distinguish the color change on the sensor but not essential since the BiOCl hydrolyzed from BiCl₃ is the UV sensing material. The fluorescent dye increases the contrast between UV exposed areas where BiOCl is darkened. This is due to a higher dye fluorescence light intensity than the sample light scattering from the paper surface. In the next chapter, two different dyes, prussian blue (PB) and rhodamine-b (RhB), were combined with BiCl₃ and their UV sensing was analyzed.

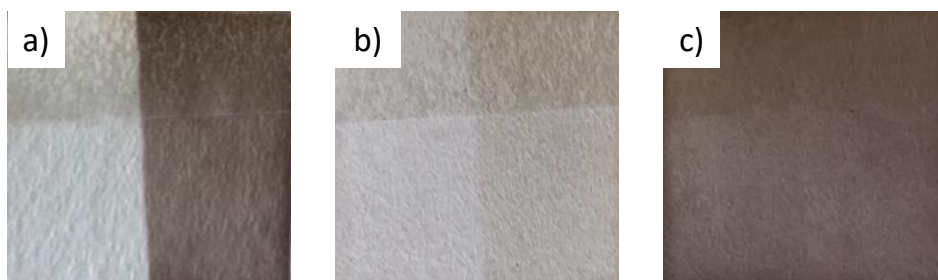


Figure 4.8. 100 mM BiCl₃ filter paper sample a) exposed to 1 hour of sunlight, b) 3 weeks after initial exposure, c) additional 1 hour exposure of sunlight on unexposed side and initially exposed side.

Chapter 5:

Other Dyes in BiCl₃ UV Sensors

BiCl₃ readily hydrolyzes in aqueous solutions to form BiOCl,³⁹⁻⁴² which is one of the well-researched photocatalyst.⁴⁹⁻⁵² Since BiOCl is identified as the key compound for UV sensitivity, we decided to test the utility of common dyes such as prussian blue (PB) and rhodamine-b (RhB) in our UV sensor measurements. Figure 5.1 shows the chemical structure of (a) PB and (b) RhB as well as the color of (c) 0.1 mM PB and (d) 0.1 mM RhB in ethanol. PB has a distinct blue color that could help distinguish the BiOCl color change in the solid-state and possibly provide a better color contrast. RhB has a deep pink color and is commonly used as an organic dye in the photocatalysis experiments to harvest the energy from the excited state BiOCl but degrades in the process.⁵³⁻⁵⁶ In this section, the two different dyes prussian blue (PB) and rhodamine-b (RhB) were tested with BiCl₃. Similar to the 6-CF and 5-CF sensors discussed in Chapter 2 and Chapter 3, both PB and RhB sensors were tested in solution and on a Whatman filter paper substrate. The RhB UV sensor could provide a unique colorimetric sensor that has a disappearance of color over an extended period of time after initial UV exposure in conduction with the initial blackened color seen in the 6-CF/5-CF dyes.

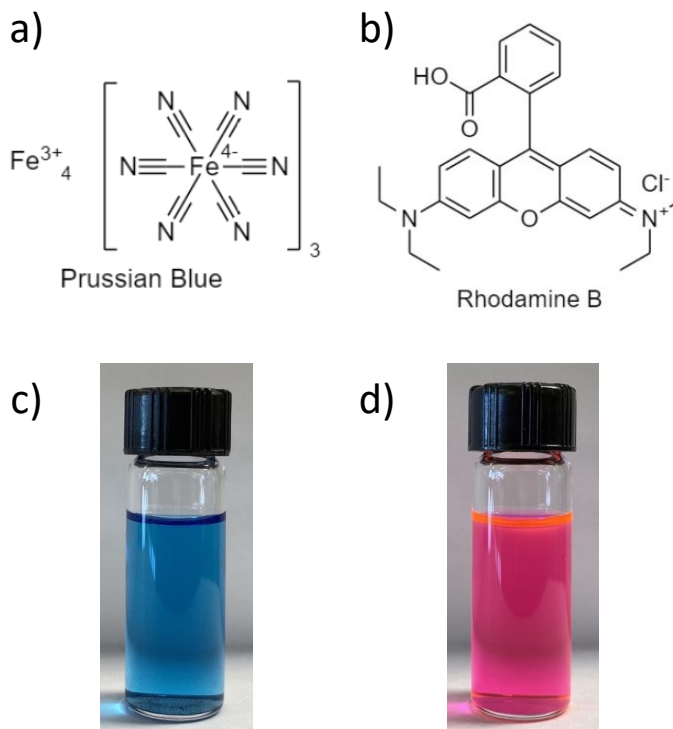


Figure 5.1. Chemical structure of a) Prussian Blue (PB) and b) Rhodamine-B (RhB) as well as photos of c) 0.1 mM PB in ethanol and d) 0.1 mM RhB in ethanol.

PB Solution Sensor

To determine a useful concentration of PB for a BiCl_3 UV sensor, three solutions of 0.01 mM, 0.1 mM, and 1 mM PB in ethanol made. Each sample's UV absorption spectrum was analyzed using a Varian Cary 50 Bio UV Vis Spectrophotometer. Each sample was not exposed to any UV radiation. Figure 5.2 compares the three dye solution's UV absorption spectrums. Figure 5.2.a. shows the UV absorption spectrum for the 0.01 mM PB solution. An absorption peaks at 200 nm can be seen on the spectrum. Figure 5.2.b. shows the UV absorption spectrum for the 0.1 mM PB solution. A low intensity absorption peak can be seen between 675 nm and 800 nm. Similar to 0.01 mM PB, the 0.1 mM PB solution has a 200 nm peak with the addition of two small shoulders at 250 nm and 275 nm. Between 300 nm and 650 nm the UV absorption

becomes negative meaning that the blank is absorbing more UV radiation than the sample, which could be due to a higher permittivity for the blank than for the PB solutions. Figure 5.2.c. shows the UV absorption spectrum for the 1 mM PB solution. Two regions of large intensity noise can be seen in the UV absorption spectrum, 200 nm to 350 nm as well as 575 nm to 800 nm. From 350 nm to 575 nm, the spectrum becomes negative similar to the 0.1 mM PB solution, which may be due to the increased opacity of the solutions. After comparing the three concentrations, it was determined that the 0.01 mM PB would provide the most useful UV absorption spectrum for a BiCl_3 sensor. Hence, we used 0.01mM PB for making the UV sensor with BiCl_3 solutions.

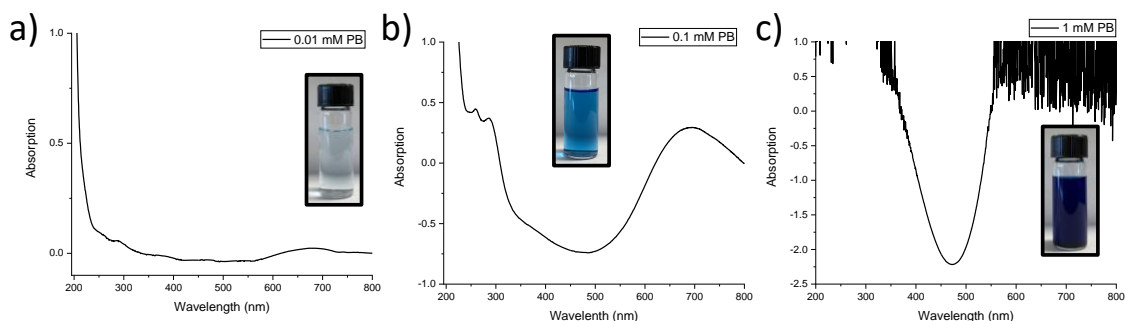


Figure 5.2. UV absorption of as prepared solutions of a) 0.01 mM PB, b) 0.1 mM PB, and c) 1 mM PB. Each inset shows the respective concentration of PB in ethanol.

Three PB solution sensors, 83% PB, 50% PB, and 17% PB were made between 0.01 mM PB and 10 mM BiCl_3 and tested. Figure 5.3 shows the UV absorption spectra of the three PB solution sensors after 1 hour exposure to 302 nm UV light. Figure 5.3.a. shows the UV absorption spectrum for 83% PB. An absorption peak from 275 nm to 325 nm can be seen. This peaks match the 1 mM BiCl_3 absorption peaks in Figure A.2. In both Figures 5.3.b. and 5.3.c., a wide 250 nm to 325 nm absorption peak with a large amount of noise can be seen, matching the absorption peaks of 5 mM BiCl_3 (Figure A.3.) and 10 mM BiCl_3 (Figure A.4.).

After 1 hour exposure to 302 UV light, some regions in the BiCl_3 peaks increased substantially for all three solutions. However, there was no change in the absorption from 350 nm to 600 nm.

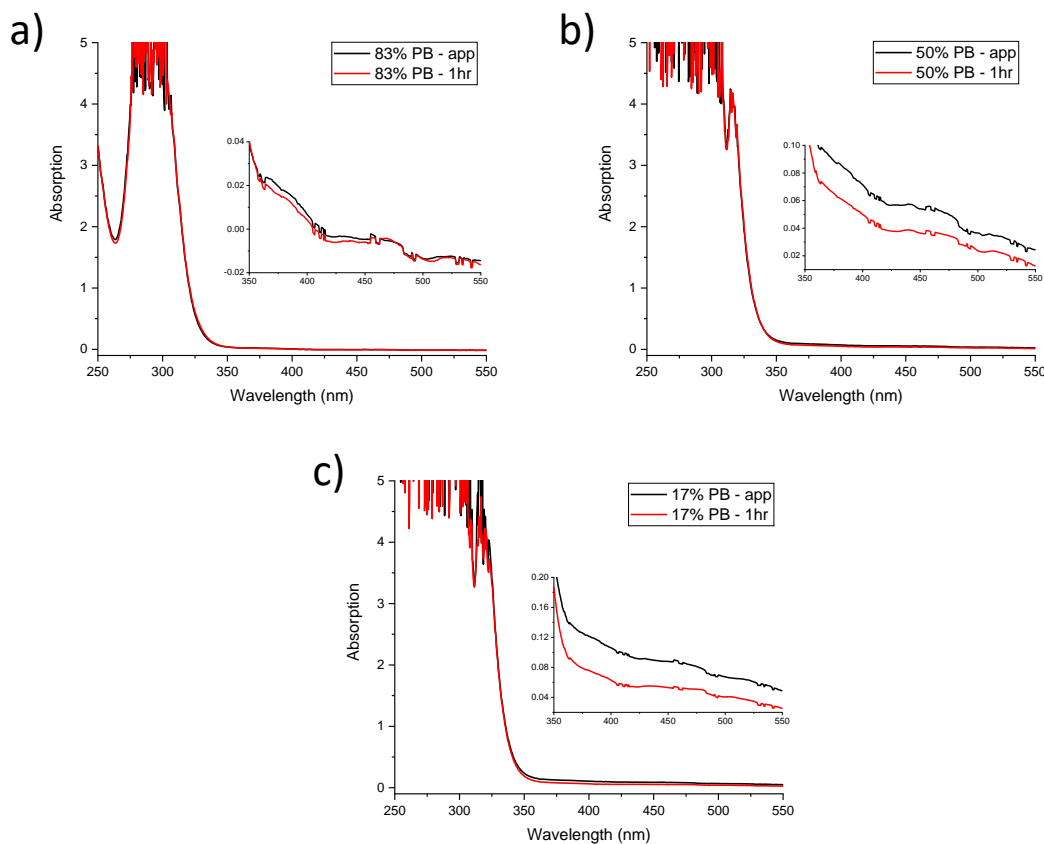


Figure 5.3. UV absorption of 0.01 mM PB and 10 mM BiCl_3 in ethanol when exposed to 302 nm UV light for 1 hour at a) 83% volume PB, b) 50% volume PB, and c) 17% volume PB.

Solid-State PB UV Sensor

Similar to the 6-CF and 5-CF solid-state sensors, filter paper was soaked in a 50% 1 mM PB and 100 mM BiCl_3 solution and dried at room temperature. Figure 5.4 depicts the PB solid-state sensors exposed to 302 nm light for various durations. Upon exposure, the right side of the filter paper turned into a similar tone of brown seen in the 6-CF, 5-CF, and undyed filter

paper samples leading to the conclusion that the dye does not interfere with the excitation process of BiOCl and hence on the performance of BiCl₃ UV sensor. The 5 minute exposure produced a darker color change than the previous 6-CF and 5-CF sensors. There is no clear color distinction between the 1 hour and 2 hour exposure times. Prussian blue although provides a bright blue color, it is not a promising alternative to 6-CF as the contrast between the blue and black color may not be better than the contrast between the yellow and black. Further, the color gradient seen in Figure 5.4 for PB based sensor is more difficult to distinguish than the 6-CF counterpart.

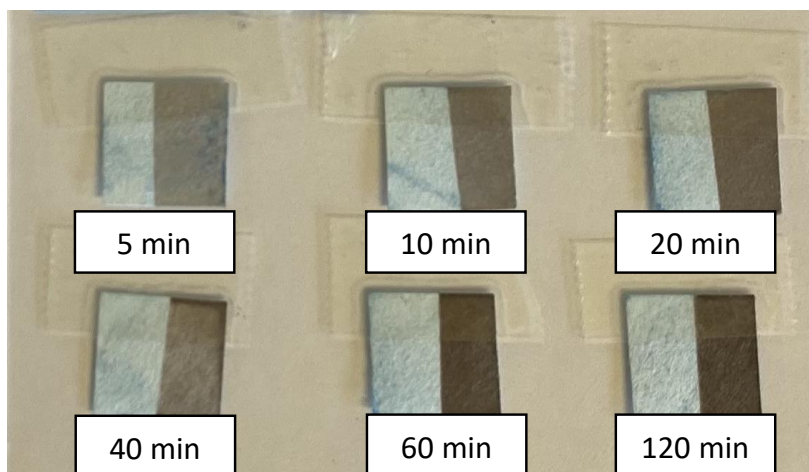


Figure 5.4. Soaked and dried filter paper squares in 50% 1 mM PB and 100 mM BiCl₃ in ethanol exposed to 302 nm UV light at various times.

RhB Solution Sensor

In order to evaluate the RhB for application in our UV sensor devices, first an analysis of RhB's UV stability under 302 nm UV light was conducted before assembling a RhB solution sensor. Figure 5.5 shows the UV absorption spectrum of 0.1 mM RhB in ethanol when exposed to 302 nm UV light. The solution was exposed to 302 nm UV light at 1 hour intervals for a total of 5 hours. The UV spectrum has an absorption peak range from 510 nm to 575 nm. After 5

hours of exposure, there was no change seen in the absorption peak meaning that RhB is stable under 302 nm UV light.

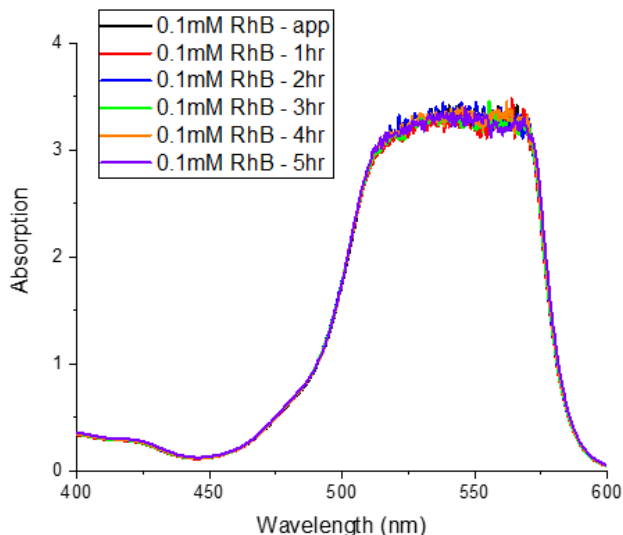


Figure 5.5. UV absorption spectrum of 0.1 mM RhB in ethanol when exposed to 302 nm UV light for 1, 2, 3, 4, and 5 hours.

Two RhB solution sensors were tested to determine the appropriate concentration of RhB to use. The two solution sensors were made with for RhB concentration of 0.1 mM and 1 mM 50% RhB and 100 mM BiCl₃. Figure 5.6 compares the UV absorption spectra of 0.1 mM RhB and 1 mM RhB upon exposure to 302 nm UV light. Figure 5.6.a. shows the UV absorption spectrum for the 0.1 mM RhB sensor. The 510 nm to 575 nm RhB peak was seen in the as prepared spectrum. After 5 hours of 302 nm UV light exposure the RhB absorption peak was almost entirely quenched. Figure 5.6.b. shows the UV absorption spectrum for the 1 mM RhB sensor. The RhB peak seen in the 0.1 mM sensor was widened to 475 nm to 575 nm. A 400 nm RhB peak and 425 nm shoulder were also formed at the higher concentration. After 2 hours of 302 nm UV light exposure, the 475-575 nm peak decreased slightly in peak intensity while the 400 nm peak and 425 nm shoulder saw an increase in peak intensity. Moving forward with

the RhB solution sensor, the 0.1 mM RhB concentration produced a more promising UV absorption than the 1 mM RhB counterpart.

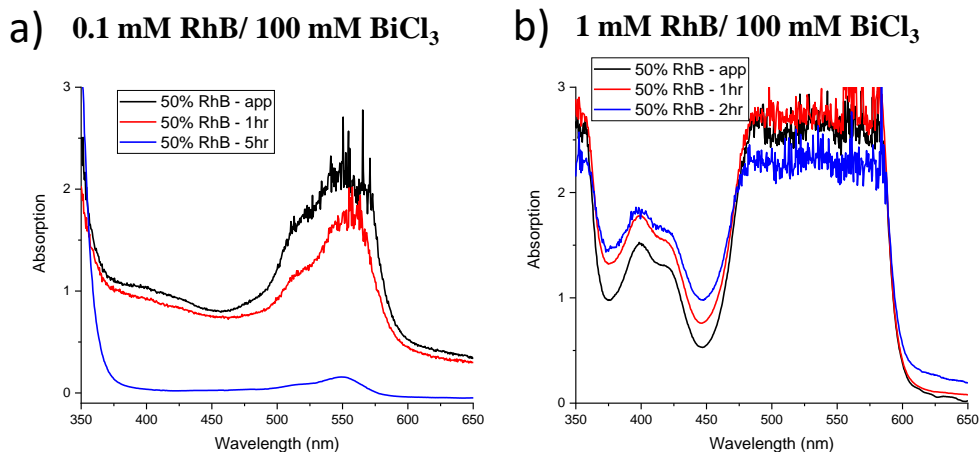


Figure 5.6. UV absorption of a) 50% 0.1 mM RhB and 100 mM BiCl₃ and b) 50% 1 mM RhB and 100 mM BiCl₃ in ethanol when exposed to 302 nm UV light for 1 and b) 2 hours and a) 5 hours.

Following the RhB UV stability test and combination of BiCl₃, a 0.1 mM RhB and 100 mM BiCl₃ solution sensor was made at 83% RhB, 50% RhB, and 17% RhB volumetric percentages. Figure 5.7 shows the UV absorption spectra for the three volumetric percentages of the RhB and BiCl₃ sensors when exposed to 302 nm UV light. Figure 5.7.a. shows the UV absorption spectrum for the 83% RhB sensor. A similar 510 nm to 575 nm RhB peak as the unexposed RhB is seen. An increase in exposure resulted in a large decrease in the intensity of the RhB peak. Figure 5.7.b. shows the UV absorption spectrum for the 50% RhB sensor. The RhB peak intensity observed around 510 nm to 575 nm decreased from that of the 83% RhB sensor. After 4 hours of 302 nm UV light exposure, the RhB absorption peak was completely quenched and UV spectra resembling that of the BiCl₃ absorption spectrum in the 400 nm to 600 nm range. Figure 5.7.c. shows the UV absorption spectrum for the 17% RhB sensor. Similar to the 50% RhB sensor, the 17% RhB sensor saw another decrease in the conventional RhB peak intensity

between 510 nm to 574 nm. After 2 hours, the RhB absorption peak was completely quenched. The quenching seen in the UV absorption spectra of the RhB sensors is due to the degradation of RhB in the presence of BiOCl and UV radiation. This is a well-known process where the excited BiOCl transfers its energy to RhB which in turn causes the RhB bonds to break.⁵³ The solutions state sensor between RhB and BiCl₃ clearly showed a linear trend in peak intensity decrease specially at high RhB concentrations. This property could be used for monitoring the UV exposure although the solution state UV sensors pose challenges for practical applications along with the need for UV absorption equipment to quantify the UV exposure.

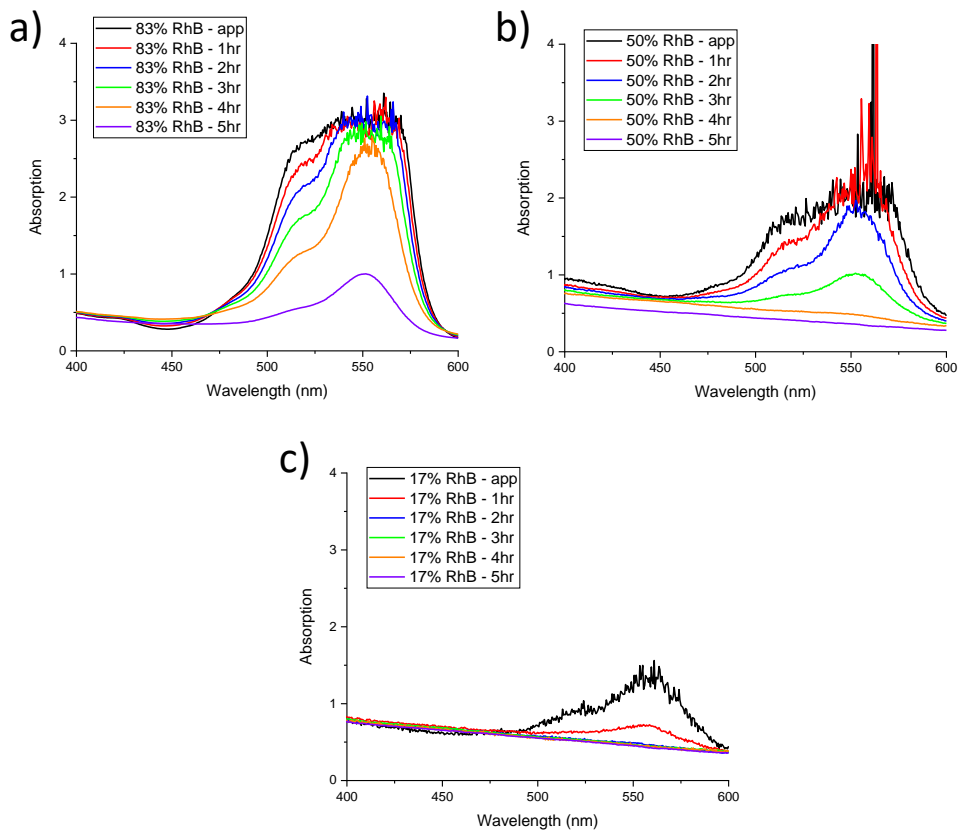


Figure 5.7. UV absorption of 0.1 mM RhB and 100 mM BiCl₃ in ethanol when exposed to 302 nm UV light for 1, 2, 3, 4, and 5 hours at a) 83% volume RhB, b) 50% volume 6-RhB, and c) 17% volume RhB.

Figure 5.8 shows the photographic images of the 0.1 mM RhB and 100 mM BiCl₃ solution sensors. The following volumetric percentages seen in Figure 5.8.a-d. are listed left to right, 100% 0.1 mM RhB, 83% RhB, 66% RhB, 50% RhB, 33% RhB, 17% RhB, and 100% 100 mM BiCl₃. Figure 5.8.a. shows the solution sensors prior to 302 nm UV exposure. The 0.1 mM RhB was a slightly transparent vibrant red with the increasing BiCl₃ concentration caused each solution to turn cloudier and pink while the 100 mM BiCl₃ solution was a cloudy white. Figure 5.8.b. shows the solutions after exposure to 302 nm UV light for a total of 5 hours. The 100% 0.1 mM RhB solution remained unchanged while every other RhB solutions containing BiCl₃ changed in appearance. The 83% RhB solution turned a pale yellow color while the 66-17% RhB solutions became clear with a white precipitate. The 17% RhB solution is cloudy due to the suspension of BiCl₃ particles not given enough time to settle at the bottom of the vial. Figure 5.8.c. shows the solutions after 5 straight hours of 302 nm UV exposure. Again, the 100% 0.1 mM RhB solution color was unchanged. However, the solutions containing BiCl₃ turned black or dark grey. Interestingly, the darkest color change occurred from the smallest BiCl₃ percentage, the 83% RhB solution, and fading to a dark grey in the 100 mM BiCl₃ solution. Figure 5.8.d. shows the solutions after 1 day of settling following the continuous 5 hour 302 nm UV light exposure. Black and white precipitate condensed at the bottom of the vials of the BiCl₃ solutions. The darkest color change seen in Figure 5.8.c. corresponded to a larger ratio of black precipitate to white precipitate. The 83% RhB solution produced more black precipitate while the 100 mM BiCl₃ produced a combination of black and white precipitate with visible estimation indicating more white precipitate. This is contrary to the expectation since while excited state BiOCl is observed to form black color upon exposure to UV radiation, here maximum black precipitate was observed in the mixture with least BiCl₃

concentration. It could be due to the decomposed products of RhB forming a black color or there could be further changes in BiOCl. In order to understand this, we carried out powder XRD measurements on the black precipitate obtained from solution mixtures containing both RhB and BiCl₃.

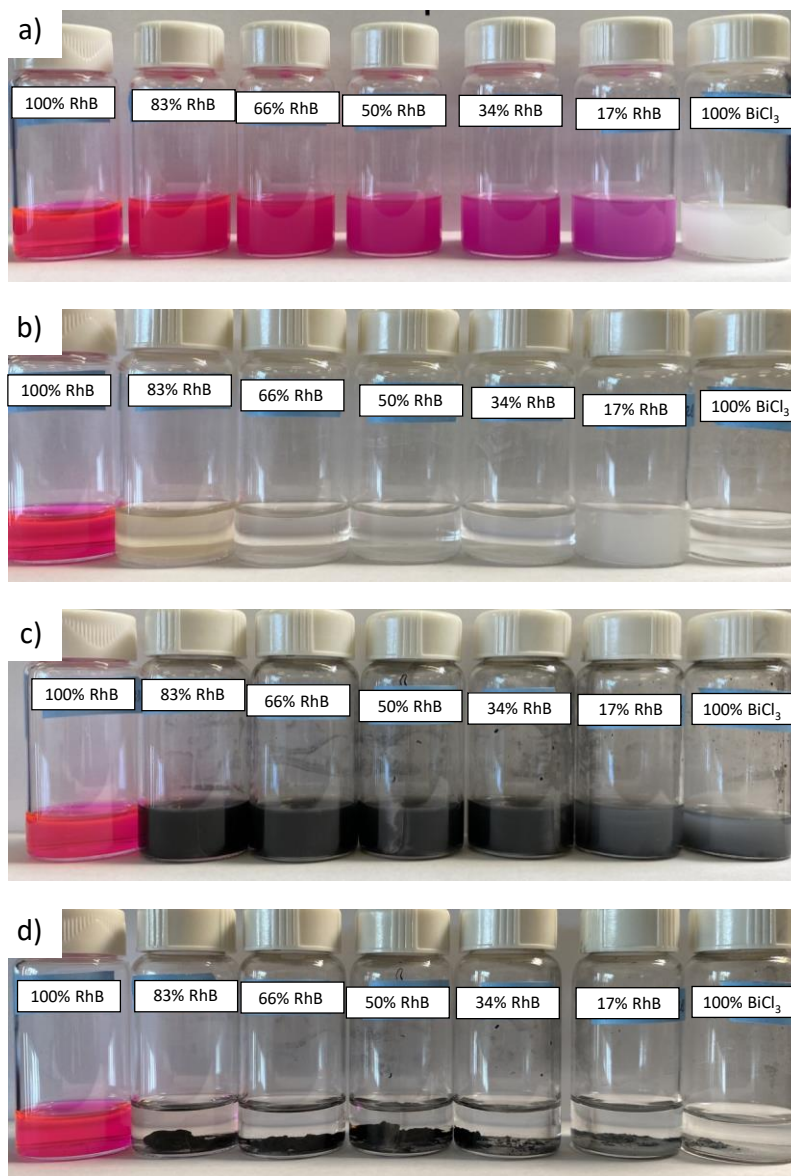


Figure 5.8. Picture of 0.1 mM RhB and 100 mM BiCl₃ solution sensor a) as prepared, b) after 1 hour intervals for a total of 5 hours of 302 nm UV light exposure, c) after 5 hours of continuous 302 nm UV light exposure, and d) 1 day settling after 5 hours of continuous 302 nm UV light exposure.

XRD Analysis

The black precipitate formed in the 50% 0.1 mM RhB and 100 mM BiCl₃ solution sensor from 5 continuous hours of 302 nm UV light exposure was used for carrying out the powder XRD measurements and the obtained patterns were further analyzed using XRD whole pattern fitting using the JADE software. The results are shown in Figure 5.9. The XRD pattern was initially fitted with only BiOCl however, there were few peaks remained unaccounted. These unaccounted peaks were matching well with that of metallic bismuth and the addition of peaks corresponding to bismuth metal dramatically improved the fit. The precipitate analyzed had a 56.9 wt% metallic Bi (JCPDS: 01-071-4642 and Space Group: R-3m) and 43.1 wt% BiOCl (JCPDS: 01-073-2060 and Space Group: P4/nmm). This analysis has proven that Bi nanoparticles are produced in conjunction with the excited BiOCl particles in the presence of RhB. The formation of Bi nanoparticles was not seen in the other solution tests, so their formation is likely the result of the RhB acting as a reducing agent while decomposing upon exposure to UV radiation in the presence of BiOCl. Hence, the increased black precipitate in the RhB-BiCl₃ mixtures could be due to the formation of metallic bismuth along with excited state BiOCl.

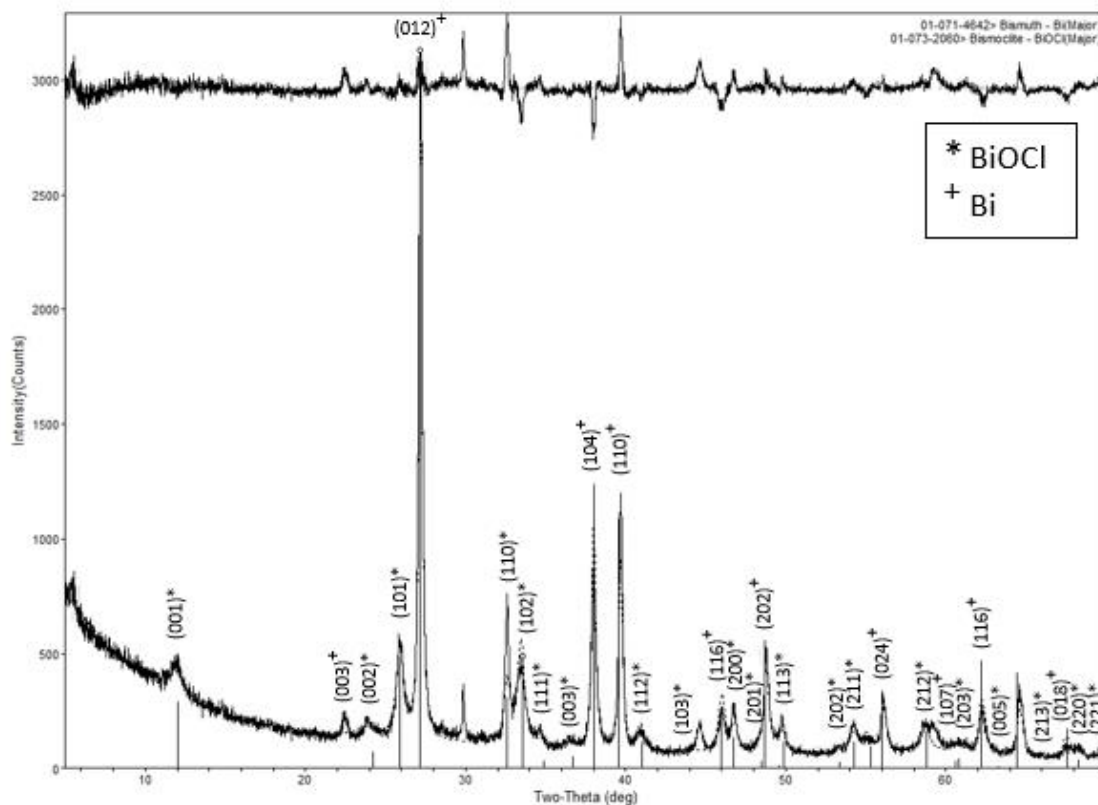


Figure 5.9. XRD Whole Pattern Fitting of black precipitate formed from 5 continuous hours of 302 nm UV light exposure of 50% 0.1 mM RhB and 100 BiCl₃ solution sensor. The star represents peaks associated with BiOCl and the plus represents peaks with Bi metal.

Solid-State RhB UV Sensor

For fabricating the solid-state UV sensor using RhB and BiCl₃, we first soaked the filter paper in 0.1 mM RhB solution. However, soaking filter paper squares in a 0.1 mM RhB solution dyed the filter paper with only a faint purple while a 1 mM RhB solution dyed the filter paper a uniform purple. Hence, for the RhB filter paper sensor, a mixture of 50% 1 mM RhB and 100 mM BiCl₃ solution was used because of the uniform color achieved by the 1 mM RhB solution. Figure 5.10.a. shows the filter paper sensors after exposure to 302 nm UV light. The 5 minute exposure didn't produce a noticeable color change while a slight color gradient can be seen until 40 minute exposure whereas the same color change can be seen in the 1 hour

exposure. The color change between the 1 hour exposure and 2 hour exposure is more pronounced. Figure 5.10.b. shows the same RhB filter paper sensors 1 month after initial exposure. The exposed area of the 10 minute, 40 minute, 1 hour, and 2 hour exposure turned only back to pale pink. The excited BiOCl releases its energy to the RhB molecules causing them to degrade. The RhB solution state sensors as well as the RhB solid-state sensors provide a unique response to UV radiation. For the solution state sensor, RhB's degradation when combined with BiOCl produces a fluorescent quenching that can be measured using a UV-Vis spectrometer. For the solid-state sensor, a distinguishable color change can be seen after 20 minutes of 302 nm UV exposure as well as a noticeable color fading a few days after the initial exposure. In the next chapter, two practical applications will be tested on our 50% 1 mM 6-CF and 100 mM BiCl₃ solid-state sensor.

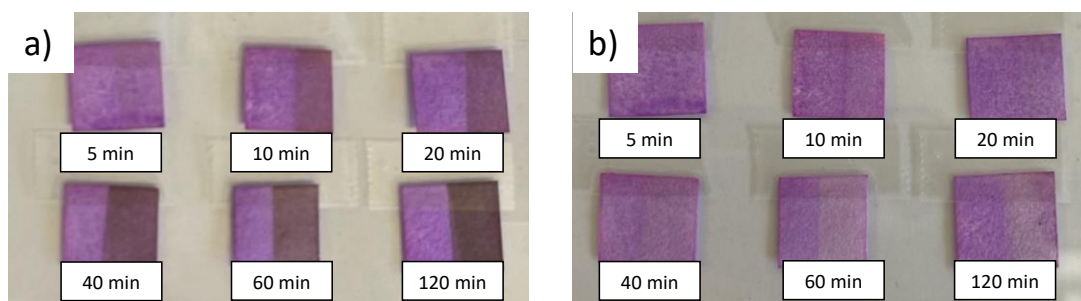


Figure 5.10. Soaked and dried filter paper squares in 50% 1 mM RhB and 100 mM BiCl₃ in ethanol exposed to 302 nm UV light at various times. a) Picture taken immediately after exposure. b) Picture taken 1 month after exposure.

Chapter 6:

Practical Applications for the UV Solid-State Sensors

After carefully analyzing our results, it became clear that BiOCl is the photo-sensitive component for UV sensing application and the dye may only be used for enhancing the contrast between the exposed and unexposed regions. Among the four dye molecules studied, 6-CF was better suited from the perspective of providing a better contrast. Also, 6-CF is non-hazardous,³⁰ hence we decided to study the utility of this sensor in conditions closer to real world scenarios. We treated this problem in two different ways, (i) test the efficiency of commercially available sunscreens in protecting the skin for prolonged periods using our solid-state UV sensor, and (ii) quantify the exposure of sunlight using optical density measurements. Hence, in this chapter, we will present our results obtained with a commercially available sunscreen followed by optical density measurements obtained using ImageJ.³²

Sunscreen Efficiency Testing

Sunscreen efficiency measurement tests were performed using the 50% 1 mM 6-CF and 100 mM BiCl₃ solid-state sensor and the sunscreen efficiency was tested by exposing them to 302 nm UV light as well as sunlight. Filter paper strips with a size of 1 cm by 4 cm, were soaked in the sensor solution and then dried at room temperature. The UV sensor was placed on top of a glass substrate with Scotch Tape covering the sensor. A UV blocker was placed over a small area to prevent UV exposure while a layer of 3M Transpore Tape was applied to the exposed sensor area. Finally, 10 mg of Equate Sport Broad Spectrum SPF 30 Lotion was applied on top of the 3M Transpore Tape. 3M Transpore Tape was used as an in vitro skin substrate recommended by the FDA.⁵⁷ The 10 mg of sunscreen applied on top of the 3M

Transpore Tape was roughly ten times the FDA recommended value 0.75 mg/cm^2 of sunscreen⁵⁷ in order to ensure complete covering of the UV sensor surface. Equate Sport Broad Spectrum SPF 30 Lotion sunscreen was used for both tests.

302 nm SPF 30 Testing

A schematic of the experimental setup and a photographic image of the experimental setup for the 302 nm UV test are given in Figure 6.1.a. and 6.1.b. Two stacked filter paper squares were used as a UV blocker for this test. The glass substrate used was an inverted watch glass to provide a non-uniform distribution of light to the UV sensors. This preparation setup was exposed to 302 nm UV radiation for various time durations from an hour to about 26 hours.

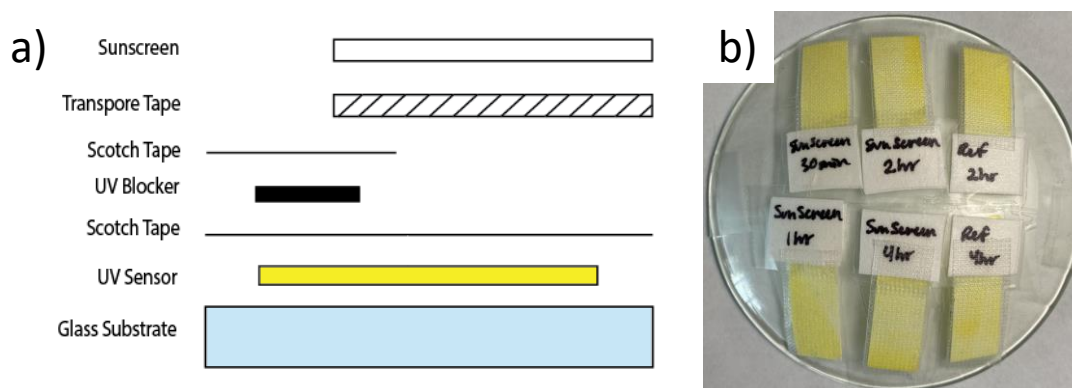


Figure 6.1. a) schematic and b) picture of experimental setup of 302 nm UV light SPF 30 sunscreen test.

The results of the 302 nm UV light sunscreen test are shown in Figure 6.2. Figure 6.2.a. and 6.2.b. represent the reference sensors with no sunscreen applied and were exposed to 2 and 4 hours of 302 nm UV light respectively. It should be noted that the reference samples did have a layer of 3M Transpore Tape applied. The next three sensors shown in Figure 6.2.c-e. were UV sensors with SPF 30 sunscreen applied. Their 302 nm UV exposure was 1 hour, 2 hours, and 26 hours respectfully. The two reference samples turned to a dark brown color upon

exposure to UV radiation with no noticeable difference between the 2 and 4 hour exposure times. This is in line with the experiment results obtained for solid-state UV sensors fabricated with 6-CF and BiCl_3 and discussed in Chapter 2. However, the 1 hour, 2 hour, and 26 hour sensors covered in sunscreen showed no discernible color change on heavily applied areas. However, the 3M tape showed dark spots in the convex regions of the 3M Transpore Tape that could be possible due to the edges of the mesh like 3M tape receiving/retaining lower sunscreen application. The dark spots in the 26 hour sunscreen sensor has considerably darker spots compared to the other two sensors. This could be due to the convex region retaining less sunscreen than the concave regions. Nevertheless, we did not try to reduce the sunscreen applied and repeat these measurements as the disparity between concave and convex region may increase. Figure 6.2.b. and 6.2.e. show a large amount of darkening in the area that was supposed to be covered and unexposed. This can be attributed to the inverted watch glass scattering the UV light and the poor UV blocking of two filter paper squares. This result made it difficult to distinguish the unexposed area from the exposed area but did not affect the results of sunscreen test.

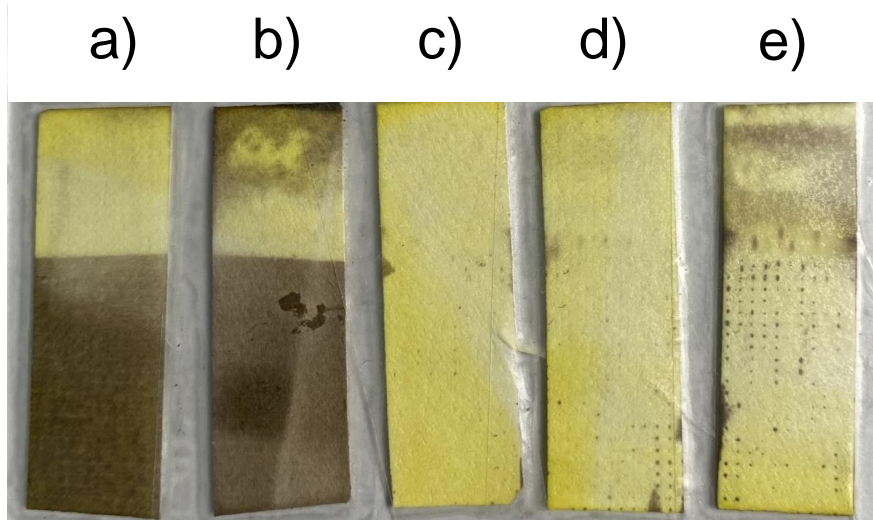


Figure 6.2. 50% 1 mM 6-CF and 100 mM BiCl₃ UV sensor SPF 30 sunscreen test with 302 nm UV light. a) 2 hour and b) 4 hour exposure with no sunscreen. c) 1 hour, d) 2 hour, and e) 26 hour exposure with sunscreen.

Sunlight SFP 30 Testing

A similar sunscreen test was performed on the same 50% 1 mM 6-CF and 100 mM BiCl₃ solid-state sensor under sunlight. Figure 6.3 shows the schematic for the sunlight sunscreen test. A few alterations were made to the 302 nm UV light sunscreen schematic. First, the 3M Transpore Tape was applied over the entire sensor and Scotch Tape. Second, the sunscreen was applied over the entire sensor even the UV blocked section. Third, the previous filter paper UV blocker was applied over the entire sensor even the UV blocked section. Third, the previous filter paper UV blocker was replaced with a metal square as the UV blocker. Finally, the inverted glass substrate was replaced with a glass slide. These changes to the schematic were expected to help eliminate the backscattered UV exposure on the unexposed area as well as limit the UV reflection seen in the 302 nm UV light sunscreen test.

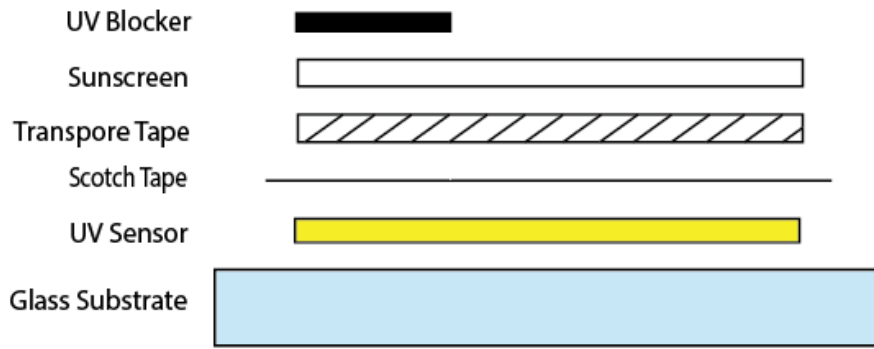


Figure 6.3. Schematic of sunlight SPF 30 sunscreen test.

For the sunlight sunscreen test, five different sunscreen environments were tested, (i) a conventional sensor with no sunscreen applied, (ii) a normal application of Equate Sport Broad Spectrum SPF 30 Lotion on the sensor, (iii) stationary addition of 44.8 mM NaCl in DI water to the sunscreen coated sensor, (iv) stationary addition of DI water to the sunscreen coated sensor, and (v) 2 minute flush of DI water to the sunscreen coated sensor. The 44.8 mM NaCl solution was made to mimic the sodium content in sweat with an average sodium ion concentrations taken from the measured values obtained by Buono et al.⁵⁸ The stationary addition of DI water was meant to simulate the effect of stagnant water on sunscreen and the a 2 minute flush of DI water was meant to simulate the effect of dynamic water on sunscreen. Figure 6.4.a-e. shows the results of the 1 hour sunlight exposure on these sensors and Figure 6.4.f-j. shows the results after 2 hour sunlight exposure on these sensors. Figure 6.4.a. and 6.4.f. are the reference sensors where no sunscreen applied to the sensor. The 2 hour sunlight exposure produced a darker shade of brown than the 1 hour sunlight exposure as expected. Both exposures produced a uniform color change in the exposed area. Figure 6.4.b. and 6.4.g. are the sensors coated with sunscreen and exposed to 1 hour and 2 hours respectively. A slight uniform color change can be seen in both sensors however, the 2 hour sunlight exposure

appears to be slightly darker. Unlike the 302 nm UV light test, no dark spots from the 3M Transpore Tape are present on these sunlight exposed sensors. Figure 6.4.c. and 6.4.h. shows the impact of a stationary sweat solution applied on top of the sunscreen and exposed to sunlight for 1 and 2 hours. The sweat solution appears to have stripped the sunscreen allowing for more sunlight to reach the sensor. Dark spots from the 3M Transpore Tape can be seen as well as a light uniform darkening of the sensor. Figure 6.4.d. and 6.4.i. shows the results obtained for sensors with stationary DI water added to the sunscreen coat and exposed to 1 and 2 hours of sunlight. The 1 hour exposure to sunlight produced a lighter uniform color change than the 1 hour sunlight sweat solution. The 2 hour exposure produced the same uniform color change as the 2 hour sweat solution as well as a noticeable dark spot where the water completely dissolved the sunscreen. Figure 6.4.e. and 6.4.j. shows the impact of a 2 minute DI water flush on the sunscreen coated sensor as well as 1 and 2 hours of sunlight exposure. The 1 hour exposure of the sensor produced the second darkest color change behind the reference, Figure 6.4.f., where no sunscreen was applied on the sensor. The sensor had light spots due to the 3M Transpore Tape's convex regions elevating the sunscreen above the flowing water. The 2 hour sunlight exposure had the same light spots seen in the 1 hour sensor. The color change was slightly lighter than the reference. From this test, we have determined that our 50% 1 mM and 100 mM BiCl_3 filter paper sensor can be used in conjunction with sunscreen to measure UV exposure.

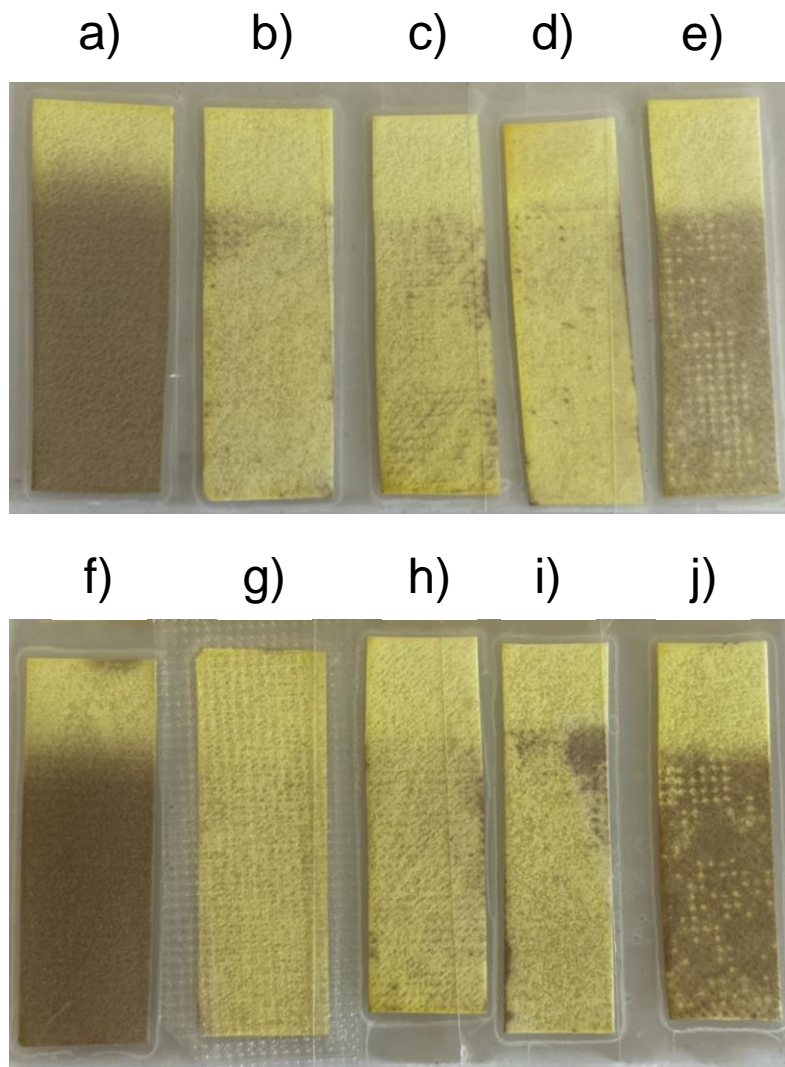


Figure 6.4. 50% 1 mM 6-CF and 100 mM BiCl_3 UV sensor SPF 30 sunscreen test with sunlight. a) 1 hour and f) 2 hour exposure with no sunscreen, b) 1 hour and g) 2 hour exposure with sunscreen, c) 1 hour and h) 2 hour exposure with sunscreen and 44.8 mM NaCl and water solution, d) 1 hour and i) 2 hour exposure with sunscreen and DI water, e) 1 hour and j) 2 hour exposure with sunscreen flushed with DI water for 2 minutes.

Optical Density Measurements on Solid-State Sensors

Colorimetric UV sensors offer a unique, inexpensive method for monitoring UV exposure that can be easily scaled up to be used in a wide variety of applications. For example, utilizing a phone camera, a user can scan the color of the sensor and using an app can easily measure the exposure dosage. The app will determine the optical density of the sensor and relate the measured optical density value to exposure time and dosage of UV radiation. Optical density can be used to measure the amount of color change in any sample and since the darkening in our solid-state UV sensor is directly proportional to the exposure to the UV radiation, it can be used to monitor the UV dosage. We tried to determine a preliminary relationship between optical density and exposure time for our sensors using the 50% 1 mM 6-CF and 100 mM BiCl₃ solid-state sensor. We used a simple and readily available software, ImageJ developed by the National Institutes of Health for calculating the optical density values for our sensors exposed to UV radiation. However, the ImageJ software only measures grayscale values so, a calibration for grayscale values to optical density values was created using Figure 6.5. The optical density value for every step of the Kodak No. 3 Step Tablet were known allowing for a straightforward calibration.

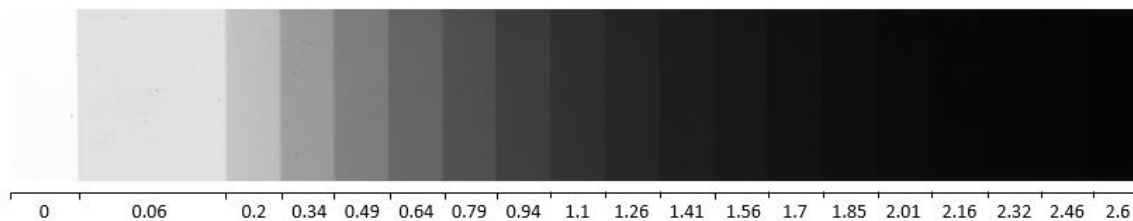


Figure 6.5. Kodak No. 3 Calibrated Step Tablet scanned with an Epson Expression 1680 Professional Scanner. The optical density values are listed below each step.

After the calibration, the solid-state sensor picture were converted to 8-bit grayscale image using ImageJ. Figure 6.6. shows an example of the 8-bit grayscale conversion. This conversion was done in an attempt to mitigate the effects of the iPhone's automatic color correction.



Figure 6.6. 8-bit gray scale conversion of 302 nm solid-state sensor image.

Using the calibration, the optical density values were obtained for the 50% 1 mM 6-CF and 100 mM BiCl₃ solid state sensor exposed to 365 nm light, 302 nm light, 254 nm light, and sunlight. Figure 6.7.a. compares the four different UV exposures' optical density values with respect to exposure time. The 365 nm UV light (black square) showed the slowest optical density increase over the 300 minute time frame ending with a value of 0.383. This 300 minute optical density value is a similar value seen in the 5 minute value for the 302 nm light, 254 nm light, and sunlight measurements. The exposure time and optical density appear to have a linear relationship. The 302 nm UV light (red circle) as well as the sunlight (green diamond) had the fastest optical density increase over a 120 minute period ending with values of 0.766 and 0.795 respectively. Similarly, the 254 UV light (blue triangle) had a slightly slower optical density increase and a sharper plateau between the 60 minute and 120 minute optical density values. The 302 nm UV radiation, 254 nm UV radiation, and sunlight all appear to have a logarithmic relationship between exposure time and optical density because of the tapering seen between the 40 minute, 60 minute and 120 minute optical density values, however longer exposure

times are needed to determine the actual trend. Figure 6.7.b. plots the optical density values as a function of time. The intensity of the UVLMS-38 EL Series 3UV Lamp at 365 nm, 302 nm, and 254 nm were determined to be 0.96 mW/cm², 1.16 mW/cm², and 0.82 mW/cm² respectfully compared to the intensity of sunlight which is approximately 4.61 mW/cm². The 365 nm sensors were exposed to roughly twice the UV dosage but produced the lightest color change. This is likely due to the 350 nm to 375 nm UV absorption edge^{42,43,52,55} associated with BiOCl which resulted in less excitation of BiOCl. The 302 nm sensors produced the second darkest color change after sunlight but with about 10 times less exposure. The 254 nm sensors produced the third darkest color change a could be caused by the low intensity of the 254 nm UV lamp or an upper UV absorption edge that hasn't been discovered. Finally, the sunlight sensors produced the darkest color change over the largest dose. The trend of these data points is a between the 365 nm and 302 nm sensors. This most likely corresponds to the 90%-95% UVA and 5%-10% UVB² present in sunlight as well as sunlight's approximately 10 times larger intensity compared to 254 nm, 302 nm, and 365 nm.

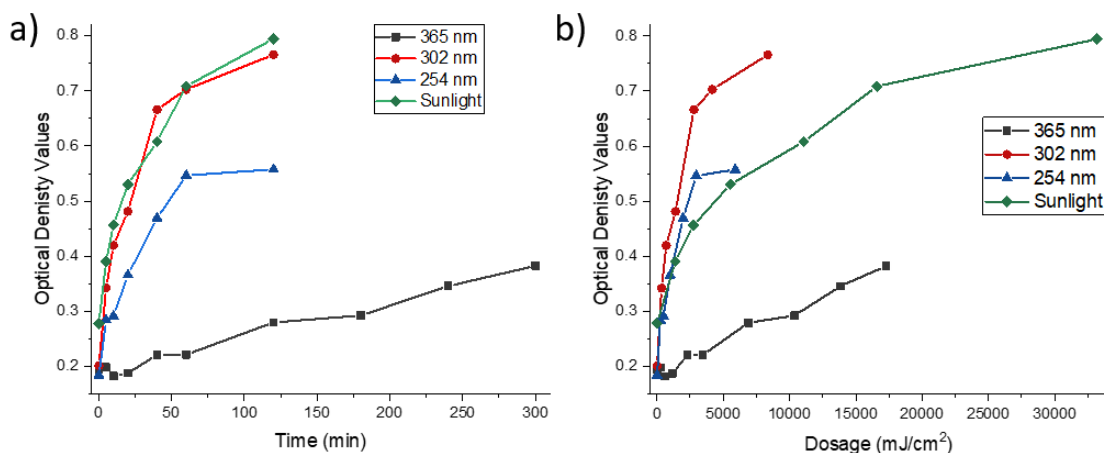


Figure 6.7. Plot of optical density values of 50% 1 mM 6-CF and 100 mM BiCl₃ solid-state sensor when exposed to 365 nm light, 302 nm light, 254 nm light, and sunlight as a function of a) time and b) dosage.

Table 6.1. lists the optical density values with respect to exposure time for all four UV exposures. It should be noted that the solid-state sensors exposed to 365 nm UV radiation were purposely exposed for 5 hours due to the slight color change induced by this UV wavelength. The solid-state sensors exposed to 254 nm, 302 nm, and sunlight UV radiation induced a significant color change after 2 hours therefore the sensors were not exposed to any additional UV radiation.

Table 6.1. Optical density values of 50% 1 mM 6-CF and 100 mM BiCl₃ solid-state UV sensor Exposed to 365 nm, 302 nm, 254 nm, and sunlight.

Time (min)	365 nm
0	0.195
5	0.198
10	0.182
20	0.188
40	0.221
60	0.221
120	0.280
180	0.293
240	0.346
300	0.383

Time (min)	302 nm	254 nm	Sunlight
0	0.201	0.184	0.278
5	0.343	0.284	0.391
10	0.420	0.291	0.457
20	0.482	0.366	0.531
40	0.666	0.469	0.608
60	0.703	0.547	0.709
120	0.766	0.558	0.795

Following the 50% 1 mM 6-CF and 100 mM BiCl₃ optical density measurements, we wanted to achieve a darker color change in our sensor since the previous sensors only achieved a maximum optical density of 0.795. A new solid-state sensor was prepared using 500 mM BiCl₃ dissolved in ethanol without 6-CF. Similar to past solid-state sensors, filter paper squares were soaked in the solution for 5 minutes and dried at room temperature. Figure 6.8.a. is a photo of the 500 mM BiCl₃ solid-state sensors after exposure to 302 nm UV light while Figure 6.8.b. is a plot of the optical density values with respect to exposure time for two tests. After 40 minutes, it appears like no further color change occurred in our sensors however, looking at the optical

density plot an optical density increase can be seen up to the maximum UV exposure time of 300 minutes. An odd trend is seen in the optical density plots where the 10 minute has a slightly higher optical density value than the 20 minute value. The same is seen for the 40 minute and 60 minute optical density values. After 60 minutes a slight increase in the optical density values is seen. It is unclear what is causing this dip in optical density, but it could be due to the placement of the sensor under the UV lamp or with the preparation of the sensor. Overall, a higher optical density value was achieved for the 500 mM BiCl_3 solid-state sensor.

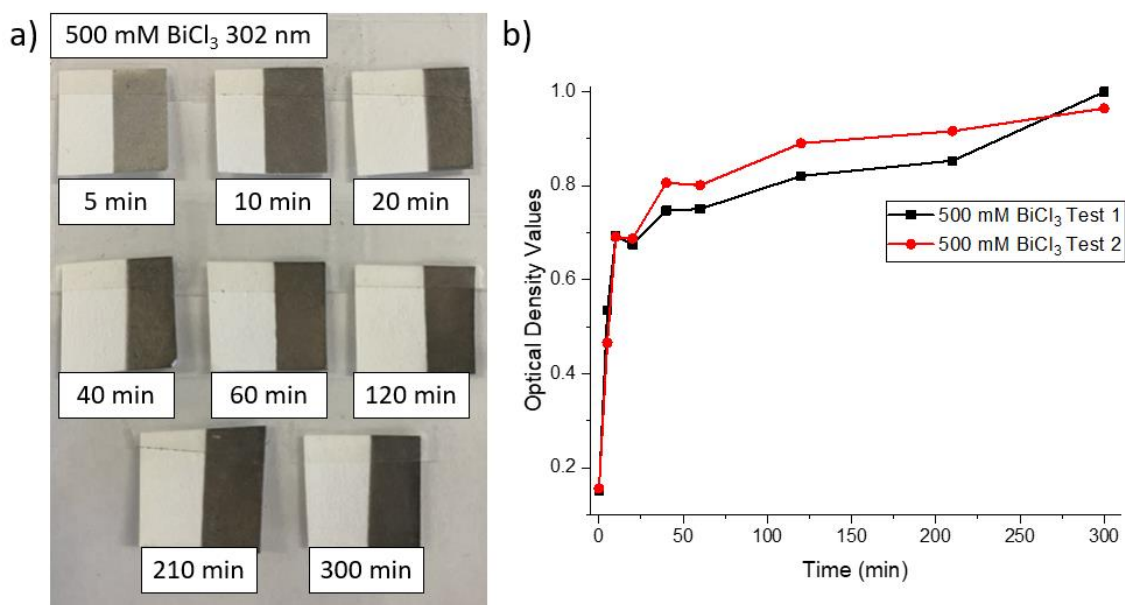




Figure 6.8. a) Filter paper squares soaked in 500 mM BiCl_3 and ethanol exposed to 302 nm UV light for various durations. b) Plot of optical density values with respect to 302 nm exposure time.

Chapter 7:

Conclusion

Long term UV exposure is known to cause many adverse effects such as sunburn, weakening of the immune system, and skin cancer.^{1,2} Therefore, UV monitoring along with UV protecting clothing and sunscreen can mitigate these adverse effects. Currently, photodiode UV sensors such as ZnO and TiO₂ are currently being researched however, their high production cost and required external monitoring tools limit the consumer range. On the other hand, current colorimetric UV sensors that use polydiacetylene or a phenylsulfonium indicator have poor chemical stability as well as chemical hazards associated with them. Three commercial UV dosimeters are compared in Table 7.1. PCE Americas Inc. offers a UVA and UVB light meter for \$224.00 while Grainger Industrial Supply offers a UVA and UVC light meter for \$896.00. The advantage of these dosimeters are the reusability and portable design, but they are expensive. Atlantic Ultraviolet Corporation supplies UVC dosimeter cards for \$5.20 per card. This dosimeter changes color based on UV irradiation, are not reusable, and only function under 254 nm UVC radiation. Currently, these UVC dosimeter cards are the only commercial colorimetric dosimeters with no commercial colorimetric dosimeters available for detecting UVA and UVB radiation.

Table 7.1. Comparison of three different commercial UV dosimeters, PCE-UV34 Light Meter, Grainger UV Light Meter, and UVC Dosimeters UVC 254 TRI Card

Dosimeter	PCE-UV34 Light Meter	Grainger UV Light Meter	UVC Dosimeters UVC 254 TRI Card
			
Measured UV	UVA and UVB	UVA and UVC	UVC
Price	\$224.00	\$896.00	\$5.20 per card

Our BiCl₃ solution state sensors were prepared and analyzed with 6-carboxyfluorescein (6-CF), 5-carboxyfluorescein (5-CF), prussian blue (PB), and rhodamine-b (RhB) dyes. The 6-CF and 5-CF based sensors produced fine black BiOCl particles under long exposure to sunlight and 302 nm UV radiation in solution. These sensors also showed a decrease in the 450 nm UV absorption peak associated with 6-CF and 5-CF. This is likely due to the increased opacity by BiOCl particles suspension in solution. The 0.1 mM and 1 mM PB/ethanol solutions had negative UV absorption 300 nm to 600 nm range. A 0.01 mM PB solution state sensor was tested to avoid this negative absorption range however, the changes in UV absorption were very slight. Our RhB solution state sensor's pink color faded completely upon UV exposure to produce a colorless solution and a black precipitate. The precipitate contained about 56.9 wt% Bi metal and 43.1 wt% BiOCl. The faded color as well as the elimination of UV absorption peaks associated with RhB is due to the excited BiOCl transferring energy to RhB. The RhB is most likely the cause for the reduction of some of the BiOCl to metallic Bi.

Our BiCl_3 solid-state sensors were prepared using the same dyes, 6-CF, 5-CF, PB and RhB. It was observed that BiCl_3 alone was able to produce a color change upon UV exposure while the use of dye helped produce a larger color contrast rather than being a UV sensing material. Both 6-CF and 5-CF solid-state sensors produced a yellow to brown color transition after UV exposure. The 6-CF solid-state UV sensor was more sensitive to UVB and UVC radiation while exposure to UVA radiation underwent a slower color change. The PB solid-state sensor produce a blue to brown color change under 302 nm UV radiation but lacked the contrast to determine a color change between 20 minutes and 120 minutes. Finally, the RhB solid-state sensor produced a purple to brown color change. The RhB sensor was slightly easier to determine a color change between short and long UV exposure than the PB sensor however, smaller intervals (10-20 minutes) were difficult. Ultimately, 6-CF provided the best color contrast out of the dyes researched. Two practical applications were assessed using the 6-CF solid-state sensor, a sunscreen efficiency test under 302 nm UV radiation and sunlight as well as optical density measurements. For the sunscreen efficiency tests, 10 mg of SPF 30 sunscreen was placed on top of 3M Transpore tape that covered the sensor. A slight color change was seen in our sensors under 302 nm UV light while a larger color change was seen under sunlight. The optical density of the 6-CF solid-state sensor was measured for each exposure time. As expected, UVA radiation produced the lowest optical density values and appeared to have a linear relationship with respect to time. UVC radiation surprisingly produced the second lowest optical density values with sunlight and UVB radiation produced the largest optical density values. UVB, UVC, and sunlight appears to have a logarithmic relationship between optical density and exposure time. Figure 7.1. illustrates a potential phone app that measures the optical density of the solid-state UV sensor and relates the value to exposure time.

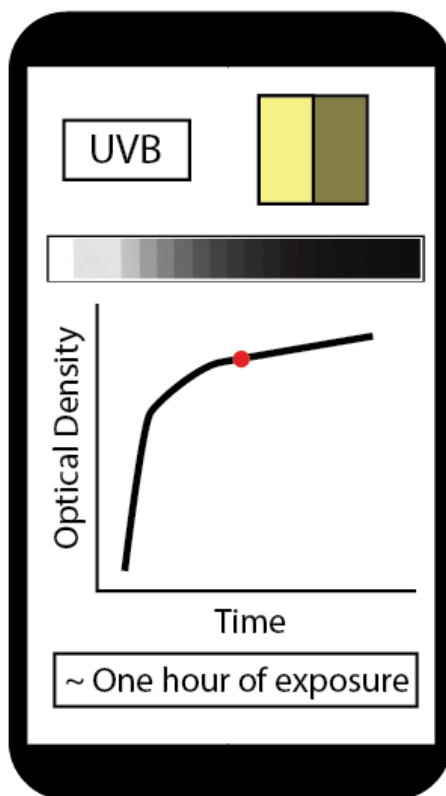


Figure 7.1. Illustration of an application that relates the optical density of a solid-state sensor to the duration of UV exposure.

Our UV sensor mechanism involves the spontaneous hydrolysis of BiCl_3 in ethanol to produce BiOCl and the excitation of BiOCl under UV radiation to produce a black precipitate in our solution state sensors and a brown color change in our solid-state sensors. In the presence of RhB and UV radiation, BiOCl is reduced to Bi metal along with the degradation of RhB. The BiCl_3 hydrolysis produced BiOCl orientated along the (001) plane. Further optical density measurements are needed under UVA, UVB, UVC, and sunlight to better relate the values to exposure time. Additional research into other dyes could lead to a better contrast than the 6-CF. In conclusion, BiOCl colorimetric UV sensors are a viable and cost-effective sensor for monitoring UV radiation with limited commercial competitors.

Appendix A:

Reference UV-Vis Absorption Spectrums

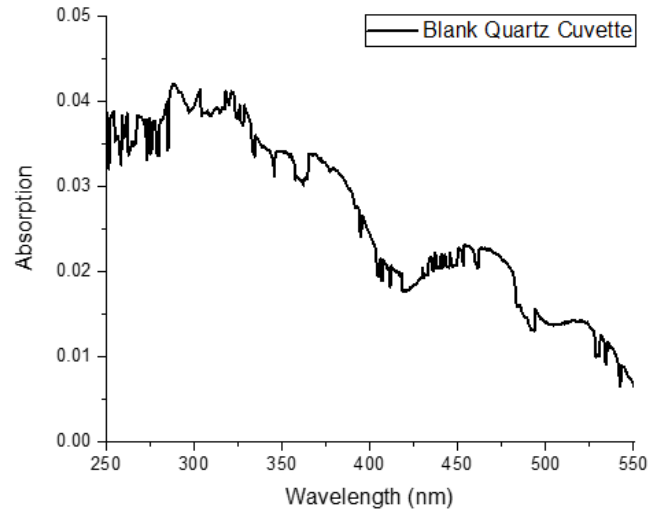


Figure A1. UV absorption spectrum of blank quartz cuvette.

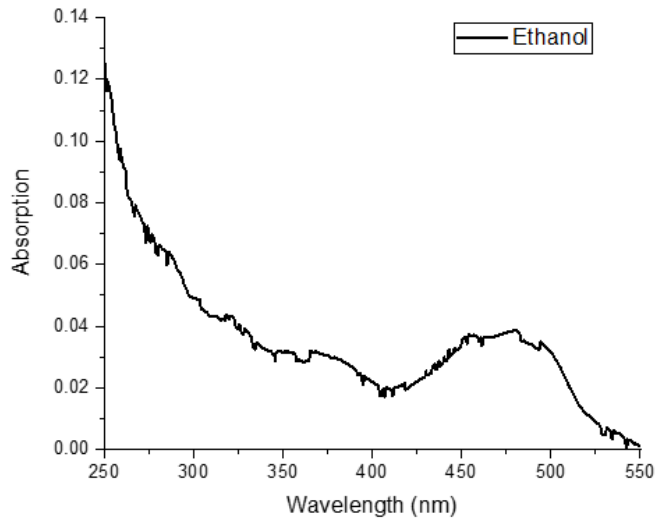


Figure A2. UV absorption spectrum of ethanol.

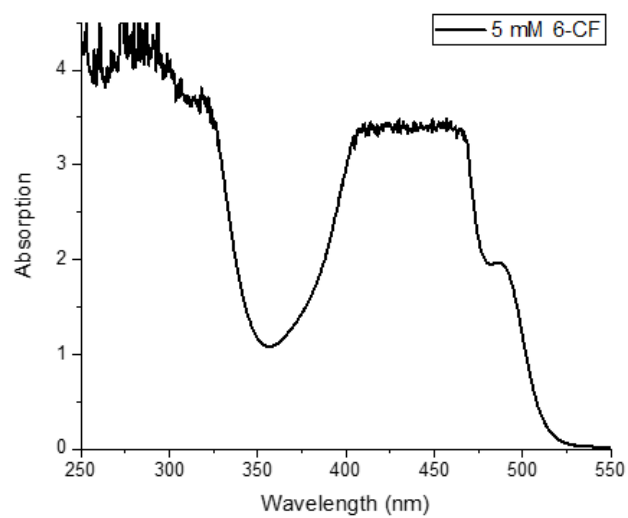


Figure A3. UV absorption spectrum of as prepared 5 mM 6-CF in ethanol.

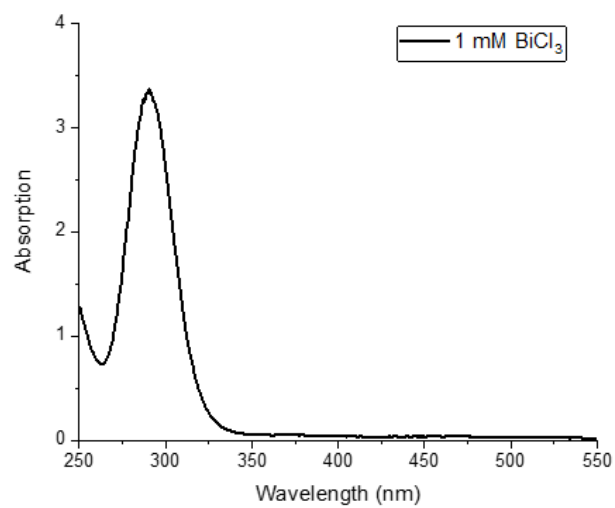


Figure A4. UV absorption spectrum of as prepared 1 mM BiCl₃ in ethanol.

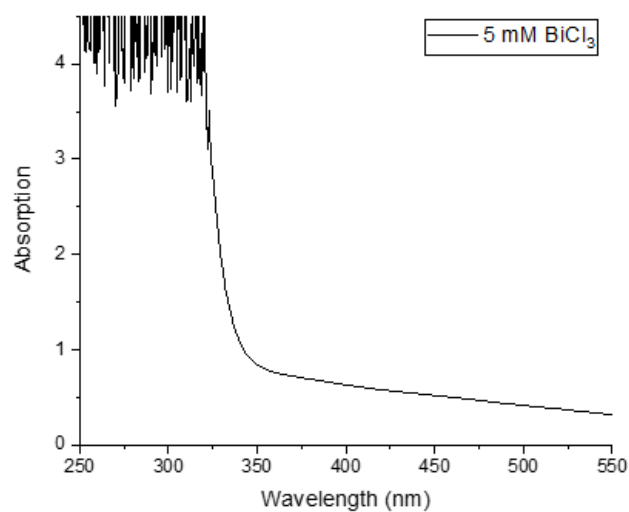


Figure A5. UV absorption spectrum of as prepared 5 mM BiCl_3 in ethanol.

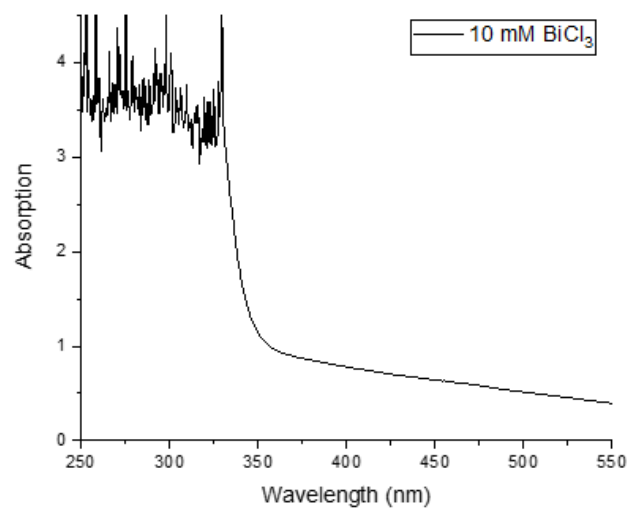


Figure A6. UV absorption spectrum of as prepared 10 mM BiCl_3 in ethanol.

Appendix B:

6-CF Fluorescence and Frontier Molecular Orbitals

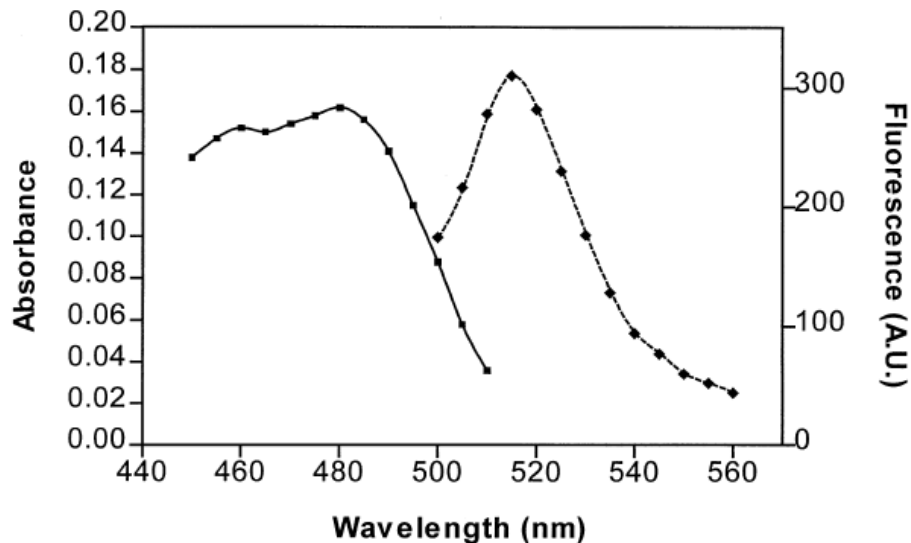


Figure B1. Absorption and emission spectra of 6-CF. The absorption spectrum is represented by the solid line while the emission spectrum is represented by the dashed line. This Figure was reused from the Massou et al. article regarding carboxyfluorescein fluorescence experiments.³⁶

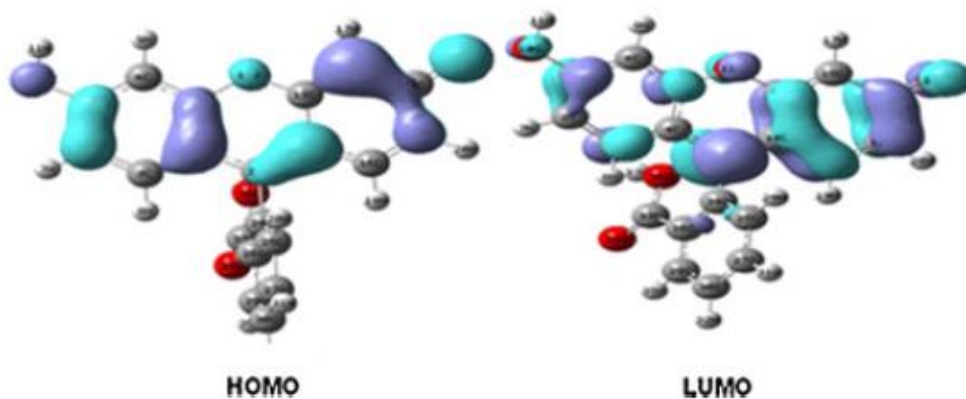


Figure B2. HOMO and LUMO frontier molecular orbitals of fluorescein. This Figure was reused from the Alvarado-González et al. article regarding a DFT study of the interaction between the conjugated fluorescein and dabcyll system.³⁵

Appendix C:

Tauc Plot for 100 mM BiCl₃

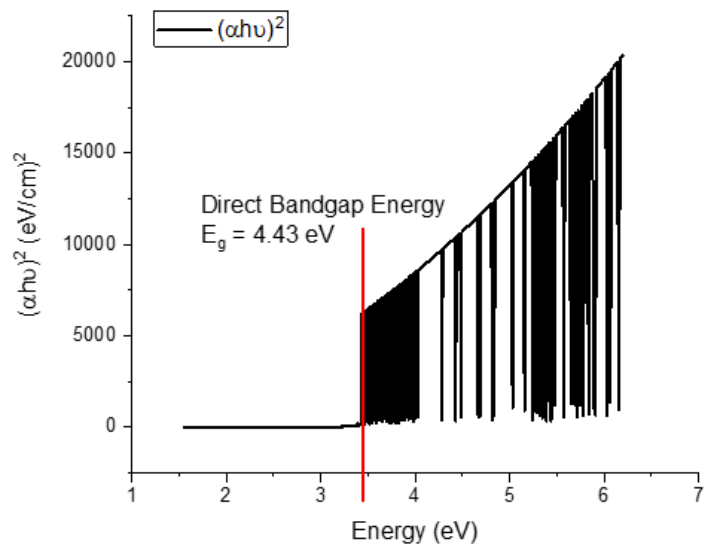


Figure C1. UV absorption spectrum of as prepared 5 mM 6-CF in ethanol.

References

- (1) Yan, J.; Wang, L.; Fu, P. P.; Yu, H. Photomutagenicity of 16 Polycyclic Aromatic Hydrocarbons from the US EPA Priority Pollutant List. *Mutat. Res. Toxicol. Environ. Mutagen.* **2004**, *557* (1), 99–108. <https://doi.org/10.1016/j.mrgentox.2003.10.004>.
- (2) D’Orazio, J.; Jarrett, S.; Amaro-Ortiz, A.; Scott, T. UV Radiation and the Skin. *Int. J. Mol. Sci.* **2013**, *14* (6), 12222–12248. <https://doi.org/10.3390/ijms140612222>.
- (3) Abidi, N.; Hequet, E.; Tarimala, S.; Dai, L. L. Cotton Fabric Surface Modification for Improved UV Radiation Protection Using Sol–Gel Process. *J. Appl. Polym. Sci.* **2007**, *104* (1), 111–117. <https://doi.org/10.1002/app.24572>.
- (4) Bai, S.; Wu, W.; Qin, Y.; Cui, N.; Bayerl, D. J.; Wang, X. High-Performance Integrated ZnO Nanowire UV Sensors on Rigid and Flexible Substrates. *Adv. Funct. Mater.* **2011**, *21* (23), 4464–4469. <https://doi.org/10.1002/adfm.201101319>.
- (5) Gedamu, D.; Paulowicz, I.; Kaps, S.; Lupan, O.; Wille, S.; Haidarschin, G.; Mishra, Y. K.; Adelung, R. Rapid Fabrication Technique for Interpenetrated ZnO Nanotetrapod Networks for Fast UV Sensors. *Adv. Mater.* **2014**, *26* (10), 1541–1550. <https://doi.org/10.1002/adma.201304363>.
- (6) Ngampeungpis, W.; Tumcharern, G.; Pienpinijtham, P.; Sukwattanasinitt, M. Colorimetric UV Sensors with Tunable Sensitivity from Diacetylenes. *Dyes Pigments* **2014**, *101*, 103–108. <https://doi.org/10.1016/j.dyepig.2013.09.033>.
- (7) Pankaew, A.; Traiphol, N.; Traiphol, R. Tuning the Sensitivity of Polydiacetylene-Based Colorimetric Sensors to UV Light and Cationic Surfactant by Co-Assembling with Various Polymers. *Colloids Surf. Physicochem. Eng. Asp.* **2021**, *608*, 125626. <https://doi.org/10.1016/j.colsurfa.2020.125626>.
- (8) Araki, H.; Kim, J.; Zhang, S.; Banks, A.; Crawford, K. E.; Sheng, X.; Gutruf, P.; Shi, Y.; Pielak, R. M.; Rogers, J. A. Materials and Device Designs for an Epidermal UV Colorimetric Dosimeter with Near Field Communication Capabilities. *Adv. Funct. Mater.* **2017**, *27* (2), 1604465. <https://doi.org/10.1002/adfm.201604465>.
- (9) Kurz, W.; Yetisen, A. K.; Kaito, M. V.; Fuchter, M. J.; Jakobi, M.; Elsner, M.; Koch, A. W. UV-Sensitive Wearable Devices for Colorimetric Monitoring of UV Exposure. *Adv. Opt. Mater.* **2020**, *8* (6), 1901969. <https://doi.org/10.1002/adom.201901969>.
- (10) Liu, J.; Liang, Y.; Wang, L.; Wang, B.; Zhang, T.; Yi, F. Fabrication and Photosensitivity of CdS Photoresistor on Silica Nanopillars Substrate. *Mater. Sci. Semicond. Process.* **2016**, *56*, 217–221. <https://doi.org/10.1016/j.mssp.2016.08.024>.
- (11) Okhonin, S.; Gureev, M.; Sallin, D.; Appel, J.; Koukab, A.; Kvasov, A.; Pastre, M.; Polzik, E. S.; Tagantsev, A. K.; Uddegard, F.; Kayal, M. A Dynamic Operation of a PIN Photodiode. *Appl. Phys. Lett.* **2015**, *106* (3), 031115. <https://doi.org/10.1063/1.4906488>.
- (12) Klingshirn, C. The Luminescence of ZnO under High One- and Two-Quantum Excitation. *Phys. Status Solidi B* **1975**, *71* (2), 547–556. <https://doi.org/10.1002/pssb.2220710216>.
- (13) Jin, Y.; Wang, J.; Sun, B.; Blakesley, J. C.; Greenham, N. C. Solution-Processed Ultraviolet Photodetectors Based on Colloidal ZnO Nanoparticles. *Nano Lett.* **2008**, *8* (6), 1649–1653. <https://doi.org/10.1021/nl0803702>.

- (14) Xu, Q.; Cheng, L.; Meng, L.; Wang, Z.; Bai, S.; Tian, X.; Jia, X.; Qin, Y. Flexible Self-Powered ZnO Film UV Sensor with a High Response. *ACS Appl. Mater. Interfaces* **2019**, *11* (29), 26127–26133. <https://doi.org/10.1021/acsami.9b09264>.
- (15) Cao, C.; Hu, C.; Wang, X.; Wang, S.; Tian, Y.; Zhang, H. UV Sensor Based on TiO₂ Nanorod Arrays on FTO Thin Film. *Sens. Actuators B Chem.* **2011**, *156* (1), 114–119. <https://doi.org/10.1016/j.snb.2011.03.080>.
- (16) Xu, X.; Chen, J.; Cai, S.; Long, Z.; Zhang, Y.; Su, L.; He, S.; Tang, C.; Liu, P.; Peng, H.; Fang, X. A Real-Time Wearable UV-Radiation Monitor Based on a High-Performance p-CuZnS/n-TiO₂ Photodetector. *Adv. Mater.* **2018**, *30* (43), 1803165. <https://doi.org/10.1002/adma.201803165>.
- (17) Kumar, S. G.; Rao, K. S. R. K. Comparison of Modification Strategies towards Enhanced Charge Carrier Separation and Photocatalytic Degradation Activity of Metal Oxide Semiconductors (TiO₂, WO₃ and ZnO). *Appl. Surf. Sci.* **2017**, *391*, 124–148. <https://doi.org/10.1016/j.apsusc.2016.07.081>.
- (18) Liu, W.-W.; Peng, R.-F. Recent Advances of Bismuth Oxychloride Photocatalytic Material: Property, Preparation and Performance Enhancement. *J. Electron. Sci. Technol.* **2020**, *18* (2), 100020. <https://doi.org/10.1016/j.jnlest.2020.100020>.
- (19) Hou, J.; Dai, D.; Wei, R.; Wu, X.; Wang, X.; Tahir, M.; Zou, J.-J. Narrowing the Band Gap of BiOCl for the Hydroxyl Radical Generation of Photocatalysis under Visible Light. *ACS Sustain. Chem. Eng.* **2019**, *7* (19), 16569–16576. <https://doi.org/10.1021/acssuschemeng.9b03885>.
- (20) Koc, H.; Akkus, H.; Mamedov, A. M. Band Structure and Optical Properties of BiOCl: Density Functional Calculation. **2012**, *9*.
- (21) Guo, M.; Zhou, Z.; Yan, S.; Zhou, P.; Miao, F.; Liang, S.; Wang, J.; Cui, X. Bi₂WO₆–BiOCl Heterostructure with Enhanced Photocatalytic Activity for Efficient Degradation of Oxytetracycline. *Sci. Rep.* **2020**, *10* (1), 18401. <https://doi.org/10.1038/s41598-020-75003-x>.
- (22) Náfrádi, M.; Hernadi, K.; Kónya, Z.; Alapi, T. Investigation of the Efficiency of BiOI/BiOCl Composite Photocatalysts Using UV, Cool and Warm White LED Light Sources - Photon Efficiency, Toxicity, Reusability, Matrix Effect, and Energy Consumption. *Chemosphere* **2021**, *280*, 130636. <https://doi.org/10.1016/j.chemosphere.2021.130636>.
- (23) Bárdos, E.; Márta, V. A.; Fodor, S.; Kedves, E.-Z.; Hernadi, K.; Pap, Z. Hydrothermal Crystallization of Bismuth Oxychlorides (BiOCl) Using Different Shape Control Reagents. *Materials* **2021**, *14* (9), 2261. <https://doi.org/10.3390/ma14092261>.
- (24) Jonas, U.; Shah, K.; Norvez, S.; Charych, D. H. Reversible Color Switching and Unusual Solution Polymerization of Hydrazide-Modified Diacetylene Lipids. *J. Am. Chem. Soc.* **1999**, *121* (19), 4580–4588. <https://doi.org/10.1021/ja984190d>.
- (25) Yuan, W.; Jiang, G.; Song, Y.; Jiang, L. Micropatterning of Polydiacetylene Based on a Photoinduced Chromatic Transition and Mechanism Study. *J. Appl. Polym. Sci.* **2007**, *103* (2), 942–946. <https://doi.org/10.1002/app.25256>.
- (26) Han, J.-M.; Xu, M.; Wang, B.; Wu, N.; Yang, X.; Yang, H.; Salter, B. J.; Zang, L. Low Dose Detection of γ Radiation via Solvent Assisted Fluorescence Quenching. *J. Am. Chem. Soc.* **2014**, *136* (13), 5090–5096. <https://doi.org/10.1021/ja500262n>.
- (27) Boyle, T.; Garzon, F. Colorimetric Radiation Detector. US 2020/0257004 A1, August 13, 2020.

- (28) Shahbazi, M.-A.; Faghfour, L.; Ferreira, M. P. A.; Figueiredo, P.; Maleki, H.; Sefat, F.; Hirvonen, J.; Santos, H. A. The Versatile Biomedical Applications of Bismuth-Based Nanoparticles and Composites: Therapeutic, Diagnostic, Biosensing, and Regenerative Properties. *Chem. Soc. Rev.* **2020**, *49* (4), 1253–1321. <https://doi.org/10.1039/C9CS00283A>.
- (29) Bartoli, M.; Jagdale, P.; Tagliaferro, A. A Short Review on Biomedical Applications of Nanostructured Bismuth Oxide and Related Nanomaterials. *Materials* **2020**, *13* (22), 5234. <https://doi.org/10.3390/ma13225234>.
- (30) 6-Carboxyfluorescein; MSDS No. 3301-79-9, 2020.
- (31) Parish, C. R. Fluorescent Dyes for Lymphocyte Migration and Proliferation Studies. *Immunol. Cell Biol.* **1999**, *77* (6), 499–508. <https://doi.org/10.1046/j.1440-1711.1999.00877.x>.
- (32) Schneider, C. A.; Rasband, W. S.; Eliceiri, K. W. NIH Image to ImageJ: 25 Years of Image Analysis. *Nat. Methods* **2012**, *9* (7), 671–675. <https://doi.org/10.1038/nmeth.2089>.
- (33) Breeuwer, P.; Drocourt, J.; Rombouts, F. M.; Abee, T. A Novel Method for Continuous Determination of the Intracellular PH in Bacteria with the Internally Conjugated Fluorescent Probe 5 (and 6-)Carboxyfluorescein Succinimidyl Ester. *Appl. Environ. Microbiol.* **1996**, *62* (1), 178–183. <https://doi.org/10.1128/aem.62.1.178-183.1996>.
- (34) International Organization for Standardization. Solar Energy — Reference Solar Spectral Irradiance at the Ground at Different Receiving Conditions — Part 1: Direct Normal and Hemispherical Solar Irradiance for Air Mass 1,5 (ISO 9845-1:1992), 1992.
- (35) Alvarado-González, M.; Gallo, M.; Lopez-Albarran, P.; Flores-Holguín, N.; Glossman-Mitnik, D. DFT Study of the Interaction between the Conjugated Fluorescein and Dabcyl System, Using Fluorescence Quenching Method. *J. Mol. Model.* **2012**, *18* (9), 4113–4120. <https://doi.org/10.1007/s00894-012-1413-4>.
- (36) Massou, S.; Albigot, R.; Prats, M. Carboxyfluorescein Fluorescence Experiments. *Biochem. Educ.* **2000**, *28* (3), 171–173. [https://doi.org/10.1016/S0307-4412\(00\)00002-9](https://doi.org/10.1016/S0307-4412(00)00002-9).
- (37) Stolte, M.; Suraru, S.-L.; Diemer, P.; He, T.; Burschka, C.; Zschieschang, U.; Klauk, H.; Würthner, F. Diketopyrrolopyrrole Organic Thin-Film Transistors: Impact of Alkyl Substituents and Tolerance of Ethylhexyl Stereoisomers. *Adv. Funct. Mater.* **2016**, *26* (41), 7415–7422. <https://doi.org/10.1002/adfm.201602994>.
- (38) Garg, S.; Ma, T.; Miller, C. J.; Waite, T. D. Mechanistic Insights into Free Chlorine and Reactive Oxygen Species Production on Irradiation of Semiconducting Silver Chloride Particles. *J. Phys. Chem. C* **2014**, *118* (46), 26659–26670. <https://doi.org/10.1021/jp5068878>.
- (39) Guo, J.; Zhao, W.; Xiong, D.; Ye, Y.; Li, S.; Zhang, B. A Hydrolysis Synthesis Route for (001)/(102) Coexposed BiOCl Nanosheets with High Visible Light-Driven Catalytic Performance. *New J. Chem.* **2021**, *45* (42), 19996–20006. <https://doi.org/10.1039/D1NJ03961J>.
- (40) Liu, X.; Fan, C.; Wang, Y.; Wang, Y.; Zhang, X.; Liang, Z. Low Temperature Preparation of Flower-like BiOCl Film and Its Photocatalytic Activity. *Sci. China Chem.* **2012**, *55* (11), 2438–2444. <https://doi.org/10.1007/s11426-012-4549-2>.

- (41) Shi, Z.; Wang, Y.; Fan, C.; Wang, Y.; Ding, G. Preparation and Photocatalytic Activity of BiOCl Catalyst. *Trans. Nonferrous Met. Soc. China* **2011**, *21* (10), 2254–2258. [https://doi.org/10.1016/S1003-6326\(11\)61004-2](https://doi.org/10.1016/S1003-6326(11)61004-2).
- (42) Myung, Y.; Wu, F.; Banerjee, S.; Park, J.; Banerjee, P. Electrical Conductivity of P-Type BiOCl Nanosheets. *Chem. Commun.* **2015**, *51* (13), 2629–2632. <https://doi.org/10.1039/C4CC09295C>.
- (43) Yan, Y.; Yang, H.; Yi, Z.; Xian, T. NaBH₄-Reduction Induced Evolution of Bi Nanoparticles from BiOCl Nanoplates and Construction of Promising Bi@BiOCl Hybrid Photocatalysts. *Catalysts* **2019**, *9* (10), 795. <https://doi.org/10.3390/catal9100795>.
- (44) Zhang, H.; Ma, Y.; Quan, F.; Huang, J.; Jia, F.; Zhang, L. Selective Electro-Reduction of CO₂ to Formate on Nanostructured Bi from Reduction of BiOCl Nanosheets. *Electrochem. Commun.* **2014**, *46*, 63–66. <https://doi.org/10.1016/j.elecom.2014.06.013>.
- (45) Shashikanth, J.; Shashank, M.; Sumedha, H. N.; Alharthi, F. A.; Nizam, A.; Reddy, M.; Nagaraju, G. Tamarindusindica Mediated Combustion Synthesis of BiOCl: Photocatalytic Degradation of Dyes and Synthesis of β -Enaminones. *J. Electron. Mater.* **2021**, *50* (8), 4650–4662. <https://doi.org/10.1007/s11664-021-08994-6>.
- (46) Li, Y.; Zhao, Z.; Song, Z.; Wan, R.; Qiu, J.; Yang, Z.; Yin, Z.; Liu, X.; Liu, Q.; Zhou, Y. Far-Red-Emitting BiOCl:Eu³⁺ Phosphor with Excellent Broadband NUV-Excitation for White-Light-Emitting Diodes. *J. Am. Ceram. Soc.* **2015**, *98* (7), 2170–2176. <https://doi.org/10.1111/jace.13589>.
- (47) Ye, L.; Deng, K.; Xu, F.; Tian, L.; Peng, T.; Zan, L. Increasing Visible-Light Absorption for Photocatalysis with Black BiOCl. *Phys Chem Chem Phys* **2012**, *14* (1), 82–85. <https://doi.org/10.1039/C1CP22876E>.
- (48) Li, Y.; Li, C.; Zhang, Z.; Zhang, Y.; Sun, X.; Si, H.; Zhang, J. Black BiOCl with Disorder Surface Structure Prepared by Fe Reduction and the Enhanced Photocatalytic Activity. *Solid State Sci.* **2014**, *34*, 107–112. <https://doi.org/10.1016/j.solidstatesciences.2014.05.011>.
- (49) Zhao, H.; Liu, X.; Dong, Y.; Xia, Y.; Wang, H. A Special Synthesis of BiOCl Photocatalyst for Efficient Pollutants Removal: New Insight into the Band Structure Regulation and Molecular Oxygen Activation. *Appl. Catal. B Environ.* **2019**, *256*, 117872. <https://doi.org/10.1016/j.apcatb.2019.117872>.
- (50) Chai, S. Y.; Kim, Y. J.; Jung, M. H.; Chakraborty, A. K.; Jung, D.; Lee, W. I. Heterojunctioned BiOCl/Bi₂O₃, a New Visible Light Photocatalyst. *J. Catal.* **2009**, *262* (1), 144–149. <https://doi.org/10.1016/j.jcat.2008.12.020>.
- (51) Chen, F.; Liu, H.; Bagwasi, S.; Shen, X.; Zhang, J. Photocatalytic Study of BiOCl for Degradation of Organic Pollutants under UV Irradiation. *J. Photochem. Photobiol. Chem.* **2010**, *215* (1), 76–80. <https://doi.org/10.1016/j.jphotochem.2010.07.026>.
- (52) Zhang, K.; Liu, C.; Huang, F.; Zheng, C.; Wang, W. Study of the Electronic Structure and Photocatalytic Activity of the BiOCl Photocatalyst. *Appl. Catal. B Environ.* **2006**, *68* (3–4), 125–129. <https://doi.org/10.1016/j.apcatb.2006.08.002>.
- (53) Chang, X.; Gondal, M. A.; Al-Saadi, A. A.; Ali, M. A.; Shen, H.; Zhou, Q.; Zhang, J.; Du, M.; Liu, Y.; Ji, G. Photodegradation of Rhodamine B over Unexcited Semiconductor Compounds of BiOCl and BiOBr. *J. Colloid Interface Sci.* **2012**, *377* (1), 291–298. <https://doi.org/10.1016/j.jcis.2012.03.021>.

- (54) Li, G.; Jiang, B.; Xiao, S.; Lian, Z.; Zhang, D.; Yu, J. C.; Li, H. An Efficient Dye-Sensitized BiOCl Photocatalyst for Air and Water Purification under Visible Light Irradiation. *Env. Sci Process. Impacts* **2014**, *16* (8), 1975–1980. <https://doi.org/10.1039/C4EM00196F>.
- (55) Li, Z.; Ma, B.; Zhang, X.; Sang, Y.; Liu, H. One-Pot Synthesis of BiOCl Nanosheets with Dual Functional Carbon for Ultra-Highly Efficient Photocatalytic Degradation of RhB. *Environ. Res.* **2020**, *182*, 109077. <https://doi.org/10.1016/j.envres.2019.109077>.
- (56) Wang, Q.; Hui, J.; Huang, Y.; Ding, Y.; Cai, Y.; Yin, S.; Li, Z.; Su, B. The Preparation of BiOCl Photocatalyst and Its Performance of Photodegradation on Dyes. *Mater. Sci. Semicond. Process.* **2014**, *17*, 87–93. <https://doi.org/10.1016/j.mssp.2013.08.018>.
- (57) Padera, F. Sunscreen Testing According to COLIPA 2011/FDA Final Rule 2011 Using UV/Vis LAMBDA Spectrophotometers. *PerkinElmer Inc* 9.
- (58) Buono, M. J.; Ball, K. D.; Kolkhorst, F. W. Sodium Ion Concentration vs. Sweat Rate Relationship in Humans. *J. Appl. Physiol.* **2007**, *103* (3), 990–994. <https://doi.org/10.1152/jappphysiol.00015.2007>.